ABSTRACT

Title of Document: ANALYSIS OF OCEAN POWER EXTRACTION CAPABILITIES OF A ROTARY WAVE ENERGY CONVERSION SYSTEM

Sean P. Henely, Laura K. Hereford, Mary Y. Jung, Tatsuya Saito, Edward P. Toumayan, Sarah K. Watt, Melanie K. Wong

Directed By: Professor James Duncan, Mechanical Engineering

In recent years, there has been a shift towards renewable energy sources to help alleviate the dependence on fossil fuels. Many industries have started to investigate wind, solar, and other alternative energy sources. Our research aimed to provide additional insight into the field of wave energy as a component of a comprehensive energy solution. We selected a unique wave energy converter design and analyzed potential modifications that could improve its performance. After developing design modifications, we constructed and tested a prototype of a Rotary Wave Energy Collector (R-WEC). We tested the rotor under two mooring configurations and collected data on the relationship between power output and wavelength. We also analyzed the rotor's performance under single and multiple frequency wave environments. In addition, we investigated the implementation of a full-scale device through a study of three coastal regions in the Mid-Atlantic U.S. area. This research showed that our R-WEC design could be implemented in shallow water, single frequency wave environments to generate usable power.

ANALYSIS OF OCEAN POWER EXTRACTION
CAPABILITIES OF A ROTARY WAVE ENERGY
CONVERSION SYSTEM

By
Team WAVES
(Water and Versatile Energy Systems)

Sean Henely
Laura Hereford
Mary Jung
Tatsuya Saito
Edward Toumayan
Sarah Watt
Melanie Wong

Thesis submitted in partial fulfillment of the requirements of the
Gemstone Program, University of Maryland, 2011

Advisory Committee:
Dr. James Duncan, chair, University of Maryland
Dr. James Baeder, University of Maryland
Mr. John Zseleczky, United States Naval Academy
Dr. Kenneth Kiger, University of Maryland
Dr. Raymond Adomaitis, University of Maryland
Dr. Xinan Liu, University of Maryland

Acknowledgements

Table of Contents

List of Tables

List of Figures

List of Equations

Nomenclature

Acronyms

R-WEC: Rotary Wave Energy Collector
WEC: Wave Energy Converter
USDOE: United States Department of Energy
OPT: Ocean Power Technologies
PVC: Polyvinyl Choride
AC: Alternating current
DC: Direct current

Equation 1: Calculation of Weight and Buoyancy

V_{rod} – Volume of the aluminum rod [m^3]
$r_{rod, outer}$ – outer radius of the aluminum rod [m]
$r_{rod, inner}$ – Inner radius of the aluminum rod [m]
L_{rod} – Length of the rod [m]
V_{helix} – Volume of the helix [m^3]
R_{helix} – Radius of the helix [m]
$L_{helix, pitch}$ – Length of the helical pitch [m]
$F_{gravity}$ – Force of gravity [N]
ρ_{rod} – density of the aluminum rod [kg/m^3]
g – acceleration due to gravity [m/s^2]
ρ_{helix} – density of the helix [kg/m^3]
$F_{buoyancy}$ – Buoyancy force [N]
ρ_{water} – density of water [kg/m^3]
F_{result} – resultant force [N]

Equation 2: Macaulay's Method of Stress Analysis and Factor of Safety

z – position along the length of the rotor
W_{rod} – Weight of the aluminum rod [N]
L_{rod} – Length of the aluminum rod [m]
W_{helix} – Weight of the helix [N]
L_{helix} – Length of the helix [m]
$M(z)$ – Moment [Nm]
$I_{rod,z}(z)$ – Moment of Inertia
$r_{rod, outer}$ – outer radius of the aluminum rod [m]
$r_{rod, inner}$ – Inner radius of the aluminum rod [m]
$\sigma(z)$ – stress [Pa]
$SF(z)$ – Safety Factor
S_{yield} – yield stress [Pa]

Equation 3: Leading edge angular displacement

$\Theta_{LE}(z)$ – angular displacement of the leading edge
z – position along the length of the rotor [m]

Equation 4: Trailing edge angular displacement

$\Theta_{TE}(z)$ – angular displacement of the trailing edge
z – position along the length of the rotor [m]

Equation 5: Leading edge and trailing edge radial displacement

$r_{LE}(z)$ – radial displacement of the leading edge
$r_{TE}(z)$ – radial displacement of the trailing edge
z – position along the length of the rotor [m[

Equation 6: Definition of multi component wave parameters

$\zeta(t, \bar{x})$ – surface elevation
t – time [s]
$\bar{x}$ – position vector [m]
a_i – amplitude [m]
$\bar{k}_i$ – wave number vector
ω_i – wave frequency [radian]
Φ_i – phase shift [radian]
S – power spectrum
p – probability function
θ_{wind} – angle of rotation

Equation 7: Bretschneider wave spectrum

S – power spectrum
f – frequency [Hz]
f_{mean} – mean frequency [Hz]
H – significant wave height [m]

Equation 8: Definition of frequencies

$f_{carrier}$ – carrier frequency [Hz]
f_{mean} – mean frequency [Hz]
f_{low} – low frequency [Hz]
f_{high} – high frequency [Hz]
f_{max} – maximum frequency [Hz]

Equation 9: Water wave frequency dispersion

λ – wavelength [m]

g – acceleration due to gravity [m/s^2]
f – frequency [Hz]

Equation 10: Energy flux per unit wave front

P – energy flux per wave crest [kW/m]
ρ – density of the medium [kg/m^3]
g – acceleration due to gravity [m/s^2]
H – wave height [m]
T – wave period [s]

Equation 11: Power available to the rotor

ρ – density of the medium [kg/m^3]
g – acceleration due to gravity [m/s^2]
T – wave period [s]

Equation 12: Power calculated from the vertically lifted weight

P – power extracted [W]
m – mass lifted [kg]
g – acceleration due to gravity [m/s^2]
h – height which the mass was lifted [m]
t – time required to lift the mass m a height h [s]

Equation 13: Power available in multi frequency waves

P – power available [W]
ρ – density of the medium [kg/m^3]
$\Sigma(z^2)$ – sum of the wave amplitudes squared [m^2]
Δt – time required to rise 0.3 meters (12 inches) [s]
g – acceleration due to gravity [m/s^2]

Chapter 1:   Introduction

The research described hereafter aims to modify, construct, and test a device to extract power from ocean waves.   The wave motion causes the device to engage in continuous rotation as the waves propagate along its axis.   The rotary movement of the device can be converted into usable energy.

1.1 Background

The use of wave power to do work can be traced back to the early Roman times when ocean currents were used in mills to process grain (Charlier & Finkl, 2009).   However, a real fascination with wave power did not develop until more recently.   Since the oil crisis of the 1970s, wave power has had increasing interest throughout the United States and the world. During this time, data was taken from weather monitoring ships and buoys to show the potential of wave energy.   Statisticians calculated that waves passing over a one meter wide section of water in a typical location with a depth of fifty meters carried an average of forty kilowatts of power (Barras, 2010).   In the many years since then, researchers have been studying wave energy closely, in order to determine its true capabilities. In recent years, wave energy converting systems are being designed and tested to use the kinetic energy of oceans and other bodies of water to produce electricity.

The pending global energy crisis requires an examination of renewable energy sources, including wave energy.   In 2008, 91.1 percent of electricity in the United States was produced by non-renewable energy sources, including the burning of fossil fuels (Industry statistics, 2008). Eventually, this finite resource will be depleted and new energy sources will have to replace

fossil fuels as a dominant electricity source.   Throughout the past several years, researchers have strived to find cost-effect ways to harness energy from new sources.   Also, in the recent years, there has been a societal shift towards environmentally friendly practices in all industries. This desire to "go green" has further pushed engineers and researcher towards renewable energy sources as an alternative to fossil fuels and other non-renewable sources.   Renewable energy sources, including wave energy, have the potential to provide clean, abundant energy for the global community.

Wave energy, in conjunction with other renewable energy sources, could help alleviate our dependence on non-renewable energy sources.   In addition, wave energy has great potential to meet our future electrical energy needs with relatively less environmental impact than current methods used to generate power from fossil fuels.   According to data taken in 2006, there are two terawatts of kinetic energy stored in the ocean, which is the equivalent of twice the world's electricity production (AquaBUOY, 2006).   Although not all of this energy is usable, there is great potential to significantly decrease the global dependence on fossil fuels.   As shown in Figure 1, there is potential energy stored along coasts all throughout the world.   Engineers and researchers are making every effort to develop a cost effective, environmentally friendly way to convert the energy stored in ocean waves into energy suitable for human use (Leijon, 2009).

Figure 1: Worldwide Wave Power Levels (kW/m of Wave Front)

(http://www.freewebs.com/frenchsociety/energypoweredchange.htm)

1.2   Current methods and trends

Currently, there are many types of wave energy converters being designed and researched in the field of wave energy.   Each category of design uses different techniques and mechanical subsystems to harness energy from ocean waves.   Figure 2-6 show computer generated models of each category of design.   Point absorbers are floating structures which harness the energy through vertical motion.   The components of a point absorber move relative to each other and are driven by the oscillation of ocean waves.   This motion drives an electromechanical or hydraulic energy converter, which extracts usable energy from the wave motion.   Attenuators are floating structures composed of multiple, connected segments oriented perpendicular to the waves.   The differing heights of waves cause flexing between the segments, which produces

6

energy, usually through a hydraulic pump.   Overtopping devices gather water from incoming

waves into a reservoir.   When the energy is released, gravity causes the water to fall back, and

the energy of the water causes hydro turbines to turn.   Oscillating water columns are terminator

devices which extend perpendicular to the direction of wave travel.   Water enters a chamber,

which is connected to a turbine, and the water column moves up and down like a piston as the

wave action passes.
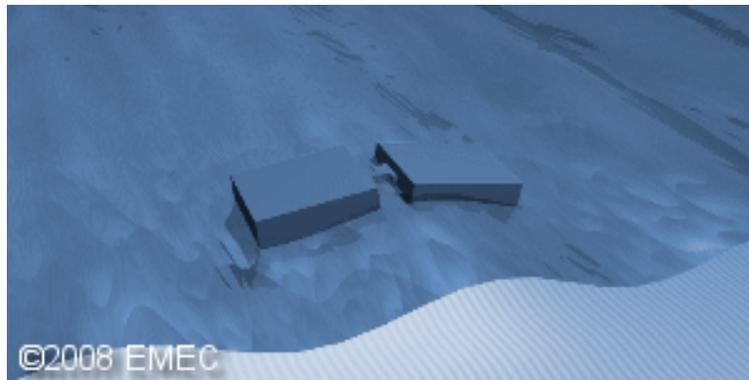
Figure 2: Model of an attenuating wave energy conversion device (EMEC, 2008)
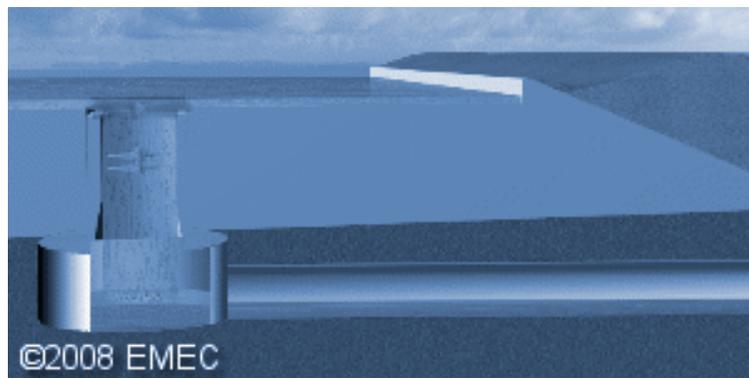
Figure 3: Model of an overtopping wave energy conversion device (EMEC, 2008)
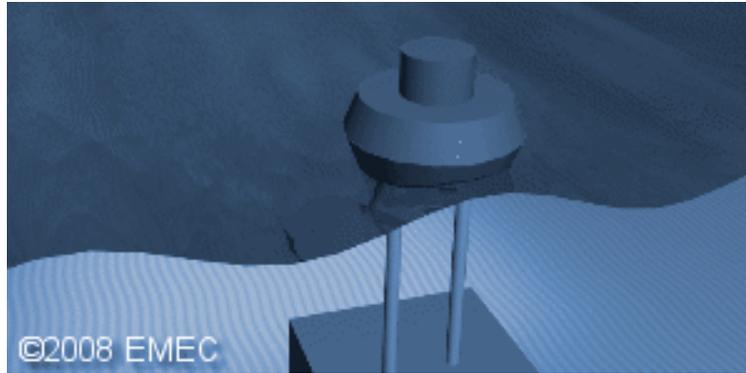
Figure 4: Model of a point absorber wave energy conversion device (EMEC, 2008)
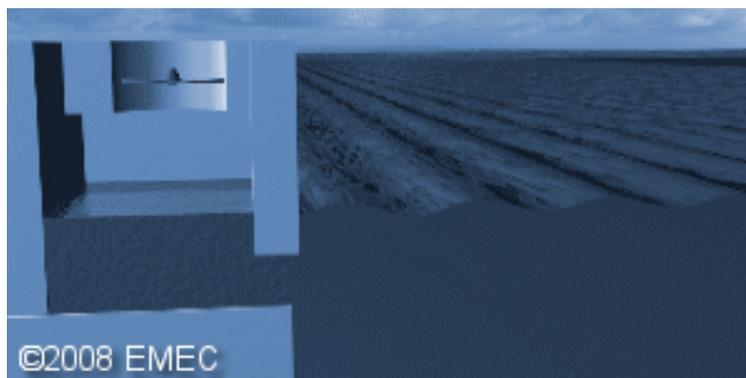
Figure 5: Model of an oscillating water column wave energy conversion device (EMEC, 2008)
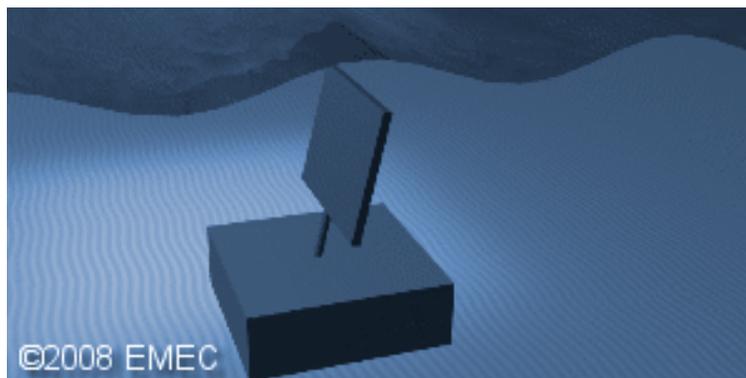
Figure 6: Model of an oscillating wave surge wave energy conversion device (EMEC, 2008)

A small number of wave energy farms have been installed in various areas of the world. These wave farms show how configuring wave energy devices at an offshore location can yield increased electrical output, in comparison to a single device acting on its own.

One of the main issues facing today's society surrounding wave energy is the question of how to best utilize this resource.   There is currently great debate over determining how the maximum amount of energy can be extracted with the smallest negative impact to the environment.   The field of alternative energy also struggles with lack of public support for research (Beyene & Wilson, 2008).   Continuous studying of ocean energy will increase the viability of renewable technologies.   Without valuable ocean energy research, the possibility of wave energy remains somewhat of a mystery to the general population.   This research was designed to show that Wave Energy Converters are capable of providing a significant portion of energy demands in regions with sufficient wave energy potential.   Research in the field of renewable energy is instrumental in further developing wave energy conversion systems.   With research that shows proof of success, public support will increase, leading to additional funding and access to this renewable energy source.   Our hope is that one day wave energy will be a reliable contribution to energy consumption worldwide.

The research described in this thesis focuses on maximizing the performance of a single device, a Rotary Wave Energy Collector, and showing the potential of that device to act as a single converter.   The research involves determining what modifications to an existing design will optimize the performance of the device, facilitating the construction the rotor, and testing it under various wave conditions and mooring setups.   This research is intended to contribute to the study of wave energy by showing the potential of Wave Energy Converters as an important component in a global energy solution.

1.3   Research question

How is the power output of a Rotary Wave Energy Collector (R-WEC) affected by wave

conditions, including amplitude, wave length, and sea state? Furthermore, how will the performance of the rotor be affected by adjusting the mooring system to approximate real world situations within the bounds of a laboratory setting?

1.4 Hypothesis

Increasing the wave amplitude beyond the radius of the prototype will have negligible effects on the power output. The power output will be a maximum when the wave length is equal to the pitch, the length of one full spiral rotation on the rotor. When operating under randomly generated wave conditions, the rotor's performance will degrade, in comparison to single frequency waves. When operating under mooring systems which approximate real world situations, the rotor's performance will degrade, in comparison to a laboratory based mooring design.

1.5 Limitations

Due to the difficulty of obtaining permits for open water testing, testing was not performed in open waters, thus limiting the research to testing under the simulated conditions of a wave tank. Therefore, the R-WEC's behavior in the ocean can only be predicted, not measured.

Another limitation inherent in testing in the wave tank is the disadvantage of testing a scale model of the actual prototype. Although the models of the prototype were constructed to best reflect the full scale R-WEC, testing the R-WEC at its actual size would be ideal. The full scale model testing would eliminate any error from extrapolating data obtained using a scale model (Cruz, 2008).

1.6 Overview of methodology

After a review of existing wave energy converters, the team selected the R-WEC design to study and optimize. The R-WEC design was patented in 1983 by Daniel DeMenthon (DeMenthon, 1983). The R-WEC consists of a helical shape surrounding a rod that rotates with the motion of incoming waves. The team constructed the rotor according DeMenthon's basic parameters, but used different construction methods and materials.

The dimensions of the R-WEC prototype were six feet in length and four inches in diameter. The rotor was constructed using a six-foot-long aluminum rod, and closed cell syntactic foam to create the helical portion. Small circular foam pieces with increasing and decreasing segments of a circle were cut out and attached to the aluminum with epoxy. The surface was sanded and coated in epoxy to create a smooth spiral.

For the initial round of testing, the R-WEC was rigidly moored at both ends to the top of the wave tank. A pulley system was attached at one end of the rod. This pulley system was also attached to a weight, and the power output was measured based on the time it took the rotor to lift the weight a certain height.

This initial round of testing indicated that the optimum wavelength corresponded to the length of our rotor. For our six foot rotor, this meant that the optimum wavelength was six feet.

Chapter 2:   Literature review

The literature review section will provide a discussion on prototype designs, construction materials and approaches, wave farm configurations, and mooring systems.

2.1 Wave energy as a renewable energy

In recent years, society has been faced with the challenge to develop alternative energies in order to alleviate the global dependence on fossil fuels.   A unique study by Birol investigated the likely differences between a future where an Alternative Energy Plan was enacted and a future with no attention to alternative energy.   Birol hypothesized that, without an Alternative Energy Plan, the global community, including the United States, would suffer greatly from an increasing dependence on and eventual depletion of non-renewable energy sources (Birol, 2007). Increasing energy prices and various geopolitical events have recently made the public aware of the fact that the global energy supply is in an extremely vulnerable state.   Birol emphasized the growing public knowledge and reiterated the need to restrain the growing demand for fossil fuels, alleviate harmful fuel emissions, and increase the diversity of available energies (Birol, 2007).   Ultimately, this research concluded that there is a great urgency for political action with regards to an Alternative Energy Policy.   If the policies were appropriately enacted, Birol concludes that the rate of increase in energy demand would be greatly reduced (Birol, 2007).

As the global society continues in a quest for renewable energy sources, there is some question about which sources can survive in an energy dependent world.   Research has found that wave energy has great potential to significantly decrease the dependence on non-renewable sources.   However, extracting ocean wave power and producing energy is not a quick fix.   The

technology required can only be procured with government support, regulation streamlining, and additional research and data collection (Holzman, 2007). Currently, the field of wave power faces numerous obstacles. Although there is research being done, there is a lack of unified collaboration within the field. Government support and regulation streamlining would help to focus the additional research on areas that can show the feasibility of wave energy. As of 2007, there were over 25 wave power technologies in existence and undergoing testing. However, because of the high costs associated with research and prototype testing, it is extremely difficult to achieve the standards for wave power implementation (Holzman, 2007). Although the high standards for implementation cause the most resistance to wave energy, many of the current technologies require specific water parameters in order to be economically efficient (Holzman, 2007). The field of wave energy requires additional focus on developing and testing technologies that will reduce the need for certain wave speeds and make wave energy viable for any area.

Much of the current research will show that wave energy is still in its earliest stages. In addition to research focused on developing this new technology, there is a substantial amount of research being conducted aimed at determining what performance and cost are necessary for wave energy to become a successful energy source. Ringwood (2006) studied the challenges and benefits of wave energy to determine how it compared with other renewable sources and what the future held. One of the main conclusions of the research was that a basic configuration and a stable control system were necessary in order to develop an efficient wave energy converter (Ringwood, 2006). In comparison to wind, solar, and other alternative energies, wave energy needed to accomplish these things and achieve efficiency in order to compete. Based on similar renewable energy programs, research has also shown that an

13

extremely solid legal and regulatory framework is required for wave energy programs to be successful (Holahan, 2008).

Annete von Jouanne, a leading proponent and driving force behind wave energy, tells audiences across the world that ocean waves are a useful energy source. Ocean waves aren't scarce, fleeting, or dirty. Harnessing wave energy is said to have no harmful pollutant dispersion. Von Jouanne also says that, unlike wind and solar power, wave energy is always available in that the ocean swells are constantly moving water up and down enough to generate electricity (von Jouanne, 2006).

2.2   Wave energy conversion

As stated in the previous section, research of ocean waves continually shows great potential for harnessing the energy stored in waves. Wind over the ocean surface creates waves and water motion almost constantly. The consistency and force of the winds over the ocean cause waves to be constant and allows them to store a significant amount of energy (OCS, 2010). There are many parameters taken into consideration when analyzing the options for wave energy conversion. The most common things to consider are method of extraction, location of harnessing, manner of energy conversion, and type of device (OCS, 2010). These parameters are inter-related and some of them are dependent on others. Although each of these major considerations is important, it is also necessary to make decisions holistically when it comes to determining wave energy conversion methods.

There are two well-known methods used to extract energy from ocean waves. However, wave energy research is still in the beginning stages and new technologies are constantly being researched. Currently, the most commonly tested methods are either directly from the surface

motion of ocean waves, or from the pressure fluctuations occurring deeper below the surface (OCS, 2010).

With regards to location of extraction, current research categorizes the sites as nearshore, offshore, and far offshore.   Nearshore includes the sites closest to land and those most easily reached for maintenance and upkeep.   Offshore is slightly further into the ocean and far offshore is sites where the water is at least 40 meters deep (OCS, 2010).   Many devices are designed and constructed for use in one location and they are able to maximize their energy conversion in that location classification only.

Another parameter to consider when working to harness wave energy is the method of energy conversion.   Different from the method of energy extraction, the conversion manner involves how the extracted energy is turned into usable energy, most commonly electricity (OCS, 2010).   The decision of how to convert energy requires research into pumps and generators.   It is also dependent on many of the other parameters considered.

There are currently five main categories of wave energy conversion devices with various tested prototypes within each category.   These classifications will be discussed in greater detail in the next section.

As mentioned previously, many of these parameters are inter-related.   The method of extraction is directly related to the type of device used for conversion.   Certain devices are designed to pull energy from the surface of the waves, while other categories are dependent on being deeper underwater.   The location of extraction also affects the method mainly through the type of device.   Devices are also designed to be optimally used either nearshore, offshore, or far offshore.   This determination connects the type of device to the method of extraction.   Finally, the manner of energy conversion is only loosely dependent on the other categories.   It is most

directly tied to the type of device based on the results of current tests.   Ultimately, there exist

numerous combinations of these parameters, but current testing has shown which combinations

allow for the most optimal energy extraction and conversion for usable consumption.

Current testing of wave energy conversion involves various combinations of the above

parameters in various locations throughout the world.   The United Stated Department of Energy

reported in 2008 that there were sixty-two developers of wave energy technology.   Of those

developers, only a few were reported to have full-scale prototypes for testing (USDOE, 2008).

In the report, the Department of Energy indicated that the majority of the developed devices were

either attenuators or point absorbers and they were in the design or testing phases (USDOE,

2008).   This reflects the early stages of wave energy testing and, due to the longevity of testing

required, it is likely that wave energy converters will continue to be tested for several years

before full scale implementation and use.   All of the currently tested conversion technologies

are designed for installation at or near the ocean surface (OSC, 2010).   This creates a larger

impact with regards to visual aesthetics and interference with other maritime activities.

2.3 *Prototype designs*

In general, wave energy converters (WECs) can be grouped into five main categories:

oscillating water columns, point absorbers (including floating and submerged pressure

differential devices), attenuators, overtopping devices, and oscillating wave surge converters.

These categories comprise the current research and testing that exists for harnessing wave

energy.   In addition to these categories, there are wave energy converter designs which can be

categorized as a combination of these groups and wave energy converter designs which cannot

be placed into these categories at all.   These groups serve to outline the mechanical components

and systems which are most commonly used to extract energy from ocean waves.   Each category was researched with regards to the concepts behind the design, examples currently being developed and/or tested, and the advantages and disadvantages that come with each design.

2.3.1: Oscillating Water Columns

Oscillating water columns are considered to be one of the more attractive wave energy converter designs in terms of efficiency, economics, and aesthetics.   They are partially submerged, hollow devices which use turbines to generate electricity (EMEC, 2008). Wave movements cause a water column in the device to rise and fall which compresses and decompresses a column of air above.   These changes in pressure cause air flow through rotating turbines, thus generating electricity (EMEC, 2008).   A model of an oscillating water column device is shown in Figure 7 below.
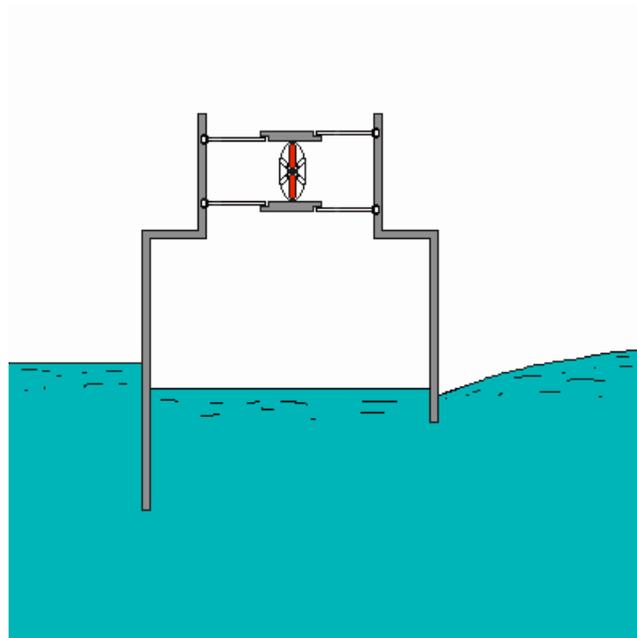
Figure 7: A model of the oscillating water column technology (Daedalus, 2008)

The device is primarily composed of a vertical cylinder which is partially submerged. The lower end of the cylinder is left open so that water may enter the chamber. As waves pass by the device, oscillating pressures are formed at the open, lower end (Evans, 1978). A water column is formed in the vertical chamber with air at the upper end. The motion of the waves, as they pass by the device, creates a rise and fall motion of the water column. The vertical, oscillating motion allows the water column to act as a piston within the cylinder (de O. Flacao).

As the water column rises during the wave crest formation, the air at the top of the chamber is compressed to a value slightly greater than atmospheric pressure (Daedalus, 2008). The compressed air is then forced out of the cylindrical chamber by turning an air turbine. Oscillating water columns generally employ Wells turbines in order to convert the energy into electricity (USDOE, 2008). After the compressed air is forced out of the chamber, the wave trough formation causes the water column to fall. This motion decompresses the air to a value slightly less than atmospheric pressure, drawing new air into the chamber (Daedalus, 2008).

Oscillating water columns have an opening at the top of the chamber through which the air is forced out and drawn in. This opening is connected to the turbine which converts the air movement into electricity. The air movement is created from the wave motion in that the oscillation of the water column within the chamber closely follows the waves in sequence and amplitude (Daedalus, 2008). The use of a Wells turbine allows the oscillating water column device to benefit from air flow in both directions as the waves rise and fall.

Wavegen, a Scotland based company, has already began testing on the most commonly known wave energy converter prototype that follows the oscillating water column design. Installed off the coast of Islay, Scotland in 2000, it was the world's first commercially oriented approach for the capture of ocean wave power (de O. Flacao). Wavegen's system is called the

Land-Installed Marine-Powered Energy Transformer, or LIMPET.   The Wavegen oscillating

water column system is comprised of a concrete chamber built into the shoreline as shown in the

model in Figure 8 and the photograph in Figure 9.   After installation, the system has been able

to reliably generate about 500 kilowatts of power, which is enough to supply about 400 homes

(Staedter, 2002). The capability and success of the LIMPET devices have had a significant

impact on the wave energy conversion community.   It has been well received and is viewed as a

key test bed for furthering developments in wave energy technology (Staedter, 2002).
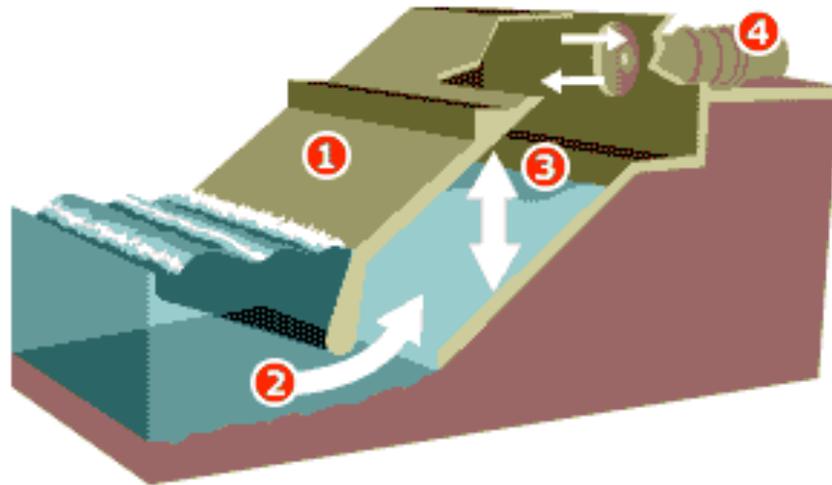
Figure 8: A model of the Wavegen LIMPET oscillating water column system installed at a
shoreline (bbc.news.co.uk)

Figure 9: A photo of the LIMPET wave energy turbine system installed in Scotland

Research shows many advantages associated with harnessing wave energy through oscillating water column devices.   The United States Department of Energy states one benefit is that the devices can be mounted, near shore or break waters, or floating further into the ocean (USDOE, 2008).   An advantage that comes with mounting close to shore is that it provides for easier access to the device and easier ability to conduct regular maintenance and perform repairs. In addition, the moving, mechanical parts used in oscillating water columns, including the turbines used for electricity conversion, are housed outside of the ocean water.   This increases the lifetime of the device by decreasing the likelihood for corrosion and other wear from the water (de O. Flacao).

2.3.2: Point Absorbers

A point absorber wave energy converter is a device with components which move relative to each other due to the motion of the ocean waves.   The relative motion of the components is used to drive an electromechanical or hydraulic energy converter (OCS, 2010). Point absorbers are classified as either floating or submerged pressure differential devices.

Floating point absorbers are wave energy converters which follow the mechanics of a point absorber and float on the ocean's surface.   They are typically deployed in water depths between 40 and 100 meters and have been found to be most efficient when deployed in arrays with a distance of several meters between each device (de O Falcao).   The devices are able to absorb energy in all directions through movements at or near the ocean surface (USDOE, 2008). The converter itself is generally small in its horizontal dimensions, when compared to the representative wavelength in the area (de O Falcao).

Submerged pressure differential point absorbers are composed of an air-filled chamber which rests atop a shaft anchored to the ocean floor.   The motion of the passing waves causes the sea level to rise and fall above the air-filled chamber.   This creates a pressure differential within the device and causes the air-filled chamber to move up and down.   Ultimately, the motion of the chamber can either serve as a water pump or can be directly converted to electricity through a hydraulic system (USDOE, 2008).

Both classifications of point absorbers extract energy through the relative motion of the device's components.   The significant difference is merely the placement of the device. Floating point absorbers are at the surface of the ocean, while submerged pressure differential point absorbers are anchored to the ocean floor.

Ocean Power Technologies of Pennington, NJ has chosen to implement a wave farm off the coast of Oregon with floating point absorber devices.   The coast of Oregon was identified by Ocean Power Technologies as an area with attractive wave energy levels as shown in Figure 10 (OPT, 2011).   The device, named PowerBuoy, is about 150 feet in length, 40 feet in diameter, and about 220 tons in weight and is shown in Figure 11.   The original design allowed the converter to capture about 150 kW of energy.   However, the United States Department of Energy recently awarded Ocean Power Technologies 1.5 million dollars to ramp up the device's capability to 500 kW (Russell, 2010).   The prototypes generate electricity through a hydraulic generator (von Jouanne, 2006).   Ocean Power Technologies has contracted Oregon Iron Works as the constructor of the prototypes, which are placed about two and a half miles off the coast (Russell, 2010).   As development and testing continue, Ocean Power Technologies is contributing valuable research to the question of wave energy's reliability and validity.   The Vice President of Business Development and Marketing for Ocean Power Technologies, Phil Pellegrino, has stated that wave energy would cost about 15 cents per kWh, which is on par with current costs for wind and solar energy (Russell, 2010).

●●● Attractive Wave Energy Levels

■ Current OPT Focus
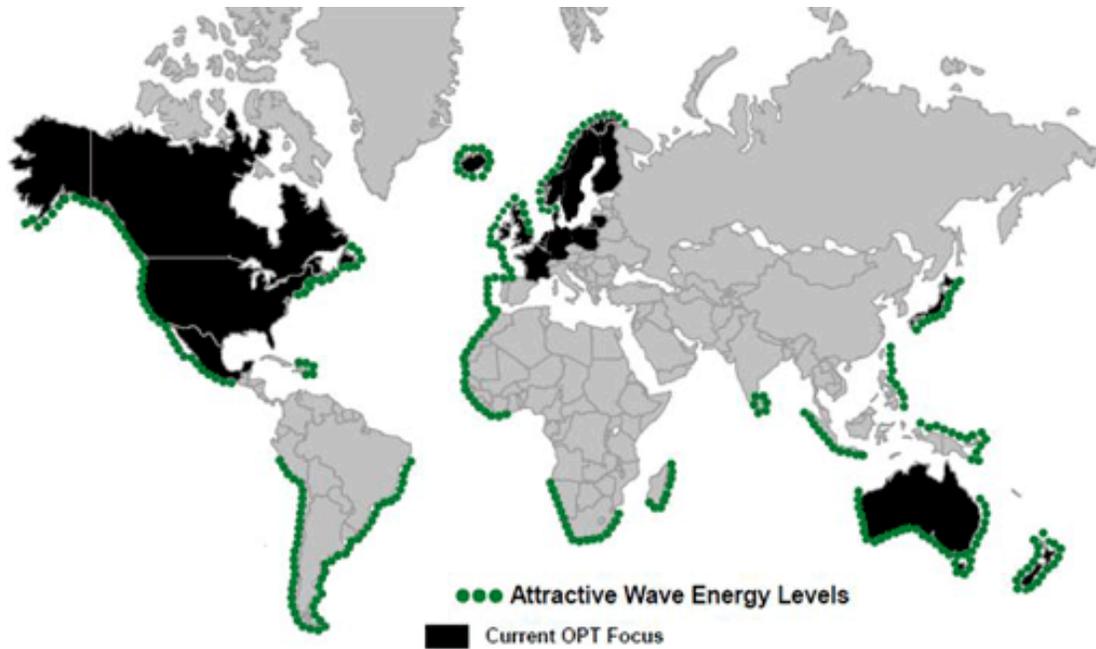
Figure 10: A map showing the areas of coastline with attractive wave energy levels as well as Ocean Power Technologies' areas of focus (OPT, 2011)

Figure 11: The Ocean Power Technologies PowerBuoy installed off the coast of Oregon (OPT, 2011)

AQUABuoy is another prototype of a floating point absorber currently being developed and tested.   It consists of a long cylinder which hangs down into the ocean off of a floating buoy as shown in Figure 12.   The cylinder contains a solid steel piston which is sprung from both the top and bottom by steel-reinforced rubber hosing (Holzman, 2007).   As the floating point absorber technology allows, when a wave passes by the device, the buoy bobs up and down with the swells of the waves.   The movement allows the inertia of the piston to stretch one end of the hosing and decompress the other (depending on whether the buoy is in a trough or atop a crest) (Holzman, 2007).   Through the relative movements of the buoy and the piston, potential energy is released, which pumps water through a turbine to generate electricity (Holzman, 2007).
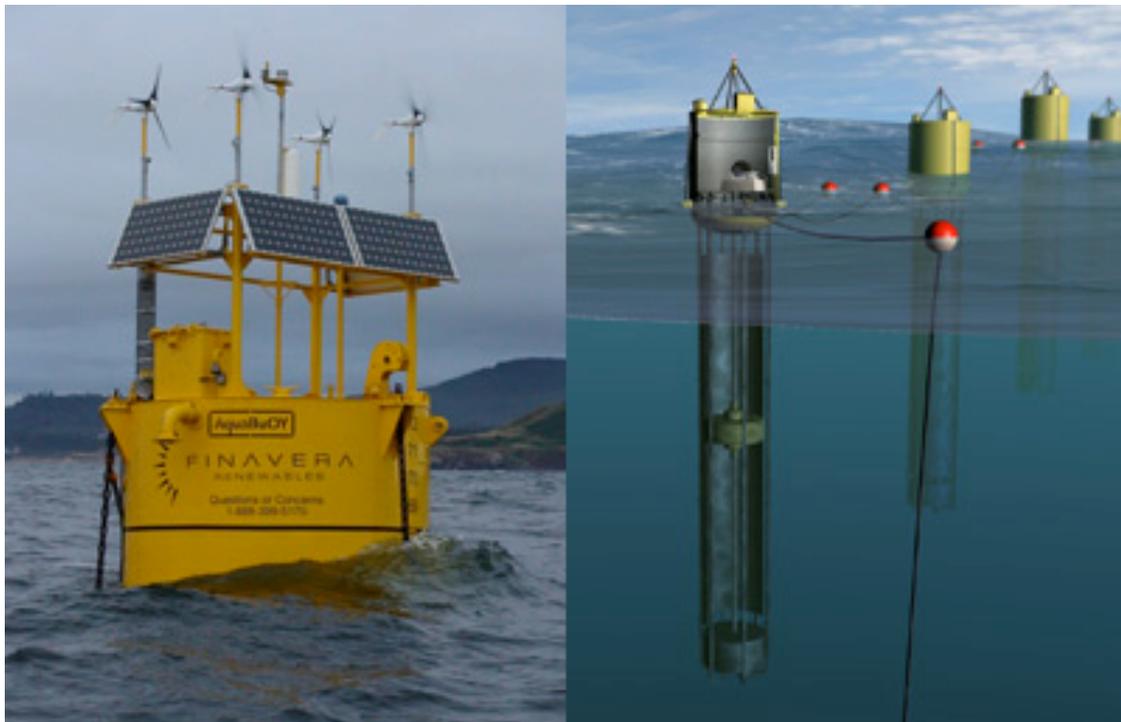
Figure 12: A photo of the Finavera AQUABuoy (left) and a model of the AQUABuoy technology under sea level (right).   (Chopra, 2007)

The Archimedes Wave Swing is an example of a point absorber which follows the submerged pressure differential design.   It is an air-filled chamber of cylindrical shape with a partially detached lid (de Sousa Prado).   The device is anchored to the bottom of the ocean floor
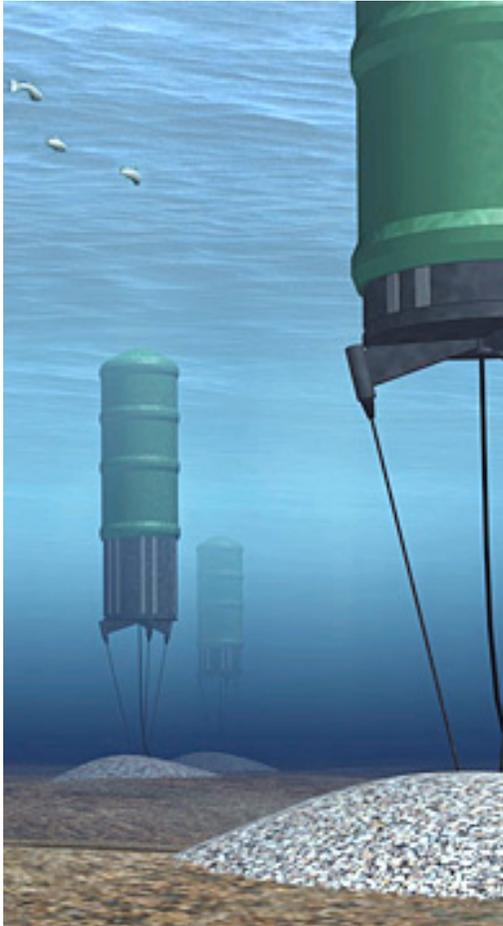
as shown in

Figure 13.   As waves pass over the device, the lid of the chamber, called the floater, is moved up and down in a vertical direction (de Sousa Prado).   The energy is extracted from the linear motion of the waves and converted to electrical energy.   Figure 14 shows the basic motion of the device as a wave propagates past.   A pilot plant of the Archimedes Wave Swing prototypes was built off a Portuguese coast in 2001 (de Sousa Prado).
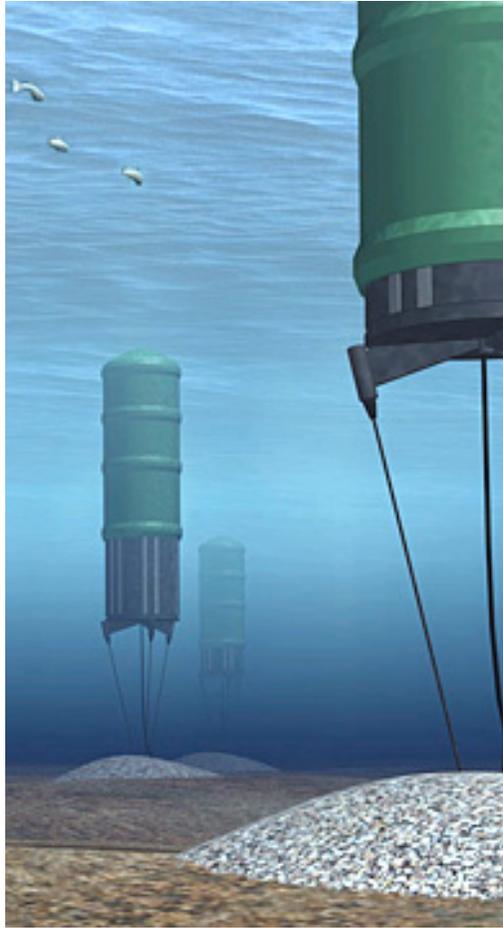
Figure 13: An underwater model of the Archimedes Wave Swing anchored to the ocean floor
(AWS Ocean Energy, 2011)
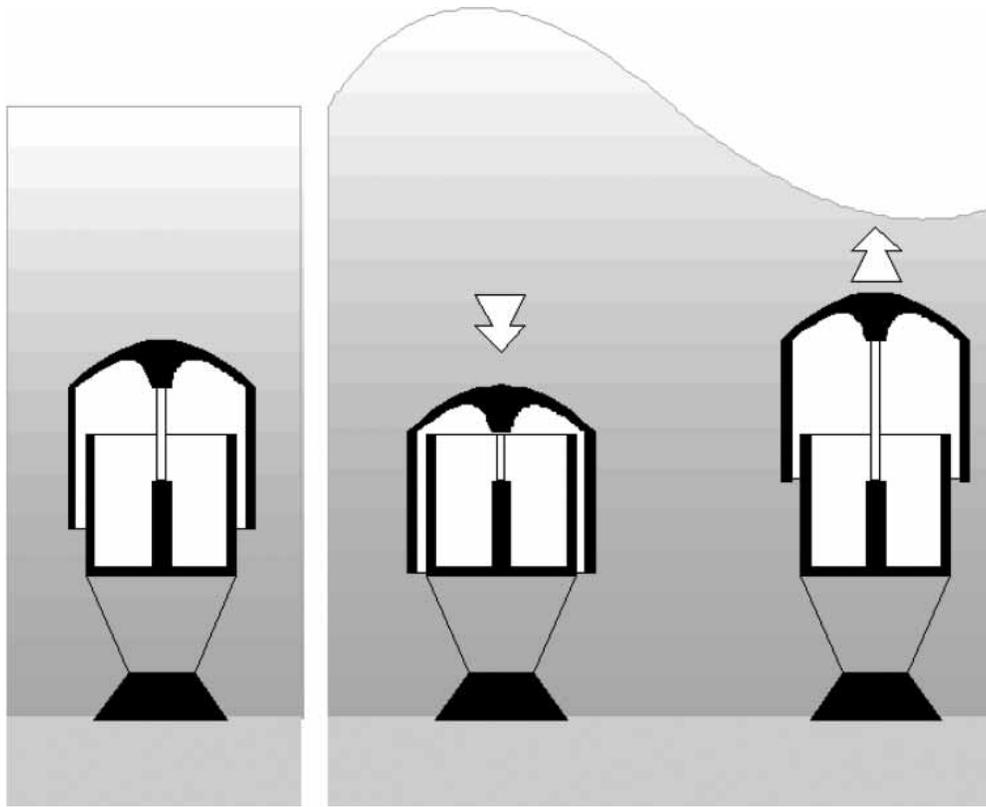
Figure 14: A model of how the Archimedes Wave Swing works as waves pass over it. (de Sousa Prado)

A profound advantage of floating point absorbers is their ability to absorb energy in all directions through wave movements near the surface (EMEC, 2008).   They are said to be able to pull tens to hundreds of kW of power out of ocean waves (de O Falcao).   A downside of floating point absorbers is that they float and, as a result, are extremely subject to drift forces. Because of this, these devices require strong and stable mooring configurations (de O Falcao).

Point absorbers which follow the submerged pressure differential design are seen to be advantageous for many reasons.   These devices are completely submerged, which makes them less vulnerable in storms (de Sousa Prado).   As opposed to the floating devices and many other types of wave energy converters, this may result in less failure and required maintenance due to irregular weather patterns.   Another benefit of being completely submerged is that they are not

visible, which leads to greater public acceptance and less interference with aesthetics (de Sousa Prado).

Point Absorbers in general also have many benefits, whether they are of the floating design or the submerged pressure differential design. The devices are relatively small compared to the most common sea wavelengths (McCabe, 2009). This makes their footprint significantly smaller than some devices and creates less interference with the ocean environment. They are also said to have the potential for more efficient power conversion in terms of output per unit volume than many other types of wave energy converters (McCabe, 2009). This indicates that point absorbers require design and implementation with a specific area in mind, in order to reach that potential. They tend to have a narrow bandwidth and only achieve the highest efficiency when excited by waves with a frequency around their resonance point (McCabe, 2009). When implemented in areas where the average wavelengths follow this requirement, point absorbers are capable of extracting ocean wave energy very efficiently.

2.3.3: Attenuators

Attenuators are wave energy converters which consist of multiple floating sections oriented in a line and hinged together at joints. The sections pivot and move with the motion of the waves as they pass by. The segments tend to rotate relative to each other in a pitch and heave motion (USDOE, 2008) as the waves pass by. This motion causes flexing at the joints, where a hydraulic pump is used to convert the energy (EMEC, 2008) and (OCS, 2010).

Pelamis, one of the most well known wave energy converter prototypes, follows the attenuator design. Pelamis Wave Power, a company in Portugal, is currently building the world's largest wave farm with attenuator devices named after the sea snake, pelamis (Holzman,

2007). The ultimate goal of the Pelamis testing is to be able to extract twenty mega-watts of power, or enough to power 4,000 homes (Holzman, 2007). As the attenuator device was described, Pelamis is comprised of multiple adjoined segments, which bend at the joints as waves pass by as shown in Figure 15. Each of the Pelamis device's segments is about the size of a train car (Holzman, 2007). Hydraulic rams at the joints work to resist the bending motion as waves pass. The rams push oil at a high pressure through hydraulic motors which drive electrical generators (Holzman, 2007).

Figure 15: The Pelamis attenuating wave energy converter (pelamiswave.com)

The success of attenuating devices has been found to be largely dependent on how well they are designed for a specific area of operation (The pelamis prototype, 2008). One major requirement of this is that, in order to be successful, the device needs to be oriented parallel to the motion of the waves. This suggests that areas where wave motion is difficult to track or areas where there is great variation in wave direction would not be suitable for attenuating devices.

2.3.4: Overtopping Devices

Overtopping devices are those that capture water from waves and then return the water to sea through a turbine which generates power.   The device is mainly composed of a reservoir which fills with water as incoming waves pass by.   The reservoir continues to gather water from passing waves until the water level within the reservoir is above the average surrounding ocean water level (OCS, 2010).   The water in the reservoir is then released, and, because the water level is higher, gravity pulls the captured water back to the ocean surface.   The falling water turns hydro turbines, converting the energy stored in the falling water into usable power (OCS, 2010).

The components of an overtopping device can be categorized into collectors, ramps, and reservoirs.   Collectors, often reflective arms, are used to collect the water as waves pass by the device.   Ramps allow the collected water to enter the terminating reservoir, where the water is stored until it is time to be released (USDOE, 2008).   The hydro turbines, or other type of conversion device, are used to capture the energy as the water flows back into the ocean.

An example of an overtopping device that is currently being tested is made by WaveDragon Ltd.   The device, called WaveDragon, is composed of two reflectors which focus the waves toward a ramp, a reservoir, which collects the overtopping water, and several turbines which convert the pressure of the water into power (Kofoed, et. al., 2004).   Figure 16 shows the various parts of the WaveDragon overtopping device and a photo of the actual device is shown in Figure 17.   The WaveDragon resembles a kite, which allows it to move as the ocean water moves.   A cable is used to attach the device to the sea bed, while still allowing it to adjust to the direction of incoming waves (Leung, 2005).   The turbines are positioned at the bottom of the reservoir and spin as the water fills the reservoir.   The electricity produced by the spinning

turbines is transferred to shore through the use of a cable (Leung, 2005).   Initial cost estimates showed that the WaveDragon would produce electricity at approximately 18 cents per kilowatt-hour.   At a capacity of 4 MW, the WaveDragon developers project that cost to decrease within the next few years to an ultimate goal of about 6 cents per kilowatt-hour (Leung, 2005).
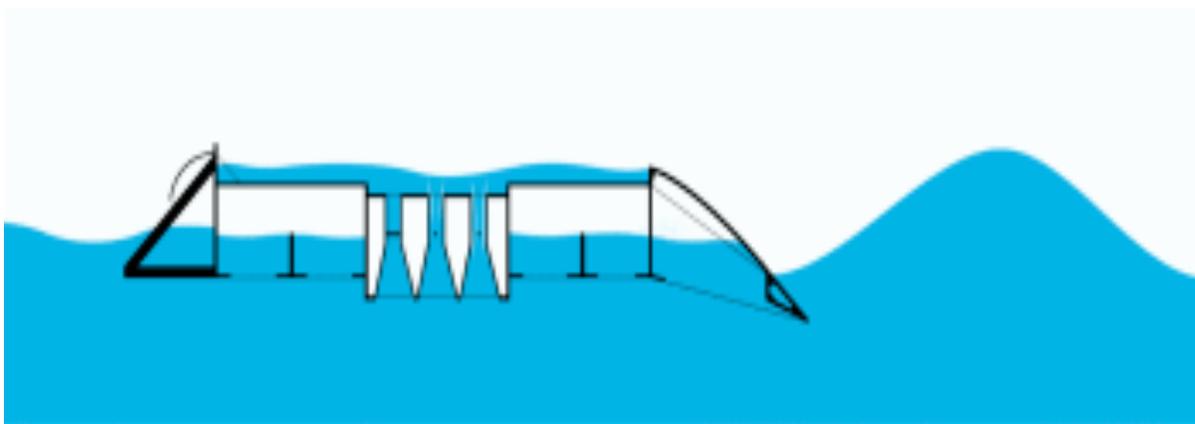
Figure 16: A model of how the WaveDragon overtopping device captures wave energy
(wavedragon.co.uk)

Figure 17: The WaveDragon overtopping device captures water in a reservoir as waves pass over the device (wavedragon.co.uk)

2.3.5: Oscillating Wave Surge Converters

Oscillating wave surge converters extract energy from wave surges and the movement of water particles (EMEC, 2008). They are placed on the shoreline or near the shore and are situated perpendicular to the direction of the waves. The motion of water particles within the passing waves allows the device to extract the horizontal energy stored in ocean waves (USDOE, 2008). The device usually consists of a paddle arm which pivots back and forth on a horizontal axis. The oscillation of the paddle arm is absorbed by a hydraulic pump, or other converter, which creates electricity (USDOE, 2008).

Various models have been developed to test the power generation of oscillating wave surge converters. In the United Kingdom, a numerical model was developed and applied to

simulate the complex fluid flow of air and water (Qian et al., 2005). This particular design took many parameters into consideration and was ultimately designed to couple strongly with the horizontal particle motion to permit large amplitudes of motion and minimal energy loss. (Folley, Whittaker, & Osterried, 2005).

Aquamarine Power has recently unveiled and started construction on a second generation oscillating wave surge converter device. Based in Aberdeen, Scotland, the device is approximately 26m by 16m and has a capacity of 800 kW (Aquamarine, 2010). The Oyster 2 device follows its predecessor, the Oyster 1 and moves towards the development of a commercial machine which could be sold on the market, says Aquamarine CEO Martin McAdam (Aquamarine, 2010). About twice as large as the first device, Oyster 2 delivers about three times more power than its predecessor (See Figure 18) (Aquamarine, 2010) . Many positive changes were made from the Oyster 1 prototype, including moving the hydraulic equipment to the end of the device and allowing it to continue operating at 75% power if one of the hydraulic pumps were to fail (Aquamarine, 2010). The device is linked to an onshore hydroelectric turbine which is used to generate usable electricity. Aquamarine currently plans to finish construction in time to deploy three test devices during summer 2011 (Aquamarine, 2010).
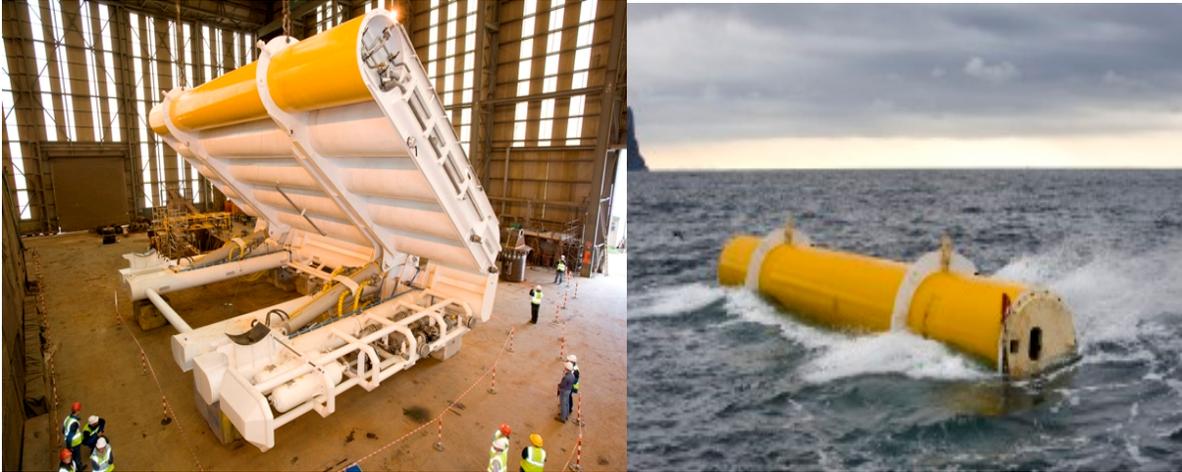
Figure 18: The Aquamarine Power Oyster 1 device during construction (left) and in the ocean (right) (Aquamarine, 2010)

Figure 19: An image of the Oyster 2 prototype design (Aquamarine, 2010)

2.4 Wave farm configurations

There is presently a limited amount of information available with regards to the strategic placement of WECs. However, the primary wave farm configurations utilized by leading wave energy companies arrange arrays of WECs in either parallel or staggered grids. The company CETO's wave energy converters are placed in parallel rows underwater, whereas Ocean Power Technologies' power buoys are placed in designs comprised of a series of staggered rows which are "spaced to maximize energy capture" (OPT, 2008). The layout of the WEC prototypes is in part based on the mechanism behind each design and how each WEC affects wave characteristics as a wave propagates past. A unique layout presented by Finavera Renewables consists of rows of WECs radiating from an open center creating a sunburst-like configuration.

Wind farms follow similar layouts and components as wave farms and have been evaluated not only for their physical parameters but also with respect to optimal electrical configurations using either alternate or direct currents (AC/DC). Wind turbines generating DC power connected in series have the greatest potential in providing the lowest energy production costs when the transmission distance is greater than 10 to 20km (Lundberg, 2004). The energy production and investment costs in the study were determined using cost analysis for models of the wind farm components. This was used as a baseline with which to compare the cost-benefit analysis performed for the R-WEC farms in the current research.

2.5 Mooring techniques

Particular consideration must be made for the dynamics of mooring lines which constrain the mechanics of floating bodies (H.O. Berteaux, 1976). For a mooring line to be effective, the elasticity of the line and the speed of the current must be taken into consideration. To compute

the physical characteristics of the optimal mooring system, which would maintain the position of the floating object, a variety of calculations are required, including but not limited to, dynamic cable analysis and vessel hydrodynamics (Pascoal, Huang, Barltrop, & Soares, 1644).

The simplest mooring system is the single point mooring system, in which there is one float, one line, one anchor, and additional equipment, if necessary (Low & Langley, 371).   A more complex system is the multi-leg mooring system in which two or more mooring lines can be used to restrain a floating structure.   This system is used to minimize the motion of the floating object while also increasing the reliability of the system.

Taut or semi-taut-leg mooring systems have been found to be favorable over the traditional catenary mooring systems due to their capability of maintaining the offset of floating structures (Wang, Guo, & Yuan, 1127).   Unlike the curved, U-shaped catenary mooring structures, taut systems hold the cables more rigidly resulting in an upside down V-shape. Regardless of the mooring array utilized, the tension distribution along the cable, the effect of slippage, and the horizontal and vertical forces must be analyzed (Wang, Guo, & Yuan, 1127). Other mooring system designs and configurations may be applied to fulfill specific needs.
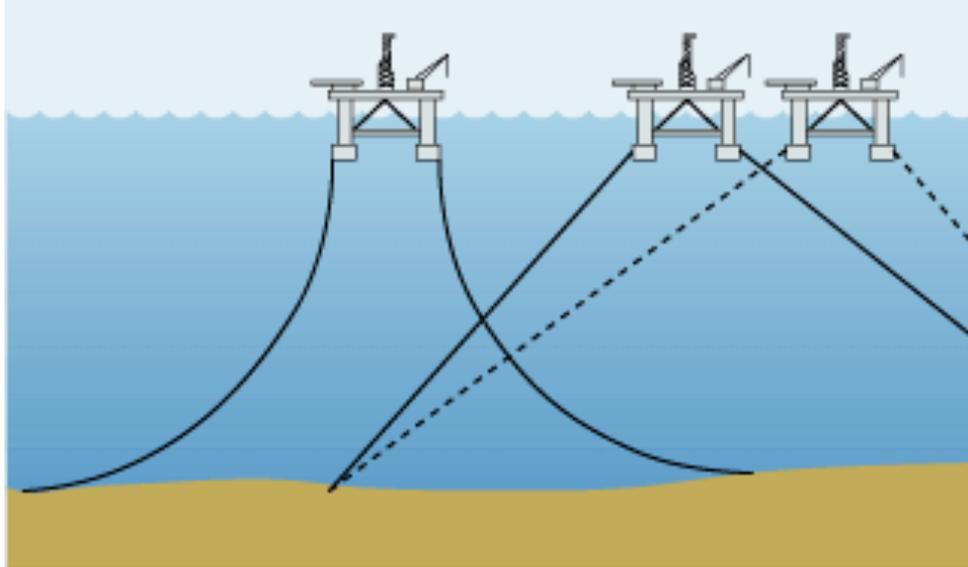
Figure 20: Catenary (left) and taut leg (right) moored floating vessels
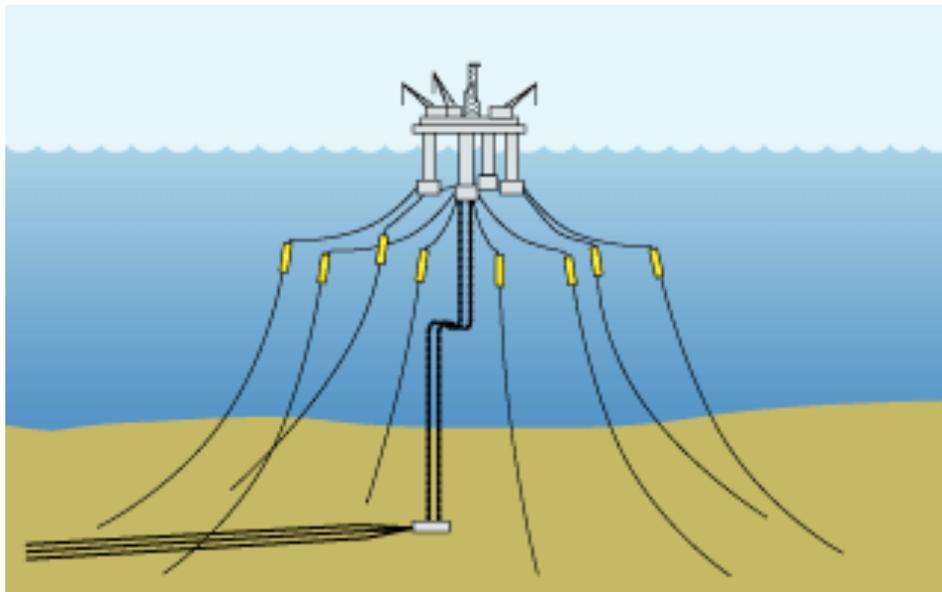
Figure 21: Semi-taut leg mooring arrangement

The article "Reliability-based Comparative Study for Mooring Lines Design Criteria" focused on the reliability and safety issues of various types of mooring systems.   Most mooring systems are affected by environmental factors such as wave elevation and wind motions.   This

study analyzed the calibration process of safety factors. They conducted simulations using various random variables, such as material strength, to test the probability of a failure for a mooring system.

Another study also focused on the reliability and maintenance of the mooring system when a single point mooring system is implemented. Although a single-point mooring system is favored for its eco-friendly and inexpensive features, its strength and reliability comes into question during a natural disaster such as a hurricane or a typhoon (Huang & Pan, 8). "Mooring line fatigue: A risk analysis for an SPM cage system" evaluated the failure risk of a mooring line over an extended period of time under various ocean conditions. The study indicated that the recommended replacement period for a polyester mooring line with a diameter of 38mm is about 6.55 years if the line's safety factor is 1 (Huang & Pan, 8). However, when the safety factor increases to 1.5, the replacement period extends to 23.81 years (Huang & Pan, 8). Therefore, the material and the strength of the cable in the mooring system must be taken into consideration after the system is defined.

2.6   The Rotary-Wave Energy Collector

The Wave Energy Converter that our team used in our experiments was designed by Dr. Daniel Dementhon, who is currently a faculty member of the National Science Foundation and associate research professor at a division of the University of Maryland Institute for Advanced Computer Studies. In 1982, Dr. Dementhon presented his design of the Rotary Wave Energy Collector (R-WEC) at the Offshore and Deepsea Systems Symposium and was issued a U.S. patent in 1983 (Dementhon, 1983).

The design does not fit neatly into any of the above defined categories of wave energy

converters, though it is most similar to a submerged pressure differential device.   However, the

R-WEC is not submerged, but rather it floats at water level.   The design calls for a series of

helical strips superimposed around a central cylinder.   The driving force behind the R-WEC is

the pressure difference on the leading edge and the trailing edge of the helical strip, causing the

device to rotate as a wave propagates past.   In order to be effective, the axis of rotation must be

at or above water level.   The device rotates in such a way that the edge of the rotor follows the

crest of the wave (See Figure 22).   The energy extracted from ocean waves depends on the

wave's amplitude and wavelength, as well as the radius and pitch of the R-WEC (Dementhon,

1983).
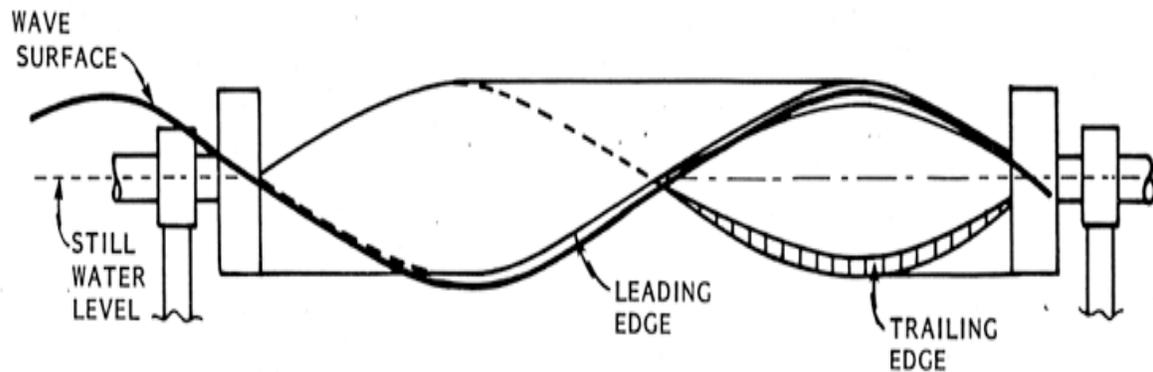
Figure 22: Thin helical rotor, clamped at still water level in sinusoidal waves (the vertical scale
has been expanded compared to the horizontal scale)

Team WAVES met with Dr. DeMenthon, and he was very enthusiastic about sharing his

design.   In addition to being an expert in the design of the prototype, Dr. DeMenthon has

provided with advice on considering issues surrounding the real-world application of the

prototype, including the effects of large storms and return on capital.
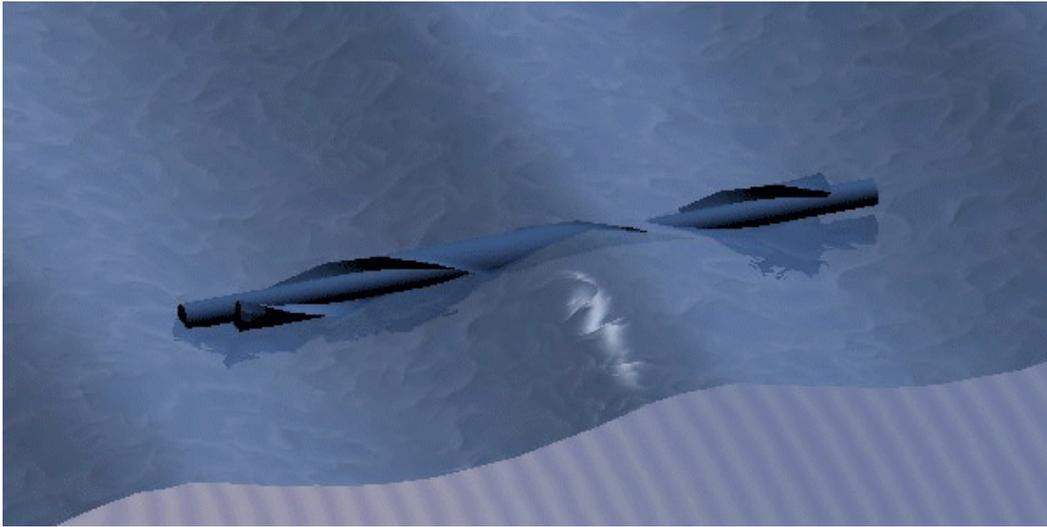
Figure 23: A 3-Dimensional prototype representation of the Rotary Wave Energy Collector created using Blender software

In DeMenthon (1983), the wave rotor was tested in a wave tank and the power output per unit volume and per unit displacement data were compared with this data for Salter cams. The experiments were conducted in a wave tank (dimensions: 20 m by 1.5 m by 1.5 m, with a water depth of 1.15 m). Three models with a pitch of 2.46 m and different radii (0.05m, 0.069m, and 0.1m) were tested.

The power extracted from the rotors was measured by "using the shafts of the rotors as winches [and] winding cables which lifted weights attached to them" (DeMenthon, 1982).

WAVE TANK
SIDE WALLS

PULLEY   ROTOR
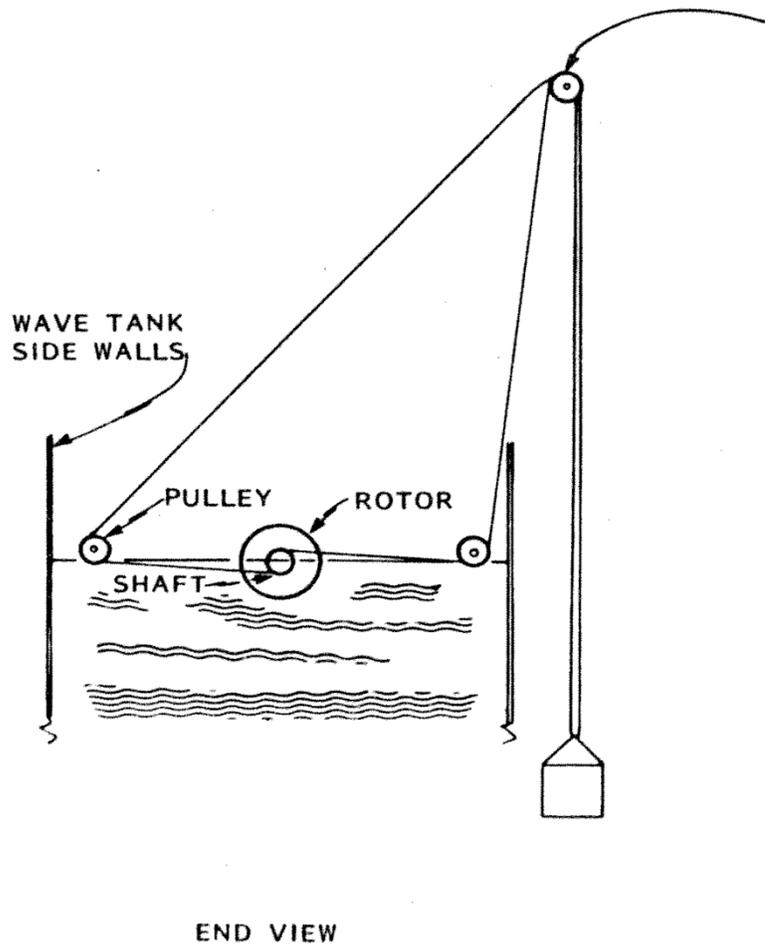
SHAFT

END VIEW

Figure 24: Using the rotor shaft as a winch to lift weights provides a measurement of power extracted from the rotor.   End view only (DeMenthon, 1982)

Under each wave condition, the maximum weight that could be lifted up one meter without stalling was recorded.   The lift time was also measured, which is independent of the weight lifted.   The power was calculated as $P = Wh/t$, where h is a fixed height of one meter (1 m), t is the time in seconds to   lift a distance h, and W is the weight lifted (Dementhon, 1).

Dementhon concluded that for each of his wave rotors, "the dimensions that yielded maximum absorption width per unit volume are a pitch 20% longer than the wave length and a radius 8% larger than the wave amplitude for this given wave slope" (Dementhon, 1982).

Dementhon's findings also showed that "elongated hulls combining helical volumes can rotate smoothly in regular waves of wave lengths between 0.5 and 1.8 times the helical pitch, and in waves of amplitudes down to a quarter of the hull radius, extracting significant amounts of power" (Dementhon, 1982).

2.7 Generation of random sea states

Wave energy converters, like many offshore structures, have uncontrollable loads exerted on them. These forces are mainly from random variation in natural occurrences, such as wind velocity or wind direction. Changes in the natural atmosphere over an ocean or another body of water result in random changes in wave height and wave period over a given period of time (Portilla, 2009). In order to characterize ocean wave behavior, sea states are used to describe the waves during a specific time period. A sea state can be defined as a wave situation that is approximately consistent during a given interval. (Portilla, 2009).

Sea states are mainly characterized by a significant wave height for that state. The significant wave height, Hs, is the average of the upper third of the size-ordered sample of all wave heights for the time interval. (Portilla, 2009). The characterization of a sea state by significant wave height shows what the expected highest wave heights should be, while accounting for outliers which may have been caused by extreme wave events. The characteristic zero crossing period is another parameter which defines a sea state. This parameter, Tz, generalizes the period of the sea state to be that of a pure sinusoid. In reality, the surface of sea can be closely modeled with a composition of superposed sinusoids with varying heights and periods. (Portilla, 2009). The zero level of a sea state refers to the undisturbed level of the water. At any position on a wave, the surface of the water has moved to a distance above

42

or below the zero level.   The characteristic zero crossing period was determined from the average time intervals between the wave's rising crossing of the zero level.

Because the natural occurrences can cause great variation in the wave height and other properties, this often results in some type of extreme wave event.   The most common characterization of extreme wave actions is rogue waves.   A wave is considered a rogue wave when the height is greater than 2.2 times the significant wave height.   (Islas, 2005)   Extreme wave events, including rogue waves, are thought to be caused by three possible ocean situations. The first is the linear interaction of waves with currents, also known as the geometrical optics theory.   This encompasses the natural phenomenon that leads to unpredictable changes in wave behavior.   The second possible cause is the simple linear superposition of Fourier phases in ocean waves.   The third possible cause is based on the Benjamin Feir instability phenomenon, which states that a monochromatic wave train can be unstable because of small side-band perturbations.   (Onorato, 2002).

In addition to natural occurrences, ocean surface currents, which may be caused by natural occurrences, also have a significant impact on wave energy converters and other maritime industries.   Wind stress and momentum transfer link the atmosphere to the ocean surface currents.   The currents are also tied into the deep ocean through eddy viscosity and additional momentum transfer. (Mao, 2008).   Both of these connections can be caused by natural occurrences or man-made phenomena.   As previously stated, the wind generates the waves by transferring momentum to the ocean through wind shear stress and pressure.   (Mao, 2008).

In researching sea states, there are many things to take into consideration when modeling random wave generation.   It is also important to research and analyze the real life sea states and

possible mooring scenarios when modeling sea states. Coasts facing an ocean have shown to be the naturally most attractive location for wave energy conversion. (Engstrom, 2009). This is largely due to the fact that these areas, on average, exhibit waves with a period greater than five seconds. Mao's study (2008) showed that fetch, or a length of water over which a given wind has blown, is another important factor for determining sea states. This research showed that the current response was different under the influence of two typical fetch conditions. Overall, Mao concluded that fetch plays a significant role in the surface current's response to wind. Another main conclusion of this research was that fetch length and wind speed are two of the most important contributors to wave size (Mao, 2008). Portilla (2002) suggested that severe weather situations, mainly high wind velocities resulting in large waves, needed to be considered when modeling random wave generation (Portilla, 2002).

When simulating random wave generation, one of the more common methods is to model a sea state by employing wave spectral properties. An ocean wave spectrum describes the distribution of total wave variance over frequency and direction (Portilla, 2002). In reality, numerous individual wave systems exist in the ocean, each originating from a different meteorological event. These individual systems overlap to form the random waves commonly seen in an ocean environment (Portilla, 2002). As stated earlier, wind is one of the most influential factors in determining wave size and distribution parameters. Random waves, caused by variation in wind sea and swell, can be modeled by partitioning an entire wave spectra into the individual wave systems. In 1992, Gerling presented the first conceptual partitioning algorithm which showed how wave spectra could be modeled through individual wave systems. Partitioning models are based on the idea that, when the total spectrum is partitioned, one part of the energy goes into the underlying random sea and another part goes into the focused transient

44

wave of the individual wave system (Portilla, 2002).

2.8   Environmental impact of wave energy

In 2005, the Spanish Ministry of Science and Innovation launched a project to determine the minimum content that any environmental impact assessment should cover for wave energy systems.   The project analyzed a variety of wave energy converters including near shore and offshore devices using an exhaustive compilation of secondary data (Bald, 2010).

It was determined that surveillance programs for wave energy systems should focus on monitoring the following components (Bald, 2010):

- Submarine cable and moorings
- Benthic communities or life found in the lowest ocean level
- Ichthyofauna or fish populations within a region
- Underwater noise
- Marine mammals
- Fishing activities
- Underwater archaeological resources
- Visual inspections
- Electromagnetic fields

In the physical environment, the study concluded that wave energy systems significantly impact swells and sediment quality, where as in the biotic environment, benthic communities, ichthyofauna, marine mammals, and marine birds are appreciably affected (Bald, 2010). **Error! Reference source not found.** below outlines the primary actions resulting in the aforementioned environmental impacts as they relate to the installation, operation and maintenance, and dismantling of wave energy systems (Bald, 2010).

Table 1: Primary actions causing environmental impacts

Installation	• Transport of material and equipment to and from the selected site • Installation of equipment/structures: WECs, moorings and submarine cables (associated noise, marine bottom and landscape alteration) and structures along the coastline • Residues storage (if required) • Small hydrocarbon leaks • Accident risk (failure of devices, crashing, etc)
Operation and maintenance	• Presence of structures • Operation of underwater cables (electromagnetic field) • Reduction of marine energy • Noise • Use of anti-fouling paints • Hydraulic/other liquid pollutants leaking • Presence of maintenance equipment/structures (associated noise, marine bottom and landscape alterations) • Accident risk (failure of devices, crashing, etc.)
Dismantling	• Transport of material and equipment to and from the selected site • Presence of dismantled equipment (associated noise, marine bottom and landscape alterations) • Final destination of dismantled structures • Small hydrocarbon leak. • Accident risk (failure of devices, crashing, etc.)

Installing WECs in areas that minimize the environmental impact is an important issue to consider when selecting a site for implementation.   There are concerns about the potential environmental effects on marine animals including fish, birds, and mammals as well as on hydrography, coastal processes, and water quality.   This disturbance for marine life would be particularly prevalent during the construction phase where the impacts are expected to be only temporary (Sorenson, 2002).   The key would be to reduce the effects present during operation and maintenance to ensure an environmentally safe WEC project.

For fish, WEC installations are likely to act as artificial reefs and provide hard substrate for algae and invertebrates (Nelson, 2008).   Mid-water and floating surface components of

wave energy converters could become the center for fish aggregations depending on the specific location of the device and on fish response. For marine birds, concerns include seabird collision for nocturnal species due to navigation lights, disturbance to local breeding colonies, and changes in distribution or availability of forage fishes (Sorenson, 2002). For marine mammals, issues such as collision, interference with migratory behavior, and the disruption of sensory mechanisms are potential impacts (Sorenson, 2002). The effect of electromagnetic fields on marine life particularly fish have been found to be negligible assuming that electrical transmission cables have been sufficiently shielded (Nelson, 2008). An assessment of the local mammal population and whether the specific site is located in the vicinity of colonies would be important factors in order for a project to receive approval (Sorenson, 2002).

Wave energy converters may have a variety of effects on hydrography and coastal processes including the wave climate, patterns of vertical mixing, tidal propagation, and residual drift currents with the most pronounced effect most likely being the wave regime (Sorenson, 2002). A decrease in wave energy could influence the nature of the shore and the communities of plants and animals they support. Impacts on sea currents and hydrography may occur for large wave energy projects, where a significant portion of the wave energy is captured or reflected depending on the area covered and distance to shore (Sorenson, 2002). These impacts may be positive or negative depending on the project layout and location. An example of a positive impact would be reduced coastal erosion and a negative impact would be permanent changes in sediment structure which could change the composition of the shoreline (Sorenson, 2002). Detailed modeling would be necessary prior to implementation and be depend on size the of the project, proximity to shoreline, shallowness of water, and general sensitivity of the local sea currents.

In addition, it would be essential to sustain water quality, especially following severe storms or emergencies where the device might be at a high risk for damage. This would necessitate some type of Hazard and Contingency Prevention Plan to prevent possible contamination from liquids leaking into the ocean (Bald, 2010). Regulations would also have to be set in place for the use of oils, which should be biodegradable, as well as anti-fouling paints, which should follow the regulations of the International Convention on the Control of Harmful Anti-fouling Systems on Ships. To study any of the environmental impacts of a project, baseline data collection before any installation would be critical for evaluating post-installation effects.

2.9   Societal impact of wave energy

A group of researchers from the European Thematic Network on Wave Energy compiled a comprehensive summary of the various impacts of wave energy technologies on the public. The most important factor in ensuring public acceptance of new wave energy technologies is for the companies implementing the technology to keep the public informed and involved. Public awareness can be spread through websites, newsletters, television, and politicians (Sorenson, 2002).

Wave energy is beneficial to the public as it provides jobs to the local population, as employees are needed to construct, install, and maintain the devices. Not all benefit from the installation of WECs; fishermen are likely to disapprove of the presence of WECs. In circumstances where the WECs are even beneficial to the local fish population, the fishermen still do not support WECs installation. However, situations in the past have been resolved with financial compensation for the fishermen. There is also a concern that WECs would interfere

with marine transportation and recreational boating (Nelson, 2008).   This is less of a problem in shallow areas, as the WECs can be made more visible with lighting structures.   The boating issue is not fully resolved and is also unique to each WEC and location (Sorenson, 2002).   In addition, the construction, deployment, operations, and maintenance of WECs could offer job opportunities and income to local communities (Nelson, 2008).

2.10 Materials and construction

Ozcivici and Singh (2005) studied the fabrication process for closed-cell, silicon carbide-based foams.   The study looks at the properties of fluid-filled spheres, cenospheres, and how they affect the properties of polymer foams.   It serves as a great reference for understanding how closed-cell foams work and how they differ from open-cell foams, as shown in Figure 25**Error! Reference source not found.**.   The study concludes that closed-cell foams are more suitable for resisting the ingress of air and corrosive fluids.   Closed-cell foams also have higher specific strength and rigidity.
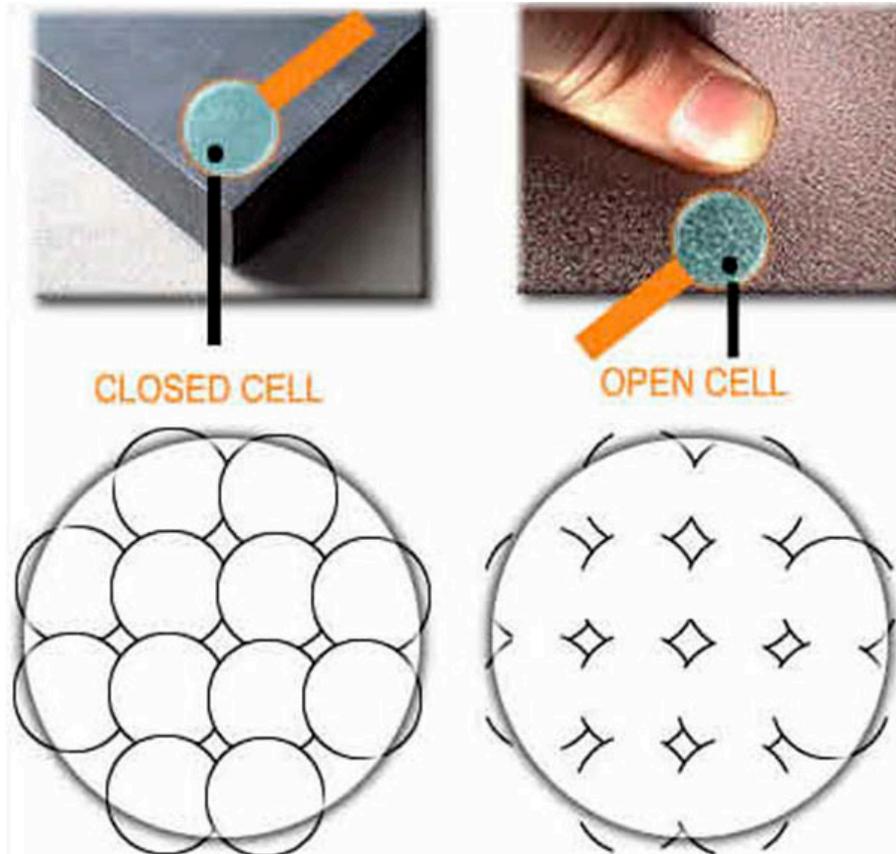
Figure 25: Closed Cell foam vs. Open Cell foam (MDI, 2011)

Ionita and Weitsman (2007) modeled the ingress of fluids into closed-cell polyvinyl-chloride (PVC) foam.   Their study quantitatively expresses the absorption of fluid by the PVC foam as a function of time exposed to sea water.   The study concluded that long term exposure to sea water can decrease the foam's integrity.   The damage that the foam undergoes is isolated to the exterior of the foam which is in direct contact with the water.

Chapter 3: Methodology

Upon completion of the literature review, the team chose a design based on the needs identified in the review and parameters specific to the current study.   A functional prototype was then constructed based on the design and constraints.   Upon completion of the prototype, the team conducted a series of tests in an effort to gain an understanding of the governing parameters of the system.

3.1 Design selection

The methods utilized during development and design can be categorized into several over-arching phases that needed to be accomplished sequentially in order to deliver the optimal design:

- Identify the constraints imposed by the testing environment, and quantify these into concrete specifications
- Create a point-by-point comparison of possible design choices
- Select design
- Identify alterations with justifications for each.
- Finalize design and describe in detail.

Simplified assumptions on linear wave theory, beam theory, and hydrostatics were used to develop design concepts.

3.1.1: Design assumptions

The team applied a simplified assumption of wave motion, device action, and load distributions to each system under consideration.   These assumptions followed first-order

theories.   Although higher-order theories were available, the application of these to specific

scenarios was beyond the scope of the research and the first-order theories were sufficient.   As

such, the design candidates were those which could be modeled by simple physical phenomena

(i.e. single degree of freedom systems).   This specification allowed the device to be properly

analyzed with the tools, equipment, and experience at hand.

The first assumption, linear wave theory, restricts the motion of waves to the one-

dimensional periodic.   This theory is a form of potential flow and assumes that the water flow

shall be laminar, inviscid, incompressible, and irrotational.   Applying these assumptions to

water waves, the mean wave height shall remain much less than the wavelength of the wave

throughout the spectrum of frequencies to be investigated.   More specifically, the global

Reynolds number (Re) in the direction of wave motion of the device must be very large in order

to negate effects of viscosity.   The constraint this puts on the design choice is as follows: the

wave energy converter (WEC) shall operate within a specified range of wave conditions where

the wave height is much less than the wavelength.

The team assumed hydrostatic equilibrium to determine the buoyancy of the design.

This implied that a design utilizing a simple structure should be chosen in order to formulate

accurate models of volume and density as a function of the point location on the device.   Also,

the specific action of the forces produced by a passing wave on the design (i.e. pressure) must be

simple enough to obtain closed-form solutions.   In terms of the device itself, the WEC shall

remain neutrally buoyant and properly oriented upon reaching the steady state conditions within

the specific test scenario.

The final consideration aims at the design itself, specifically how it will support itself

structurally outside of the testing environment.   Drawing on the previous requirement that the

design must be able to function within the bounds of linear wave theory, the length of the device (in the direction of the wave motion) must be much greater than its other two dimensions.   With this assumption, static beam theory was applied to analyze the structural properties of the specific design.   The basic purpose of this analysis was investigated for testing purposes only: the device would have to be removed periodically from the testing environment to allow other, unassociated testing to be performed.   To summarize, the WEC shall, upon removal from the testing environment, be able to support its own weight and the weight of all affixed structures.

In summary of this phase, there are three design considerations that must each individually be met in order for the design to be valid for investigation.   The aforementioned theories used to develop these requirements must remain true within the operating conditions imposed on the device.

3.1.2: Selection process

In an effort to narrow down the design selection process, designs representing each category of devices were compared and contrasted based on the specifications previously defined.   Following this, a specific design was chosen that best suited the needs of the research.

The attenuating device is designed to operate in deep water where the wavelengths of passing waves are much longer than the wave heights.   When the ratio of the wave amplitude to the wave length is small, linear wave theory can be used to effectively model the motion of passing waves.   Given a specific design, the weight and balance of a specific device can be determined and made to match the buoyancy force.   However, the distribution of stresses would be fairly difficult to obtain due to the presence of one or more hinges.   This breaks the assumption of beam theory, escaping the theoretical knowledge currently available for the

research.

Limpet, the example given previously as a functioning oscillating water column device, is specifically designed to operate on a shoreline. Waves in this region tend to have a larger wave height to wavelength ratio than is necessary for linear wave theory to hold true. A promising feature of this type of design is the lack of a need for buoyancy. This exempts the category from one of the requirements. However, due to this design's inability to be modeled as a long, slender beam, analysis of the structural integrity may prove difficult.

The Power Buoy was given as an example representing the point absorber category. As this design is essentially a buoy coupled to a power generation system, placement of the device can range from close to the shoreline to deep water. The flexibility of location means that the predominant wave conditions of a region can be required to hold valid when analyzed using linear wave theory. Assuming that the design will basically involve retrofitting a buoy, there is a large amount of literature available related to buoyancy analysis from which to draw. This also holds for the structural analysis of the system.

The Wave Dragon is a common example of a design for an overtopping WEC. As described for this specific type of design, a passing wave deposits some of its volume into a reservoir. This could cause some issues with the assumption of linear wave theory in that the interaction relies heavily on the momentum of the passing fluid, a highly non-linear effect. The transfer of fluid from the passing wave to the reservoir also makes it difficult to predict the weight of the device. This will not only vary with time, but also vary with wave height, requiring mass transfer relationships. The stresses in the structure may also prove difficult to determine due to the platform design of the reservoir.

The final design category, the R-WEC, is exemplified by a design developed by Daniel

DeMenthon.   In this design, a passing wave effectively rotates the device on the axis of wave motion.   This device is designed to be long and slender, with a point designed for interaction with linear-like waves.   The slow and typically smooth motion of rotation experienced by the device would allow hydrostatics to model the time-averaged buoyancy of the device.   Lastly, drawing from the parameter of being long and slender, the stresses in this particular design are best suited to be modeled as a beam.

Upon review of the aforementioned categories, a ranking system was developed to select the optimal design for the current research.   In this system, a lower number is superior to a higher one on a scale from one to five.   The optimal category will have the lowest summation of all of the sub-scores, as shown in Table 2.

Table 2: Ranking system used to determine the optimal WEC design

Category	Linear waves	Hydrostatics	Beam theory	Literature available	System complexity	Total
Attenuating	3	4	2	4	5	**18**
Water column	4	1	5	1	3	**14**
Point absorber	1	2	3	5	1	**12**
Overtopping	5	5	4	3	4	**21**
R-WEC	2	3	1	2	2	**10**

The ranking system shows that the optimal category for the present research is the rotary-type WEC.   For the remainder of this thesis, the initial design chosen will be assumed to be that put forth by DeMenthon.   The modifications outlined below detail the changes made prior to construction and testing.

3.1.3: Modifications to the existing design

After selecting the rotary WEC design, modifications were necessary in order to

determine the best performance characteristics of the device.   Various aspects of the device, including length, radius, pitch, material, and construction method among others, were analyzed in detail to determine the most feasible changes.

Although the rotary WEC is ideal for the test scenarios associated with this investigation, the actual construction of the device is not ideal.   Currently, DeMenthon's design is comprised of a series of flexible strips layered in the radial direction and wrapped around a central support beam to form the helical shape.   When investigations began into the materials required to accomplish this, it was agreed upon that a new method of constructing the helical shape was necessary.   The final construction method would be based around affixing a series of disks along the length of the support.   The proper portion of each individual disk would be removed to give the required shape.

The team designed the pitch of the rotor to be 4 ft long as opposed to 2.46 m used in DeMenthon's design.   The length was determined to be 6 ft and the radius, 4 inches.   The length to pitch ratio of 1.5 was the same as DeMenthon's rotor design.   The pitches and lengths were adjusted to accommodate our laboratory setting.

3.1.4: Outcome/deliverable (R-WEC)

After completing the selection process and modifying the original design to fit the current research, the prototype was constructed. The finished prototype consisted of a smooth helix shape and was able to float autonomously at mean water level. The rotor was moored in the wave tank using 80/20 aluminum frame structures.   Two mooring systems were constructed and tested.   The first system kept the two ends of the rotor at fixed vertical and horizontal positions while allowing the device to rotate.   The second system allowed for more mobility of the device

in order to better simulate real-world conditions.   All testing was carried out with this single

rotor in the laboratory's wave tank.

3.2   Stress analysis

Prior to construction, two characteristics of the R-WEC needed to be determined:

buoyancy and strength.   For this analysis, the team used two tools: Archimedes' principle

of buoyant objects and the Euler-Bernoulli beam equation.   The results of the analysis were

the primary parameters used in the design and construction of a functional prototype.

First and foremost, the device needed to float.   This required balancing the gravitational

and buoyancy forces while leaving some margin for error and additional equipment.   The mass

of the device, comprised of the helix and rod, was determined by volume of both and multiplying

by their respective densities.   Buoyancy force, actually a mass (acceleration of gravity cancels

out), was determined by assuming that the amount of water displaced was equivalent to half of

the total volume and multiplying this volume by the density of water.   The difference between

the device mass and the buoyancy 'mass' gave an effective mass while half-submerged in water.

The goal was to get this value to be slightly positive (i.e. more buoyant than massive).

Equation 1 shows the method for determining weight and buoyancy.

$$V_{rod} = \pi(r^2_{rod,outer} - r^2_{rod,inner})L_{rod}$$

$$V_{helix} = \frac{\pi}{2}(R^2_{helix} - r^2_{rod,outer})L_{helix,pitch}$$

$$F_{gravity} = \rho_{rod}gV_{rod} + \rho_{helix}gV_{helix}$$

$$F_{buoyancy} = \rho_{water}g\frac{V_{rod} + V_{helix}}{2}$$

$$F_{result=}F_{buoyancy} - F_{buoyancy} > 0$$

Equation 1: Calculation of weight and buoyancy

57

For the purpose of construction, which was done out of water, the device needed to be able to withstand any gravitational load applied to it. This involved performing a simple stress analysis utilizing Macaulay's method for beam deflection, as shown in Equation 2. In Macaulay's method, forces are applied as distributions across a certain portion of the beam. Under this theory, the team applied two separate gravitational loads to a simply supported beam: one for the foam helix and another for the metal rod. The variation in the load from the helix was assumed to vary proportionally with angular size. The weight of the rod was modeled as uniform force along the length of the device. Once forces were determined, the team integrated along the length of the device twice to determine the shear and, finally, the moment applied. It was assumed that the rod was the only load carrying component of the device and as such only determined the moment of inertia in the axial direction of the rod. The primary purpose of the stress analysis was to determine if the device would support its own weight while out of the tank and to determine the factor of safety, a major factor when considering storage and installation.

$$q(z) = -\frac{W_{rod}}{L_{rod}}\langle z-0\rangle^0 - \frac{9}{2}\frac{W_{helix}}{L^2_{helix}}\left(\langle z-0\rangle^1 - \left\langle z-\frac{L_{helix}}{3}\right\rangle^1 - \left\langle z-2\frac{L_{helix}}{3}\right\rangle^1\right)$$

$$V(z) = \int_{z=0}^{z=L} q(z)dz$$

$$M(z) = \int_{z=0}^{z=L} V(z)dz$$

$$I_{rod,z} = \frac{\pi}{4}(r^4_{rod,outer} - r^4_{rod,inner})$$

$$\sigma(z) = \frac{M(z)r_{rod,outer}}{I_{rod,z}}$$

$$SF(z) = \frac{S_{yield}}{\sigma(z)}$$

$$\langle z-A\rangle \equiv \begin{cases} z-A & ,z > A \\ 0 & ,z \leq A \end{cases}$$

Equation 2: Macaulay's method of stress analysis and factor of safety

The results of the buoyancy and stress analyses showed that the design point for the material strength would be the middle of the rod, although for reasonable materials the factor of safety in this region was much greater than unity. As for buoyancy, it allowed the team to select the dimensions and material of the device. These same analyses were also used in the scaling-up analysis described in section 5.4. More details on these analyses are shown in Appendix B: and Appendix C:.

3.3 Rotor construction

Having decided on a specific WEC design to modify and test, a construction procedure was then developed to create a prototype using the available tools and facilities. The majority of the construction took place in the Mechanical Engineering Machine Shop located on the University of Maryland campus in the Glenn L. Martin Engineering Building. In this shop, the

team had access to a variety of power tools and machinery such as lathes, mills, drill presses, table saws, band saws, and grinders.

3.3.1: Construction method selection

Once the design of the WEC was determined, the next step was to decide on how to construct the rotor.   The design called for a foam spiral wrapped around an aluminum rod with each end tapering to a point.   The surrounding spiral can be divided into three sections along the length of the rod.   The middle section of the rotor has a constant cross-sectional area, while the other two sections at the ends have cross-sections that taper to a point.   In constructing the rotor, the team considered a radial and axial layering method, as shown in Figure 26.   The radial layering method used by Dr. DeMenthon, consists of helical strips of different widths that were layered on top of each other "in order to increase the area of the side surfaces resulting from the building of the edges" (1982) producing the rotor illustrated below.   The radius of the rotor using this method can easily be adjusted by layering additional layers of foam.
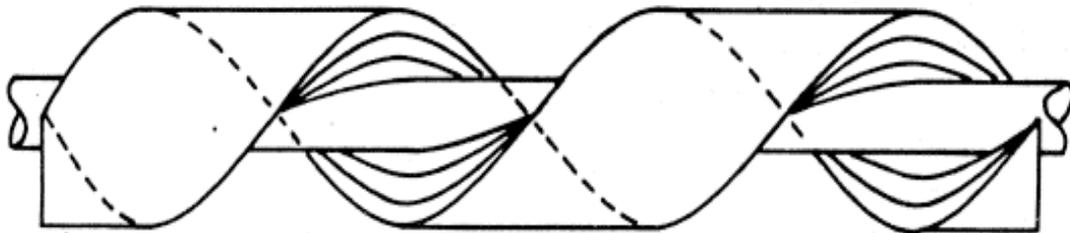
Figure 26: Rotor Construction using Radial Layering

In the axial layering method, or the wedge method, consists of placing foam wedges adjacent to one another.   The shape can easily be tailored and the foam does not necessarily have to be flexible.   Figure 27 shows the difference between the axial and radial layering

methods.   To achieve the desired helical shape using axial layering the team used a series of

foam wedges placed side by side.   First, cylinders were cut from a slab of high density, non-

porous foam using a hole saw.   The cylinders were then cut into wedges of specified angles.

The middle third of the rotor consists of 12 wedges, each measuring 195 degrees, whereas the

two remaining sections consist of 12 wedges ranging from 30 to 195 degrees in 15 degree

intervals.   The range of angles used in these two terminal sections resulted in the tapering of the

spiral both ends of the rotor.
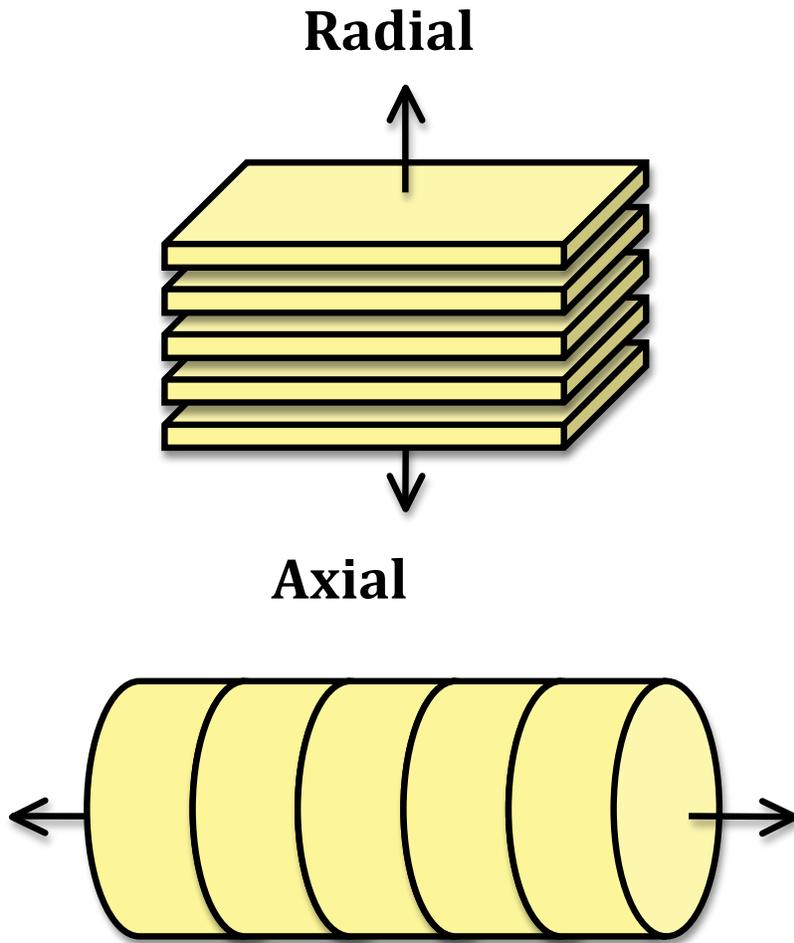
Figure 27: Radial and axial layering methods for the rotor construction

3.3.2: Material selection

A high density, non-porous, syntactic foam was selected due to its water resistance and buoyancy promoting properties. The foam could be easily manipulated and was found to be ideal in the axial layering method. The central aluminum rod was selected for its rust resistant and light weight which would be essential to the design of the rotor in water which requires the prototype to float at mean water level. The specific dimensions of the prototype as well as the materials were determined based on the dimensions of the wave tank and our laboratory setting.

A two-part epoxy mix was used to bind the foam to the aluminum rod. To prepare the aluminum rod for the epoxy work, the rod was cleaned using a fine grit sandpaper to remove the superficial layer of aluminum oxides that occurs naturally. The epoxy was then mixed in a 2:1 ratio of resin to hardener. Epoxy was applied to both the aluminum rod and to the contact surface of the foam wedge. The wedges were held in place using rubber bands to apply force to the binding surfaces. The epoxy was allowed to set for 48 hours before removing the rubber bands. The wedges then needed to be sanded down to create a smooth transition between sections. The sanding was done by hand, first with medium grit sandpaper, and then with fine grit sandpaper. After the foam was completely sanded down, the entire foam spiral was coated with two layers of epoxy with a thorough sanding job in between coats. The final layer of epoxy over the rotor marks the completion of the prototype construction.

The construction procedure and overall workmanship were greatly limited by the available tools in the Machine Shop. The drilling and cutting tools were not as precise as the team would have liked and resulted in imperfections in the final prototype; however, these

imperfections were mostly cosmetic and did not affect the performance of the device. Additionally, the epoxy and sanding applied to the exterior of the rotor helped fill and mend most imperfections.

3.3.3: Foam preparation

In order to prepare the foam, calculations were necessary to establish the angle of each foam wedge and the axial position along the length of the rotor.   To determine the angles for the foam wedges, Equation 3, Equation 4, and Equation 5were used:

$$\theta_{LE}(z[ft]) = 180° \begin{cases} \dfrac{z}{4\,ft} & ,0\,ft \leq z < 4\,ft \\ \dfrac{z+2\,ft}{2\,ft} & ,4\,ft \leq z < 6\,ft \end{cases}$$

Equation 3: Leading edge angular displacement

$$\theta_{TE}(z[ft]) = 180° \begin{cases} \dfrac{z}{2\,ft} & ,0\,ft \leq z < 2\,ft \\ \dfrac{z-2\,ft}{4\,ft} & ,2\,ft \leq z < 6\,ft \end{cases}$$

Equation 4: Trailing edge angular displacement

$$r_{LE}(z[ft]) = r_{TE}(z[ft]) = 2in$$

Equation 5: Leading edge and trailing edge radial displacement

In order to prepare the foam wedges for the rotor, 4 inch diameter circles were cut from

63

slabs of syntactic foam using a hole saw.   The angles were then drawn onto each circular piece

using a compass.   Then, a drill bit was used to cut 1 inch diameter circles from the center of the

circular foam pieces.   See Figure 28 for a diagram of how the foam discs were cut.   Using a

hand saw, the pieces were then cut along the previously drawn lines on the pieces creating

wedges of the proper angles, as shown in Figure 29 and Figure 30.
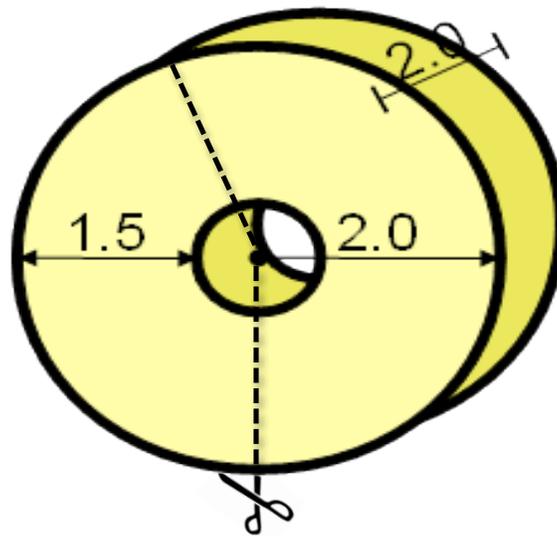
Figure 28: Schematic of a foam disc showing the dimensions and a sample cutting angle
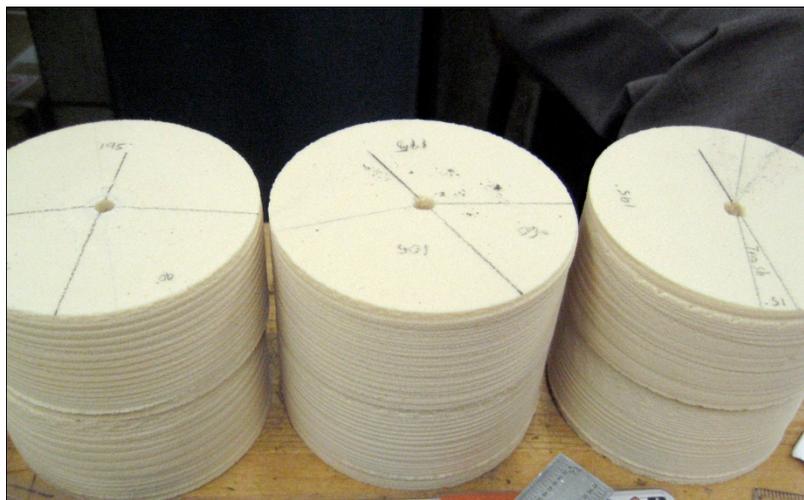
Figure 29: The 4-inch diameter foam discs marked with the proper cutting angles

Figure 30: A hand saw was used to cut the discs at the proper angles

Figure 31 below illustrates the angular displacement as a function of axial position along the rotor's length. All of the dotted lines represent the ideal positioning of each foam wedge, whereas the solid lines demonstrate the wedge positions actually achieved. The blue solid and dotted lines illustrate the trailing edge of the rotor, where as the red represent the leading edge. The solid and dotted green lines then represent the actual and ideal differences respectively among the leading and trailing edges. The area between the blue and red lines delineates the parallelogram like shape of the rotor's outline.
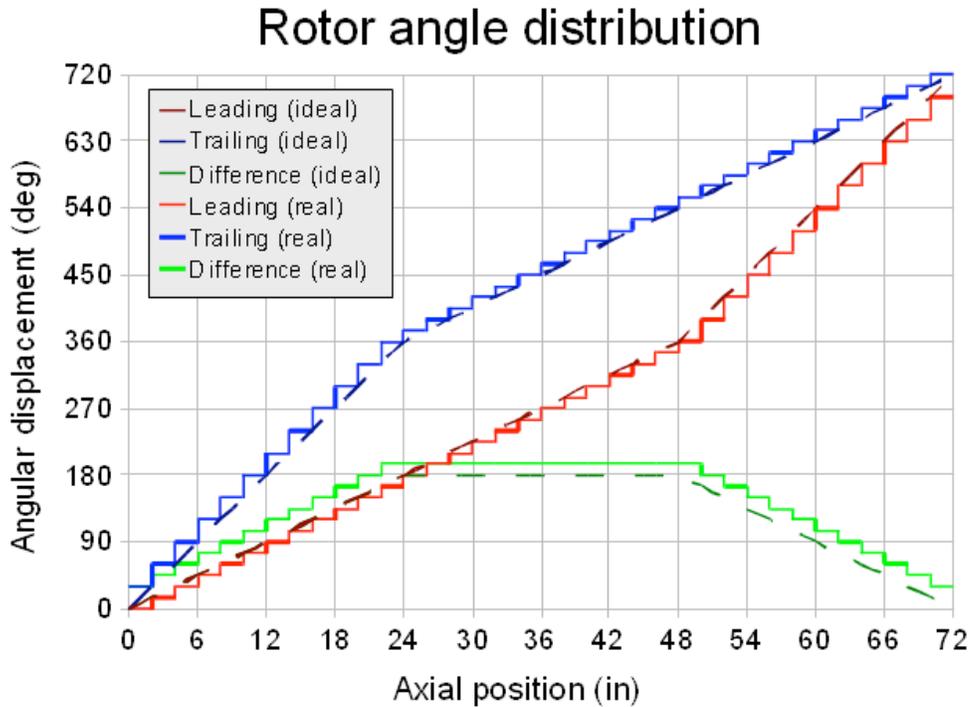
Figure 31: Rotor angle distribution

3.3.4: Putting the foam on the rod

After the foam discs were cut from syntactic foam sheets, they were sliced into wedges with different angles to be epoxied onto the rod.   First, the rod was marked with a pen showing where the wedges needed to be aligned.   The medium hardener epoxy was used to carefully glue the wedges onto the rod.   The pieces were epoxied on to the aluminum rod using rubber bands as clamps to keep the wedges on the rod, as the epoxy would take a few days to completely harden and dry.   Small wooden pieces were also placed on the opposite side of the rod from the foam to keep the rubber bands stretched out.

To avoid direct contact between the rubber bands and the foam and also to prevent the epoxy from sticking to the wooden blocks, plastic grocery bags were applied around the foam

66

and between the rod and the wooden pieces.   After a few days, the epoxy was completely dry,

and the rubber bands, along with the wooden blocks and the grocery bags were taken off.

However, pieces of the bags were glued on to the aluminum rod, so files were used to rub the

remaining pieces off.   Finally, the rotor was ready to be sanded down.

3.3.5: Sanding

The sanding process began after the epoxy was completely dry.   The foam pieces were

epoxied on a few days prior to sanding to ensure that the foams would not move while in the

process.   Sanding was necessary to shape the rotor into a hydrodynamic form.   First,

sandpaper was purchased, and cut into small square pieces to allow the sanding process to be

done manually.   Since each foam disc was cut at a specific angle, there was a gap between each

piece which had to be sanded off to make a smooth edge for the rotor.   First, a coarse sheet of

sandpaper was used to roughly shave off the edges; then a more defined sheet was used to

carefully sand the remaining pieces for a smooth edge.   After the sanding process, the rotor was

ready to be epoxied.
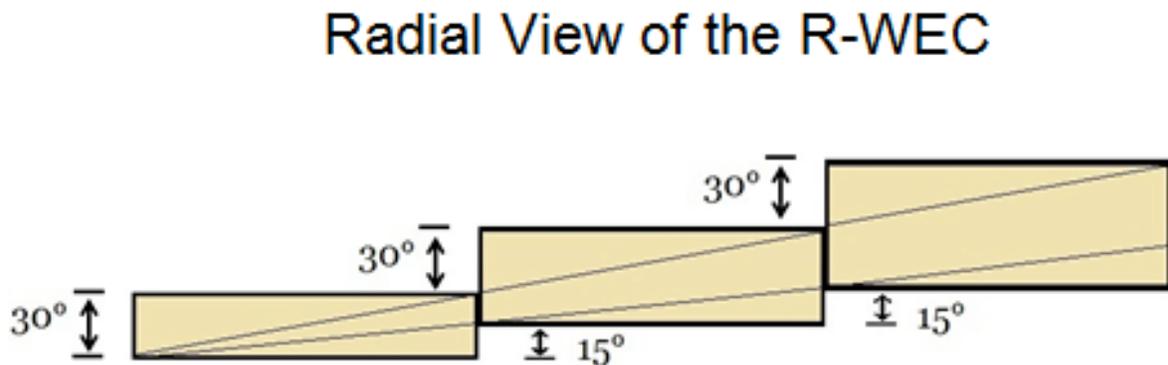
Figure 32: Radial view of sanding lines

3.3.6: Final epoxy/sealing

Directly after sanding, the rotor was set aside for final epoxy to seal the exterior surface of the foam. Although the syntactic foam used for the rotor was water-proof, epoxy was put on the exterior surface to prevent direct contact with the water. First, the medium hardener was evenly applied on the surface of the rotor as the primary layer. After the application, the rotor was set aside for a few days to allow the epoxy to dry completely. Then, again, the epoxy was applied onto the rotor which was already covered in a thin layer of the medium hardener. The second layer focused more on areas where the primary layer was thinner than the other places. Again, the rotor was set to dry for a few days to make sure the epoxy would not come off while in the process of drying. As the last step, the medium hardener was mixed in with foam dust that was collected during the sanding process, which allowed the epoxy to be more dense and close to the properties of the foam rotor itself. This mixture was used to fill in gaps that could not be covered with the first two layers of epoxy. The mixture was carefully poured into the minor gaps between two foam wedges. After epoxying the gaps, the rotor was set aside to be dried and to be tested in the wave tank.

3.4 Mooring structures

To test the R-WEC, it was necessary to develop a way of measuring the power generation of the device. In the absence of an electrical generator, a more simple and robust approach to power generation was developed. To measure the power output of the rotor, the team chose to quantify how quickly the rotor could wind up a weight of known mass a preset distance. Using the time measurements, it was possible to estimate the power generated by the device. A system of pulleys was employed to wind the rope that supported the weight.

3.4.1: Dr. Daniel DeMenthon's design

DeMenthon's R-WEC was moored so that the device would be able to rotate at mean water level.   The mooring system that DeMenthon used to hold the R-WEC in the wave tank consisted of a cable and pulley system, as shown in Figure 33.   The wave tank where DeMenthon's tests were carried out had the dimensions 20m x 1.5m, 1.5m, with a water depth of 1.15m.   Extending from the rotor was a smaller diameter shaft, around which cables were wound.   These cables then extended out perpendicular from the length of the rotor, and wound around pulleys near either side of the wave tank.   From each pulley, the two cables rose up to wrap around another pulley above one side of the wave tank.   Extending down from this pulley was a weight.   The power was measured based on the rotor's ability to lift a certain weight. The maximum power extracted from the rotor was calculated based on the maximum weight that the rotor could lift one meter, and how long it took the rotor to lift the weight this one meter (DeMenthon, 1982).
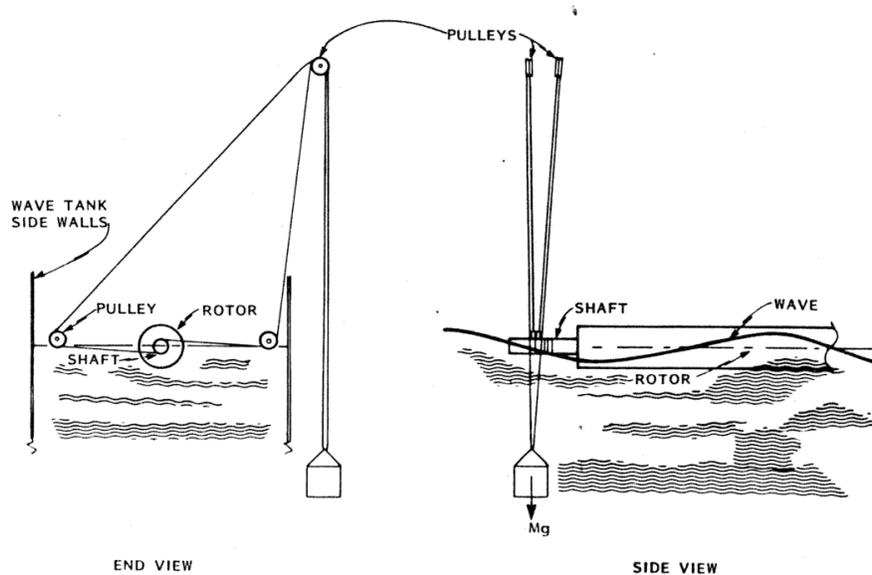
Figure 33: DeMenthon's mooring structure for the laboratory; end and side views (DeMenthon, 1982)

DeMenthon suggested a more realistic mooring system for use in open waters. In this system, two rotors float side by side as they turn in opposing directions, as shown in Figure 34. The two rotors are attached to two gear boxes on the ends of either rotor, and the two cables attach both gearboxes to a single generator. The rotors are moored with cables that extend down to anchors on the ocean floor. A buoy at the front of the rotor conveys incoming wave information to the generator. Our second mooring system mimicked characteristics of this mooring system, in that the rotor was allowed to rotate more freely (DeMenthon, 1982).
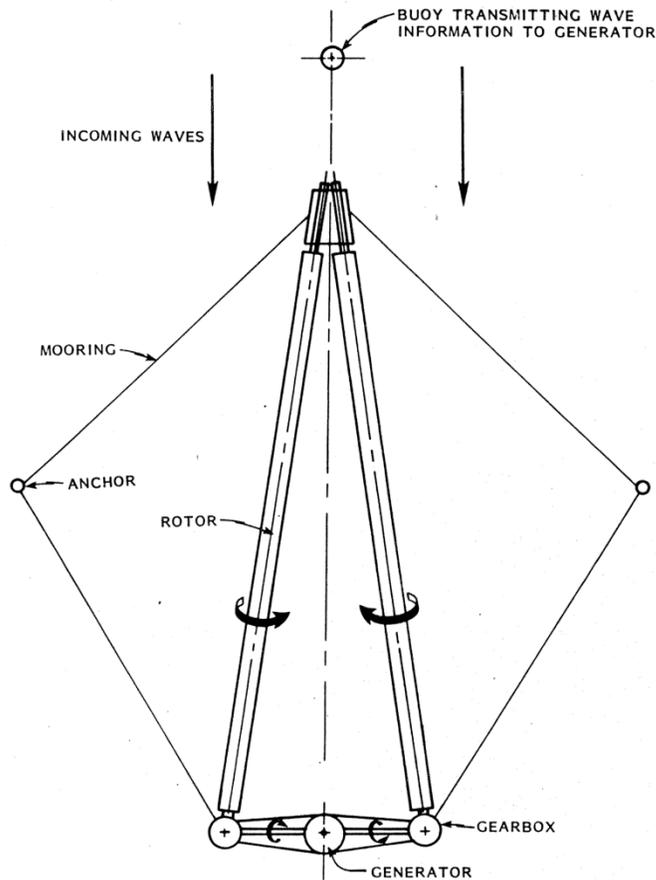
Figure 34: DeMenthon's mooring structure for open water (DeMenthon, 1982)

3.4.2: First structure - fixed end mooring

Two different support structures were used in the testing of the device. Both structures were built using 80/20® aluminum framing. The first structure was fixed at both ends of the rotor with respect to the wave tank. This structure was built with two large crosses that traversed the width of the tank and rested on the sides. The stem of each cross extended downward resting 0.10m (4 inches) above the water's surface. From each of these crosses, a Plexiglas support extended down to the water's surface.

Each end of the rotor was attached to one of the Plexiglas supports. This design fixed the axis of the rotor at the mean water level. To attach the rotor to the Plexiglas supports, a 0.013m (0.5 inch) diameter aluminum rod was inserted into each end of the rotor. To hold this smaller rod in place, a larger aluminum hollow cylinder of 0.019m (0.75 inch) outer diameter was placed at the end of the rotor on the smaller aluminum rod.

At the front end of the rotor were two Teflon pieces placed around the 0.013m (0.5 inch) aluminum rod. A wider Teflon section was followed outward from the rotor by a thinner Teflon section, that was inserted into the Plexiglas support. This Teflon structure kept the aluminum rod from slipping out of the Plexiglas, and kept the rotor in place.

Attached to the back end of the rotor was a 0.038m (1.5 inch) inch diameter Teflon spindle around which a rope was wrapped. The rope led up and out of the wave tank through a series of low-friction pulleys. A small weight of known mass was attached at the other end of the rope. As the rotor rotated the rope was wound up thus lifting the weight vertically. The time required to lift the weight 0.304m (12 inches) was recorded and used to compute the power output of the rotor. At each wavelength tested, more weight was added until the rotor could no longer lift the weight 0.304m (12 inches).
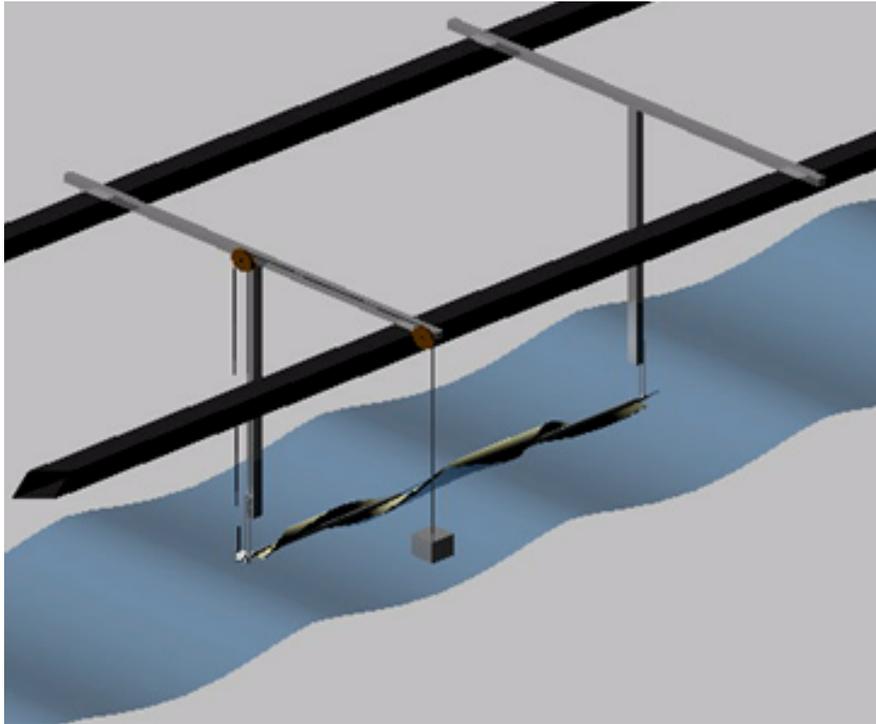
Figure 35: Graphic representing the design of the fixed end mooring structure

3.4.3: Second structure - tethered mooring

The second mooring structure that was constructed was intended to more accurately simulate a free-floating rotor in open waters. As in the first mooring structure, both ends of the rotor had a 0.013m (0.5 inch) diameter aluminum rod inserted at the end of the rotor, along with the 0.019m (0.75 inch) diameter aluminum piece around the smaller rod to keep the rod in place. One single metal cross at the front of the rotor was used as the primary structure. Attached to the vertical aluminum piece of the cross was a Plexiglas piece that descended to mean water level. A string was attached that connected the Plexiglas piece to the rotor.

Another metal structure at the back end of the rotor consisted of two vertical beams that were used to hold the pulley array that carried two ropes over and out of the tank. Under this

configuration, the two ropes were attached to two weights, one for each side of the tank. These two ropes were attached to the back end of the rotor. By having two ropes extend horizontally from the rotor to either side of the tank, the vertical force of the rope that would normally lift the rotor out of the water was eliminated.   In order to further stabilize this structure, two ropes extending from either side of the back end were hooked onto two suction cups that were attached to either side of the wave tank.   This was done to minimize the horizontal motion of the rotor as well as to keep the ropes on the pulleys so that the power output from the rotor could be measured.   During initial runs without the suction cups, the ropes carrying the weights slid off the pulleys and the weights did not lift.

Two paper cups of equal weight were attached to either rope.   An equal amount of weight was added to each cup prior to each run. The total weight lifted was calculated as the sum of the weight in each cup as well as the weight of the cups themselves.   For each wavelength tested, weights were added to the cup until the rotor could no longer lift the weights 0.304m (12 inches).
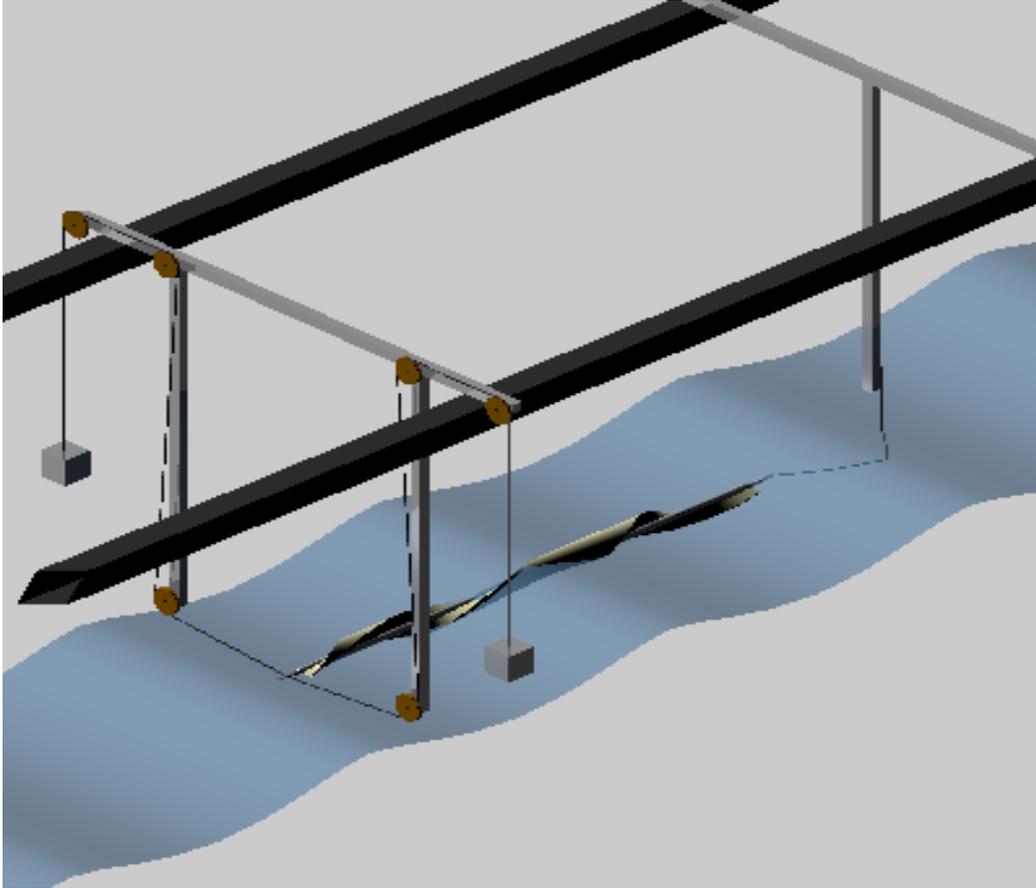
Figure 36: Graphic representing the design of the tethered mooring structure

3.5   Testing

3.5.1: Wave tank

Through the team mentor, Dr. James Duncan, access was gained to a programmable wave tank in the Hydrodynamics Laboratory.   The wave tank used for testing the RWEC prototype was 11.8m long, 4m wide, and 2.2m tall.   A side view of the tank is shown below in Figure 37.
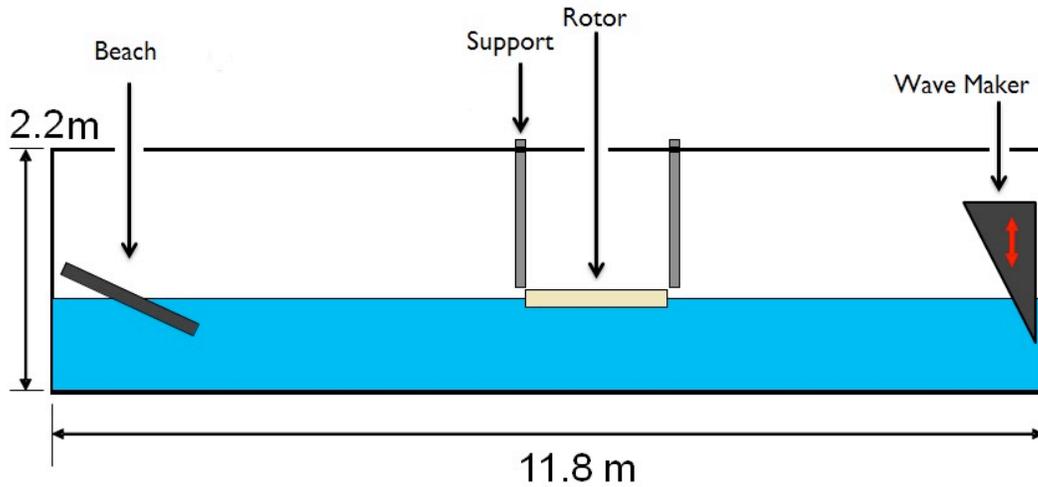
Figure 37: Schematic Cross-Section of the Hydrodynamics Laboratory Wave Tank

The tank features a wave maker system that allows for customizable wave profiles to be generated within the constraints of the wave tank.   The wave maker system consists of a motor that drives a triangular wedge vertically in and out of the water, creating the desired waves. The waves were generated on one side of the tank and on the other side of the tank there was a beach that was used to dissipate reflected waves and minimize their interference with incoming waves.   The rotor supports were fixed to the tank walls using clamps, and the rotor was placed in the middle of the tank.
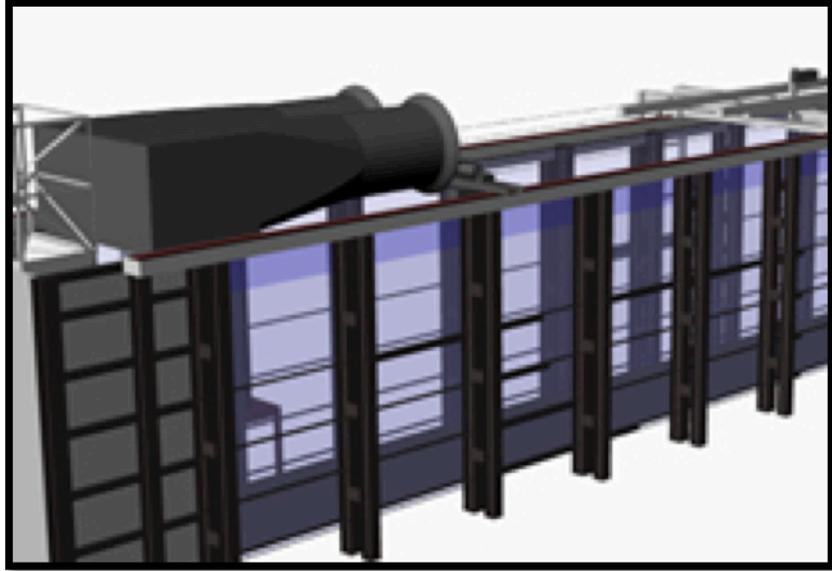
Figure 38: A CAD drawing of the hydrodynamics lab wave tank

3.5.2: Wave maker and wave profiles

The wave maker is powered by a motor that is housed outside of the tank and drives the triangular wedge up and down.   The wedge is made of plastic and spans the entire width of the tank.   The side of the wedge closest to the end of the tank is vertical and the opposite face of the wedge is declined 30° from the vertical.   The motor is designed to follow a prescribed program that defines the wave profiles that are created.   A computer control system that uses feedback from a position sensor and a tachometer is used to obtain precision over the movement of the wedge.

3.5.3: Test procedures

The objective of testing was to measure the power output of the device under different wave conditions and configurations in order to understand how the rotor behaves.   For this study, the focus was on the effect of wavelength and wave height on the power output of the RWEC.
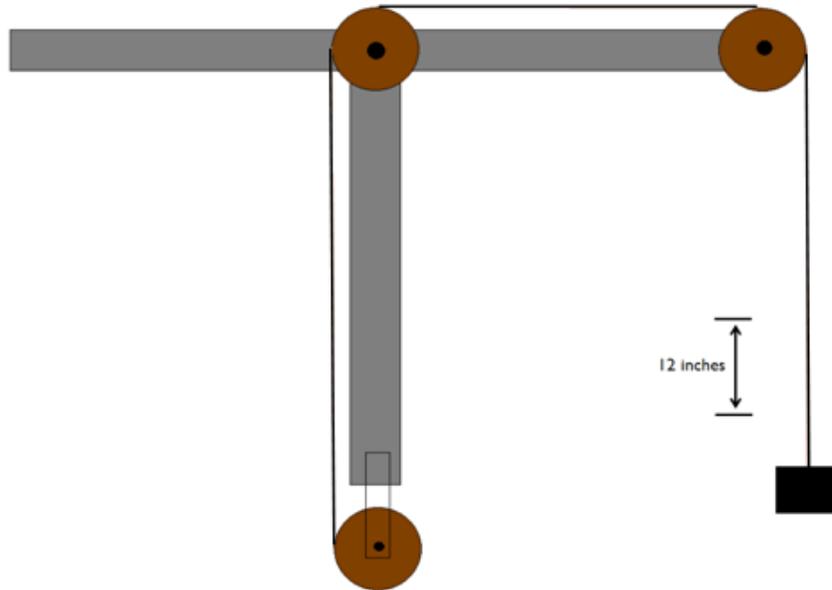
Figure 39: Schematic of the weight pulley system used to measure power capabilities

During the course of testing, three distinct experimental setups were utilized in an effort to develop an understanding the performance of the RWEC under differing conditions. The first experiments tested the RWEC in its fixed mooring configuration acted on by a single-component wave. The results of this setup were used to calibrate and verify the operation of the RWEC with the design proposed by Dr. Dementhon. Following this, the RWEC in its tethered mooring configuration was again acted on by a single frequency wave with the primary purpose of identifying deficiencies in non-rigid setups. A final set of test scenarios were applied to the RWEC involving multi-component wave patterns. Results from this were used to extrapolate performance in more realistic environments.

Prior to beginning any set of testing, the wave tank and associated equipment needed to be prepared. As a first measure, the steps listed in Appendix C: were followed prior to any steps for a particular experimental setup. These preliminary steps were followed by preparing and installing the mooring system required for the test set, including the weights and pulley

system.   The last piece of equipment to be placed in the wave tank was the RWEC itself, which was then connected to the mooring structure and pulley system.

3.5.4: Fixed mooring, single frequency waves

As mentioned above, the RWEC was first subjected to a single frequency wave in its fixed mooring configuration.   Aside from common setup procedures, the rotor often needed adjustment in order to minimize the amount of friction on the bearings.   The primary reason for this was that the mooring was fixed: everything was rigid and in place, meaning the rotor could not self-adjust to a more efficient configuration.   This was generally achieved manually by feeling for any roughness during the course of a rotation.   Once properly configured, experimentation began.   The outline of an experiment was as follows:

1) Start wave maker with sinusoidal input signal.

2) Once waves are up to amplitude or the weight has passed into the measurement region, begin timing.

3) Cease timing once the weight has moved past the measurement region (for the current experimental design, a 0.304m (12 inches) section.

4) If wave reflections started interrupting the experiment (distinguishable by the appearance of standing waves), a re-run must be done due to invalid data.

5) Record time for weight to pass through measurement region.

A minimum of three (3) runs were done for each weight and wavelength with a contingency for further runs if necessary.   The average time of all of the runs was used in data analysis.   If an outlier appeared in the results, an additional run was performed to lower the error in the results.

3.5.5: Tethered mooring, single frequency waves

The second major experimental setup involved the rotor in its tethered mooring configuration. Procedures were similar to those used to the fixed mooring, but with several minor adjustments. Due to the fact that the rotor was not fixed to any one point, adjustments were rarely needed to achieve minimum friction. The rotor would correct its own orientation depending on the incoming wave profile. In an effort to balance out the horizontal forces acting on the rotor, two weights of approximately equal mass were used, one on each side of the tank. A complication that arose during testing was that due to the resultant force of the incoming waves, the rotor had a tendency to move towards one side of the tank. Attaching strings from the rotor to suction cups on the walls of the wave tank prevented this excessive translational movement of the rotor. Beyond these considerations, measurement took place in a similar fashion to the fixed mooring system, but with the addition of tracking the second weight.

3.5.6: Multi-component wave patterns

A major shortcoming of the single frequency wave profile was its inability to properly model a realistic sea state. In open water, surface elevation is typically comprised of a series of wave components distributed across a range of amplitudes, frequencies, phase angles, and propagation directions. The range of amplitudes relates to frequency via a wave spectrum, a construct defining the distribution of available power in a given wave. The frequency and phase angle of a wave component can be considered random variables. Under a dominant wind pattern, waves propagate in the general direction of the wind.

$$\varsigma(t, \vec{x}) \approx \sum_i a_i \cos(\vec{k}_i \cdot \vec{x} - \omega_i t + \phi_i)$$

$$a_i^2 = S(\omega_i)(\omega_i - \omega_{i-1})$$

$$\vec{k}_i = \frac{\omega_i^2}{g} \angle p(\theta_{wimd})$$

$$0 \le \omega_i < \infty$$

$$0 \le \phi_i < 2\pi$$

Equation 6: Definition of multi-component wave parameters

In an effort to more closely model a realistic sea state, the RWEC was subjected to a multi-component wave envelope. Of the four aforementioned wave properties, only the relationship between wave amplitude and frequency were investigated. Due to the unidirectional nature of the testing environment, propagation direction was excluded from the experimental setup. For repeatability issues, the phase angle as a variable was excluded as well, being set to a constant value of zero (0) degrees. The wave spectrum chosen to relate amplitude to frequency was the Bretschneider spectrum, a two parameter function modeling a fully developed sea.

$$S\big(f, f_{mean}, H_{1/3}, a:0.3125, b:1.25\big) = a \frac{H_{1/3}^2}{f_{mean}} \left(\frac{f}{f_{mean}}\right)^{-5} \exp\left(-b\left(\frac{f}{f_{mean}}\right)^{-4}\right)$$

Equation 7: Bretschneider wave spectrum

A fully developed sea was defined as a state in which the fetch, the distance over which the wave has traveled, can be assumed infinite. The two parameters, the significant wave height ($H_{1/3}$) and mean frequency (f_{mean}), were chosen based on data gathered in the previous experimental setups, with values of six (6) inches (in) and 0.95 hertz (Hz).
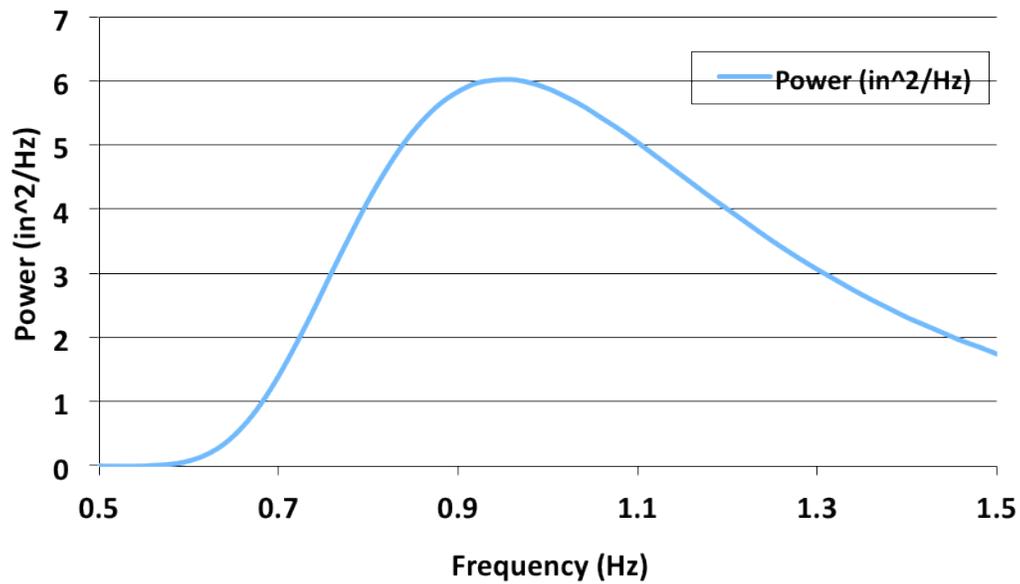
Figure 40: Wave spectrum for multi-component waves

The experimental setup consisted of the RWEC in its tethered mooring configuration exposed to a three-component wave environment.   A total of eleven wave profiles were generated with frequencies ranging from 0.80 to 1.10 hertz (Hz). As stated, each profile was comprised of three frequencies: a carrier, high, and low frequency. The carrier frequency was equivalent to the mean frequency and remained constant throughout the experiment. The high frequency was incrementally increased from the mean frequency to the maximum frequency. The low frequency was incrementally decreased from the mean frequency to the minimum frequency. For each profile, the high and low frequencies were equally distant from the carrier frequency.

$$f_{carrier,i} = f_{mean}$$

$$f_{low,i} = f_{mean} - i\Delta f$$

$$f_{high,i} = f_{mean} + i\Delta f$$

$$\Delta f = \frac{f_{max} - f_{mean}}{N} = \frac{f_{mean} - f_{min}}{N}$$

$$0 \le i \le N, i \in Z$$

Equation 8: Definition of frequencies

Each profile was designed to last forty (40) seconds regardless of the component

frequencies.   An example of a profile used during experimentation is given below in Figure 41.
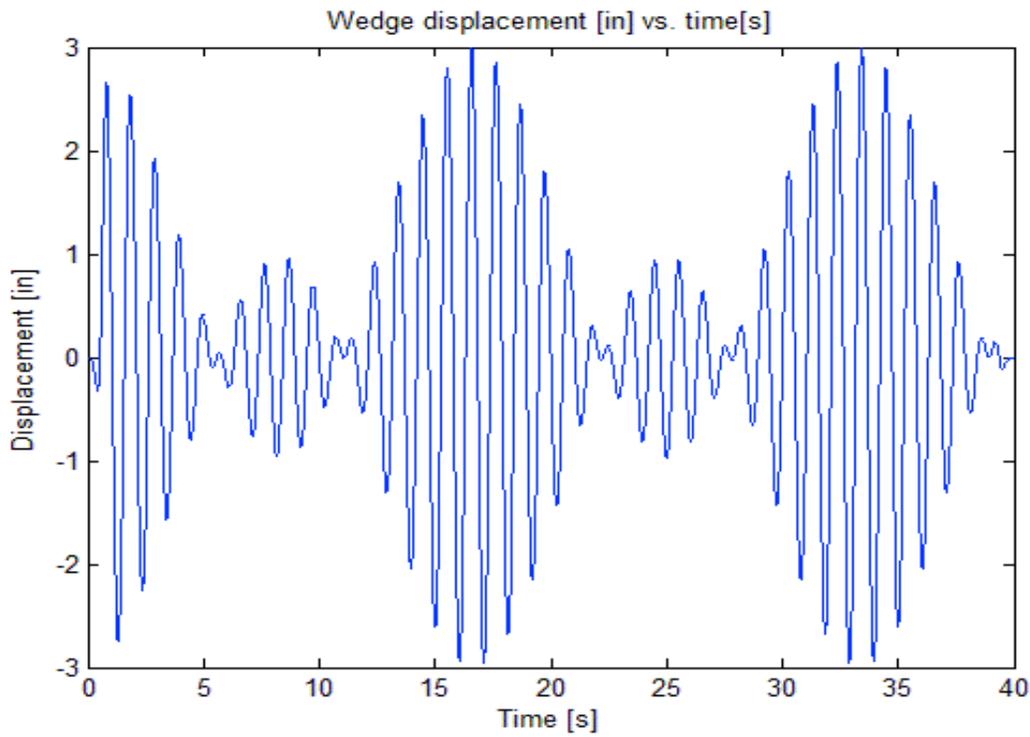
Figure 41: Example of multi-component wave profile

Due to the variation in the amplitude of the incoming waves, the method of measuring the vertical movement of weights was not a valid way of measuring power output. Instead to measure power output, the number of full forward rotations of the device was counted, excluding moments when the rotor 'unwound' due to the forces exerted by the measurement weights. This method was valid based on the assumption that in a true wave environment, the R-WEC would be restricted to forward rotation only by mechanical means.

3.5.7: Error analysis

For all time measurements, there was naturally a component of human error based on a minimum reaction time, which was fairly negligible. In addition, when quantifying the number of rotations for the multi-frequency wave profiles, the values were taken visually from outside of the tank to the closest quarter rotation. To minimize this effect, three team members recorded their numbers separately and the values were then compared for congruency for each trial.

Chapter 4:   Results

During the course of the research, three experimental configurations were evaluated based on the power extracted from available wave power.   Each configuration was chosen to simulate different mooring systems used in real world applications.   The fixed setup maintained the axis of the rotor even with water level as the waves propagated past the length of the rotor. The fixed setup simulated a partially constrained rotor in shallow water environments.   The tethered setup simulated a rotor that was moored only at the leading end of the device and allowed to float freely at the aft.

4.1 Wave profiles and available power

The first data collection was conducted with the objective of recreating the results presented by Dr. Daniel DeMenthon.   His symposium paper suggested that the rotary wave energy converter (R-WEC) was optimized for extracting waves of wavelength equal to 1.35 times the pitch of the spiral (DeMenthon 1982).   In order to mimic the data collected by Dr. DeMenthon a design of experiments (DOE) was generated that would allow us to study the relationship between the wavelength of incoming waves and the power generation of our device.

First, the desired wavelengths for the wave were determined, taking into consideration the dimensions of the tank and the rotor.   The pitch of our R-WEC was 1.22m (4 feet), and according to Dr. DeMenthon's findings, the optimal wavelength for a rotor was 1.65m (5.4 feet). Wavelengths were chosen that spanned a reasonable range above and below this value.   In addition, the experiments were constrained by the range of motion allowed considering the wave maker and the wave tank dimensions.   The range of test waves chosen for the experiments had

wavelengths ranging from 1.22m (4 feet) to 2.44m (8 feet) in 0.15m (6 in) intervals, resulting in nine (9) different profiles.

Once the desired wavelengths were decided upon, the corresponding frequencies for each wave profile were determined. To compute the frequency of a wave travelling in water from its wavelength in water, Equation 9 was used:

$$\lambda = \frac{g}{2\pi f^2}$$

Equation 9: Water wave frequency dispersion

Wavelength (expressed here as the Greek letter lambda) is measured in meters, g is the acceleration of gravity measured in meters per second squared, and f is the frequency measured in Hertz.   Using Equation 9, Table 3 below was created:

Table 3: Wavelength converted to frequency

Wavelength (m)	Frequency (Hz)
1.2192	1.137
1.3716	1.066
1.524	1.012
1.6764	0.965
1.8288	0.924
1.9812	0.887
2.1336	0.855
2.286	0.826
2.4384	0.800

These frequencies were then passed into the MATLAB script in Appendix E: to generate sinusoidal signals.   These signals were fed to wave maker input software via a software application that drives the wedge.   This wedge translated the signal into wave patterns in the tank.   The script allows the user to input the desired wave frequency, the wave amplitude factor

and the number of desired waves, while generating a text file that describes the sine wave. The wave maker software has a built-in function that converts the text files into binary signal that controls the servomotor that drives the vertical motion of the wave maker wedge.

The wave maker creates very little discrepancy between the input frequency and the frequency of the generated waves. However, the amplitude is much more difficult to control. The amplitude factor that is input to the script did not correspond to the amplitude of the generated waves. In order to determine the required amplitude factor necessary to generate the desired amplitudes, many different amplitude factors were used and the amplitude of the subsequent waves was measured. Using trial and error we determined that an amplitude factor of 0.0405 corresponded to an amplitude between 0.038m (1.5 inches) and 0.051m (2 inches), depending on the specific frequency. A wave amplitude of approximately 0.051m (2 inches) was chosen due to the hypothesis that power extraction would be optimal if the amplitude was equal to the radius of the R-WEC.

For each of the nine, single frequency, wave profiles that were created the amplitudes were measured three consecutive times. An average of the three amplitudes was used to subsequently estimate the available energy contained in a unit width of wave crest. The complete set of data that was collected can be found in Appendix H:. This measure of available energy is called the energy flux and is a measure of the amount of power that is contained in the waves for a given width of wave crest. Equation 10 was used to compute the energy flux was derived using general wave theory principles and is shown below:

$$Q = \frac{\rho g^2 A^2 T}{8\pi}$$

Equation 10: Energy flux per unit wave front

Where Q is the energy flux in kilowatts per meter of wave crest, ρ is the density of the medium, g is the acceleration of gravity, A is the wave amplitude (one half of the wave height) in meters, and T is the period of the wave in seconds. From this equation for the energy flux we can compute the total available power by multiplying by the width of crest (w) that is accessible (in this case the tank was 1.219m wide).

$$P = Q * w = \frac{\rho g^2 A^2 T}{8\pi} * w$$

Equation 11: Power available to rotor (in watts)

In this form, the only values that need to be computed are the wave height, which is equal to twice the amplitude, and the period, which is the inverse of the frequency. A sample calculation for the energy flux is shown in Appendix I:. Table 4 below shows the data collected for each wave profile.

Table 4: Amplitude and energy flux for the single frequency wave profiles

Wavelength (m)	Amplitude (in)	Amplitude (m)	Energy Flux (kW/m)
1.2192	1.54	0.0392	0.0054
1.3716	1.60	0.0407	0.0062
1.524	1.46	0.0370	0.0054
1.6764	1.44	0.0365	0.0055
1.8288	1.46	0.0370	0.0059
1.9812	1.63	0.0413	0.0077
2.1336	1.94	0.0492	0.011
2.286	2.13	0.0540	0.014
2.4384	1.96	0.0497	0.012

4.2 *Fixed mooring, single frequency waves*

Once these wave profiles had been created, our wave energy collector could be tested under the nine different wavelengths. For the first data collection, the R-WEC was held in the

tank using the fixed mooring structure that was described in section 3.4.2:   This kept the R-WEC fixed at the mean water level.   Preliminary testing of these profiles was conducted with the rotor in the tank using the fixed mooring in order to gain some insight into the behavior of the R-WEC.   Initial observations were recorded to attempt to better understand the dynamic behavior of the rotor under testing conditions.   It was noted that when the rotor had no external loading applied to it that it rotated smoothly and the contour of the foam spiral followed the wave profiles.   However, as increasing weight was applied to the rotor the rotation of the device began to degrade.   Most notably, if enough weight was applied, the rotation of the rotor would slowly move out of phase from the wave profile, resulting in discontinuous motion.   The weight would cause the rotor to rotate in the opposite direction until the rotor fell back into phase with the waves, at which point the rotor would shift out of phase once again.   This effect became more pronounced as the weight was increased, until enough weight was applied that the rotor simply could not rotate.   Additionally, for different wavelengths, this phenomenon of falling out of phase with the incoming waves occurred at lower weights than other wavelengths. Generally, wavelengths of around 1.68 or 1.82 meters (5.5 or 6 feet) could tolerate larger weights before the rotation of the R-WEC was affected.

After preliminary testing was conducted, data was collected for each of the nine wave profiles.   For each wave profile five weights were tested: 100g, 200g, 300g, 400g, and 500g. Each trial began with the lowest weight, and the attached weight was increased incrementally until the weight was too heavy for the R-WEC to raise it the prescribed height.   The power extracted from the R-WEC was computed by measuring the amount of time it took for a known weight attached to the rotor to rise twelve inches.   The time was measured three times for each trial, and the average of these times was used to compute the power.   Data was only collected

for those weights that the rotor was able to raise in a smooth, continuous manner. The entire set of raw data collected is shown in Appendix J:. Equation 12 below describes how the power extracted was computed using the data collected.

$$P = \frac{mgh}{t}$$

Equation 12: Power calculated from the vertically lifted weight

In Equation 12, "*P*" is the power in watts, "*m*" is the mass in kg, "*g*" is the acceleration of gravity in meters per second squared, "*h*" is the rise height, and "*t*" is the time in seconds it takes for the weight (*m*) to rise the fixed distance (*h*). An example calculation using Equation 12 is shown in Appendix K:, and a table of the power extracted from the R-WEC is shown in Appendix L:. Figure 42 below shows a plot of the data collected.
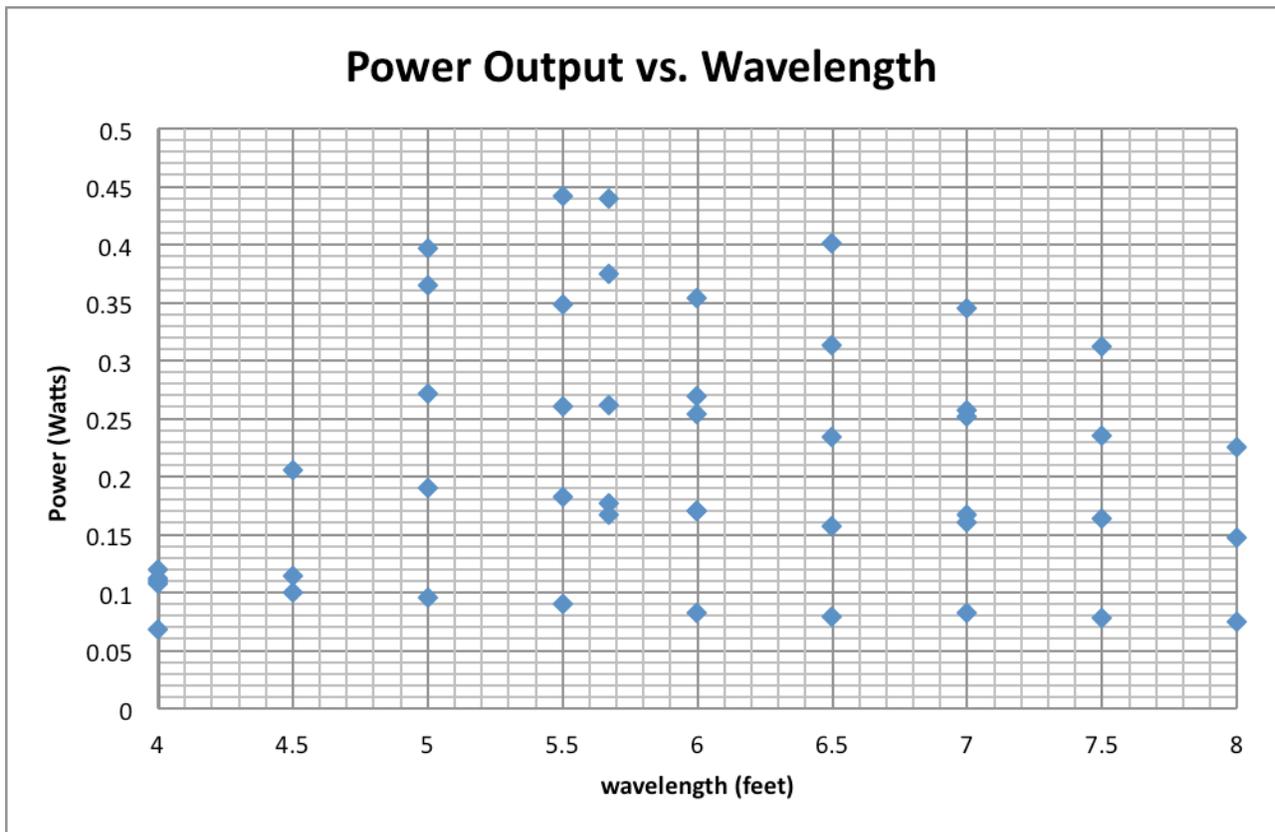
Figure 42: Power output from the R-WEC with respect to the incoming wavelength

This graph shows increments of power output for each wavelength, this corresponds to the different weights used. It is clear that a better measure for the power output of the R-WEC is the highest power that can be extracted without impeding the rotation of the device, this means measuring the power using the highest weight that can still be raised. In order to better interpret this data, only the data points for the highest weights were kept. In addition, the vertical and horizontal axes were normalized. The vertical axis was divided by the available power, which was computed by multiplying the energy flux that is given in Table 4 by the width of the tank (1.2192 m) and converting to watts. The horizontal axis was normalized by the pitch of the rotor. The resulting graph is shown in Figure 43 below.
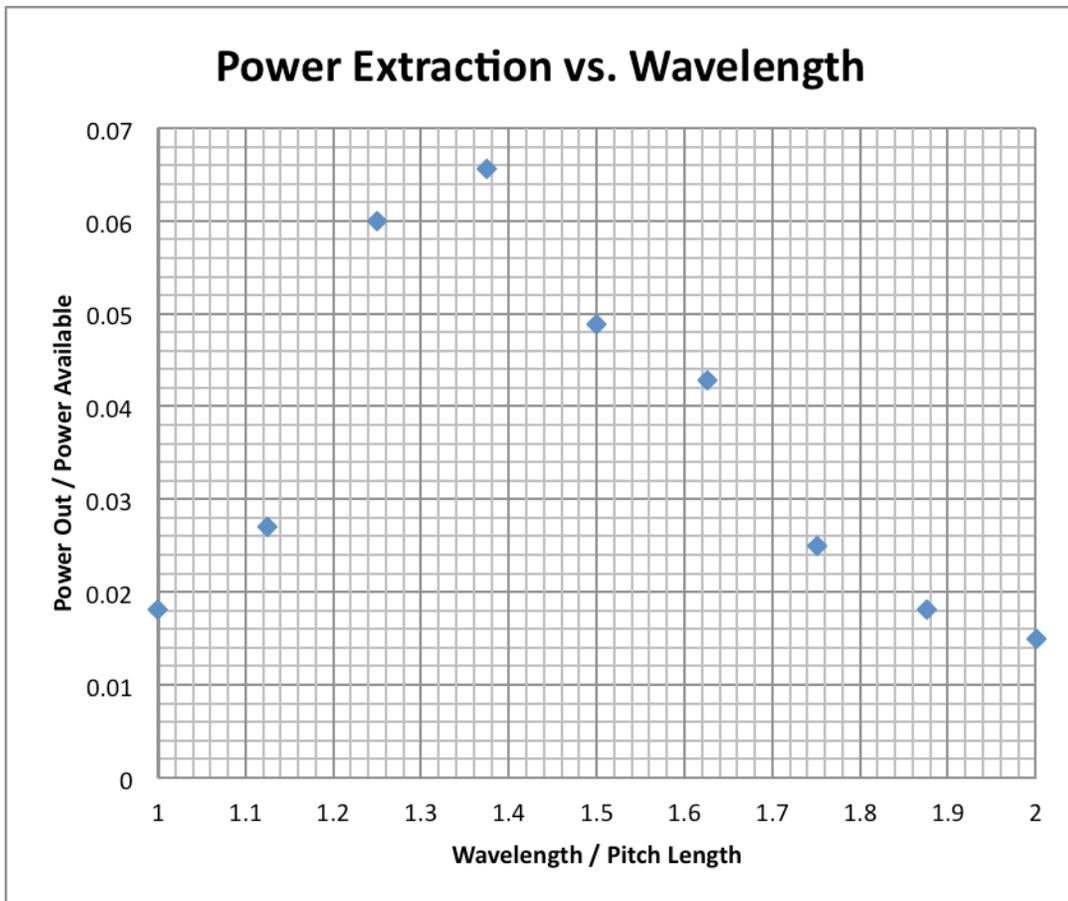
Figure 43: Normalized plot of power output from R-WEC for the fixed mooring and single frequency wave profiles

This graph is much easier to interpret and suggests that the rotor has a peak in power extraction at a wavelength that is about 1.38 times the pitch of the foam spiral (4 feet).   In addition the rotor seems to extract about 6.5% of the available energy in the wave.

4.3   *Tethered mooring, single frequency waves*

The next testing conditions also used the single frequency wave profiles, but the rotor was tethered using the tethered mooring structure that was described in section 3.4.3:   .   This mooring configuration implemented a new weight and pulley system was developed to maintain a net force of zero on the rotor as it floated at mean water level.   Specifically, this weight system had a set of weights on either side of the tank.   The same phenomenon that was observed in the fixed mooring system was seen in this experiment.   In fact, since the rotor was not held rigidly at mean water level the rotor's motion seemed to degrade a lower weights at the same wavelength compared to the first data set.   This occurred due to the lack of vertical forces to keep the rotor from rocking up and down during the testing procedure.   This rocking motion along the axis of the device is called "pitching".   At wavelengths less than the length of the rotor (less than 1.83m or 6ft) the rotor did not rotate efficiently, particularly when larger weights were used.   At wavelengths larger than the length of the rotor, the front of the rotor plunged into the trough of each wave and caused the rotor to pitch.   Pitch motion contributed to the degradation of the rotatory movement of the R-WEC.   As a result, a lower fraction of power extracted was expected for this experiment.

In order to compute the power output using this mooring setup, both weights were timed as they ascended a predetermined height.   These two times were averaged, and the measurements were taken three consecutive times.   For these trials, the weight was

91

incrementally increased until the rotor could no longer raise any more weight without affecting its rotation. Only the trials for the highest weight that allowed for continuous rotation of the R-WEC were recorded. The average of these trials was taken and used to compute the power output as shown in Equation 6. The complete set of data is shown in Appendix M:. Figure 44 below is the normalized plot of power with respect to wavelength.

Power Extraction vs. Wavelength
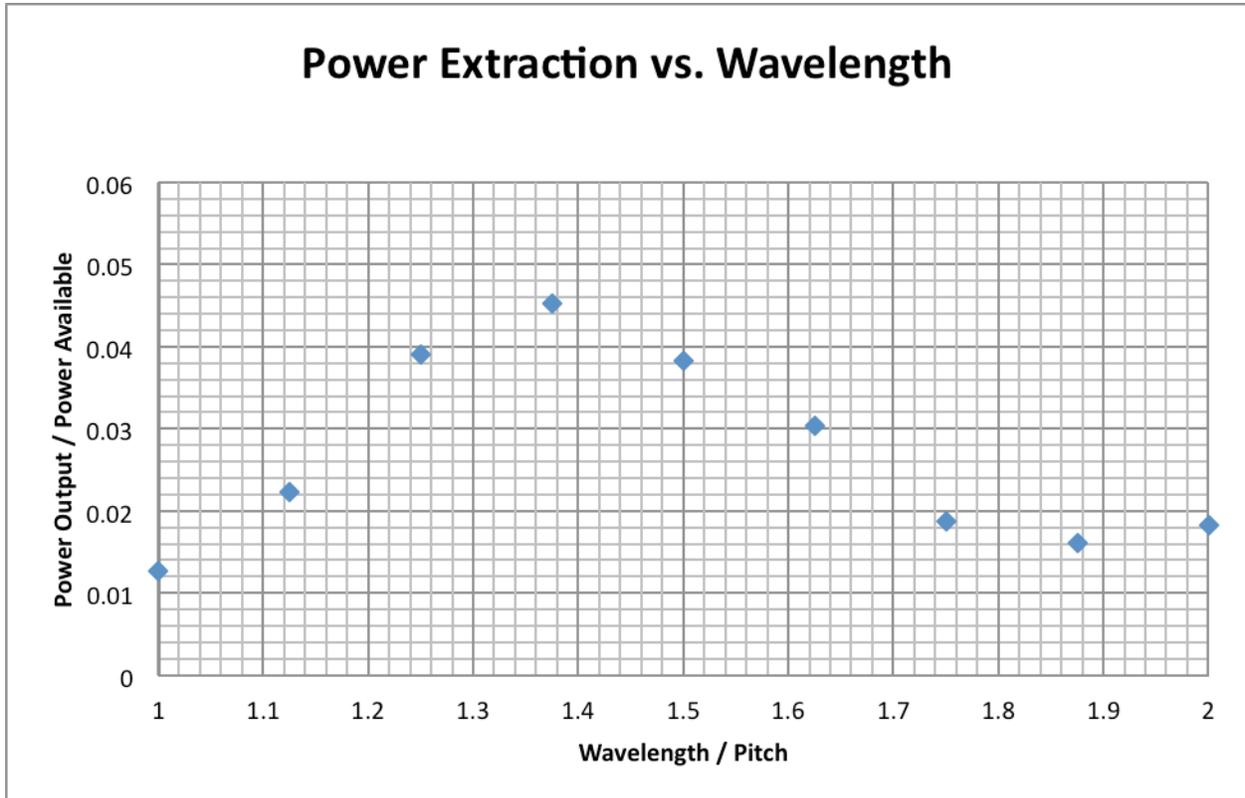
Figure 44: Normalized plot of power output from R-WEC for the tethered mooring and single frequency wave profiles

This plot also seems to reach a peak in the power extraction at wavelengths equal to 1.38 times the pitch. This is consistent with the fixed mooring experiment. The maximum power that was extracted in this setup is around 4.5% of the available power.

4.4   Tethered mooring, multi-component waves

The final data collection was conducted using the same tethered mooring as before; however, the rotor was tested under multiple frequency waves.   The objective for these multiple frequencies was to gain a measure of how the R-WEC would behave under non-ideal conditions. These multiple frequency wave profiles were made by the linear combination of three frequencies as described in section 3.5.6:   .   As described earlier there was a carrier frequency, a minimum frequency, and a maximum frequency.   To describe a system that was comparable to the single frequency waves a series of profiles spanning the entire range of frequencies tested in the previous two experiments were generated.   The carrier frequency was chosen as the middle of the range of frequencies used (0.95 Hz).   The first wave profile generated combined three frequencies, each equal to 0.95 Hz; in effect creating a single frequency wave.   Each subsequent profile increased the maximum frequency and decreased the minimum frequency by an equal amount, while maintaining the carrier frequency constant.   Ten wave profiles were generated in this manner in order to span the entire range of frequencies (from 0.8 Hz to 1.1 Hz).

Preliminary tests using these profiles made it evident that a new data collection technique would need to be implemented.   Due to the unsteady nature of these multiple frequency profiles, the rotational motion of the rotor was highly discontinuous.   In fact only the waves that had amplitudes larger than the radius of the R-WEC were able to cause any rotation of the device.   Since these wave profiles were generated in packets, there were breaks between periods of continuous rotation.   During these breaks the rotor would rotate clockwise as the weight unwound itself from the pulley system.   Then the rotor would begin to rotate counterclockwise again and wind up the weights.

93

*Due to the unpredictable nature of this rotation the power extracted from the R-WEC was measured by counting the number of rotations that the device completed (only in the counterclockwise direction) in a fixed amount of time (40 seconds for each wave profile). Since the diameter of the pulley around which the string attached to the weights was known, the amount that the weight was lifted could be calculated as a function of the number of rotations completed. Each rotation of the rotor is equivalent to a rise height of 0.127 meters (5 inches). The number of rotations completed was counted in three consecutive trials, and these three values were averaged. The power was then computed using Equation 12 as shown previously. The data collected is shown below in * The columns Run1, Run2, Run3, and Average all refer to the number of rotations.*

.

Table 5: Data using multiple frequency profiles

Δf	fmean	fmin	fmax	Run 1	Run 2	Run 3	Average*	Rise height (m)	Weight (g)	Power (W)
0.03	0.95	0.92	0.98	7	8.5	8	7.833	0.99483	182	0.0443
0.06	0.95	0.89	1.01	10.25	10.25	10	10.166	1.29116	182	0.0575
0.09	0.95	0.86	1.04	7.75	7.75	8	7.833	0.9948	182	0.0443
0.12	0.95	0.83	1.07	8.5	9.5	9	9	1.143	182	0.0509
0.15	0.95	0.8	1.1	5	5.5	5.25	5.25	0.66675	182	0.0297
0.18	0.95	0.77	1.13	6	8.5	7.75	7.416	0.94191	182	0.0420
0.21	0.95	0.74	1.16	8	7.75	6	7.25	0.92075	182	0.0410
0.24	0.95	0.71	1.19	3.5	5.25	4.75	4.5	0.5715	182	0.0254
0.27	0.95	0.68	1.22	6.25	5.75	5	5.666	0.71966	182	0.0320
0.3	0.95	0.65	1.25	5	5.25	5.75	5.333	0.67733	182	0.0302

* The columns Run1, Run2, Run3, and Average all refer to the number of rotations.

In order to be able to interpret the data properly the data was normalized by dividing the power output by the power available in the wave profile used. The power in each multiple frequency wave profile was estimated using Equation 13:

$$P = \frac{\rho g \Delta t}{F_{mean} T_{run}} \sum z^2$$

Equation 13: Power Available in Multiple Frequency Waves

In Equation 13, ρ is the density of the medium (in this case it is the density of water),

$\Sigma(z^2)$ is the sum of the squared wave amplitude, Δt is the time it takes for the

The following plot was generated in this way:
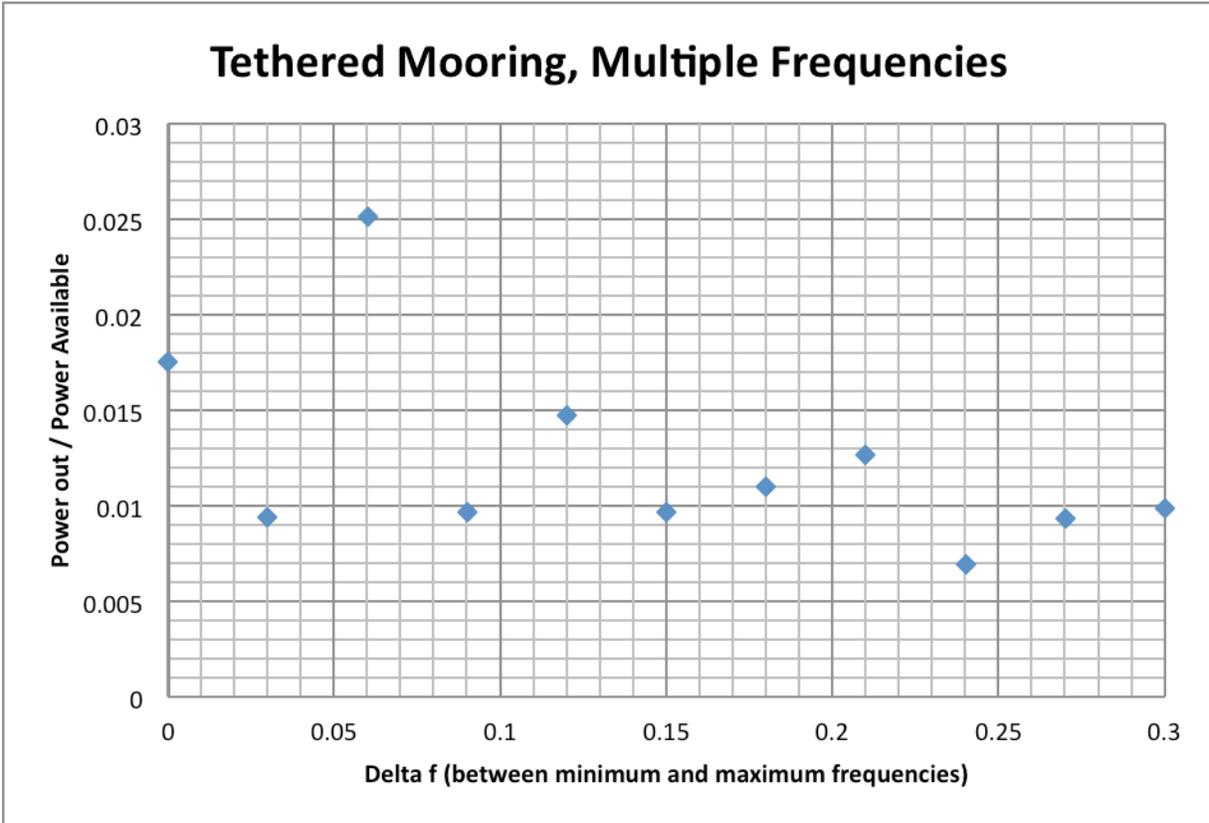
Figure 45: Normalized plot of multiple frequency data

The horizontal axis plots the difference between the maximum and minimum frequencies, that when combined with the carrier frequency, resulted in the wave profiles used. As delta f increases, the more random the profile becomes and the less it behaves like a single frequency wave. The plot in Figure 45 demonstrates a generally decreasing trend, which suggests that the R-WEC is able to extract a smaller percentage of the available power as the wave profile becomes more chaotic.

Chapter 5: Discussion and Conclusions

5.1 Single frequency wave profiles

The single frequency profiles were tested using two different mooring configurations for the R-WEC. The first configuration, or the fixed mooring system, was used to confirm the results demonstrated in DeMenthon's original design (DeMenthon, 1982). As shown inFigure 45, the peak fraction of power extracted by the R-WEC occurred at approximately 1.38 times the pitch. DeMenthon reported this value to be 1.35 times the pitch, which is reasonably close to the empirical findings in this report. Additionally, the rotor was tested using a tethered mooring system to model the R-WEC's performance in a different configuration. The tethered configuration was a typical mooring solution used in deep water applications of wave energy converters. The results of both mooring configurations are shown below in Figure 46.
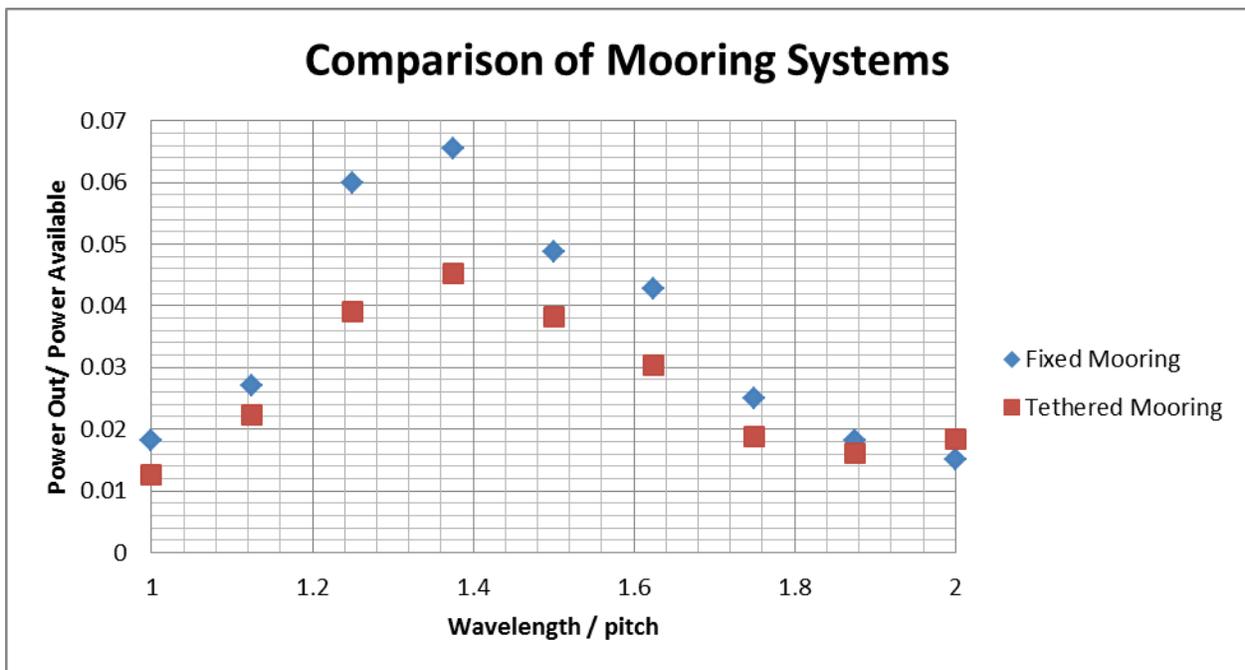
Figure 46: Plot comparing the two mooring configurations

In the tethered mooring configuration, the R-WEC did not extract as much power as it did in the fixed mooring configuration.   The only exception was the data point with the highest wavelength, which may have been affected by confounding variables.   However, the peak in power extraction occurred around the same wavelength for both mooring configurations.   This suggests that the optimal wavelength is characteristic to the rotor itself; in this case, it is equal to approximately 1.38 times the pitch.   This value provided a preliminary guide during the scaling up analysis and can be used to select additional regions for R-WEC implementation.

5.2   Multiple frequency wave profiles

The data shown in Figure 45 does not exhibit a smooth curve with an identifiable peak in power extraction, which was the case for the single frequency wave profiles (refer to Figure 44). This was mainly due to the discontinuous nature of the rotation that was observed during the experiments using multiple frequency wave profiles.   In particular, there was one outlier that did not seem to follow the general trend of the remaining data points.   Ignoring that data point revealed that the general trend suggests a decrease in power extraction as the wave profile becomes more random.   This makes sense since the R-WEC is designed to respond to waves of a certain wavelength, as seen with the single frequency wave profiles.   Consequently, the R-WEC is best suited for applications where there is a small range of frequencies in the incoming waves.

5.3   Optimization

In order to extract the largest amount of available energy using the R-WEC, it is important to consider both the mooring configuration and the wavelengths of incoming waves.   A fixed

mooring structure that maintained the axis of the rotor at mean water level produced better results than a tethered mooring.   Thus, fixed mooring structures are more easily implemented in shallow water where support structures can be fixed to the sea bed.   Additionally, shallow water environments generally have incoming waves of predictable wavelengths coming from a single direction.   The decreasing water depth acts as a filter for high and low frequency waves, resulting in a smaller range of frequencies that reach the shore.   This makes shallow water applications ideal for the R-WEC.

5.4   Economic Analysis

The team's economic analysis examined the suitability of the R-WEC in three coastal Mid-Atlantic regions of the United States, with data provided by the National Buoy Data Center and Scripps Institution of Oceanography.   The analysis used the average dominant wave periods and average significant wave heights from 2010 historical data of each region.   This section of the paper serves as a preliminary look into the cost-efficiency of implementing the R-WEC.   This analysis serves as a platform for further studies into the economic feasibility of the R-WEC device.

The scaling up analysis initialized with the calculation of the rotor pitch and radius. Given the significant wave height and dominant frequency of a specific location, the MATLAB script used in the analysis of real world implementation determined the radius and pitch of the rotary device ideal for that location, based on the area's wave profile.   In order for the radius of the device to be equal to the average wave amplitude, the significant wave height was divided by four (4).   The pitch was optimized at a specific multiple (1.38) of the wavelength, the optimal ratio as determined in the team's study.   The Bretschneider wave spectrum is a stochastic model of a fully developed sea, a scenario in which the incoming waves originate infinitely far away.

In this study, it predicted the distribution of power over a range of frequencies by displaying a wave spectrum density function for each region.   Thus, the script predicted and displayed the functional envelope of the device laid over the distribution of power, at the location as predicted by the Bretschneider wave spectrum.   The MATLAB script is located in Appendix N:.

The wave profiles of each region are as follows:

Delaware Bay

This 3-meter discus buoy is owned and maintained by the National Data Buoy Center and is located at 38°27'49" N 74°42'7" W.   It resides at a water depth of 28 meters (NBDC – Delaware Bay, 2011).

Significant wave height [m]: 1.337710953

Mean frequency [Hz]: 0.119883359

Rotor pitch: 78.6892 [m]

Rotor radius: 0.3344 [m]

with a minimum frequency of 0.0996 [Hz] and maximum frequency of 0.1408 [Hz]
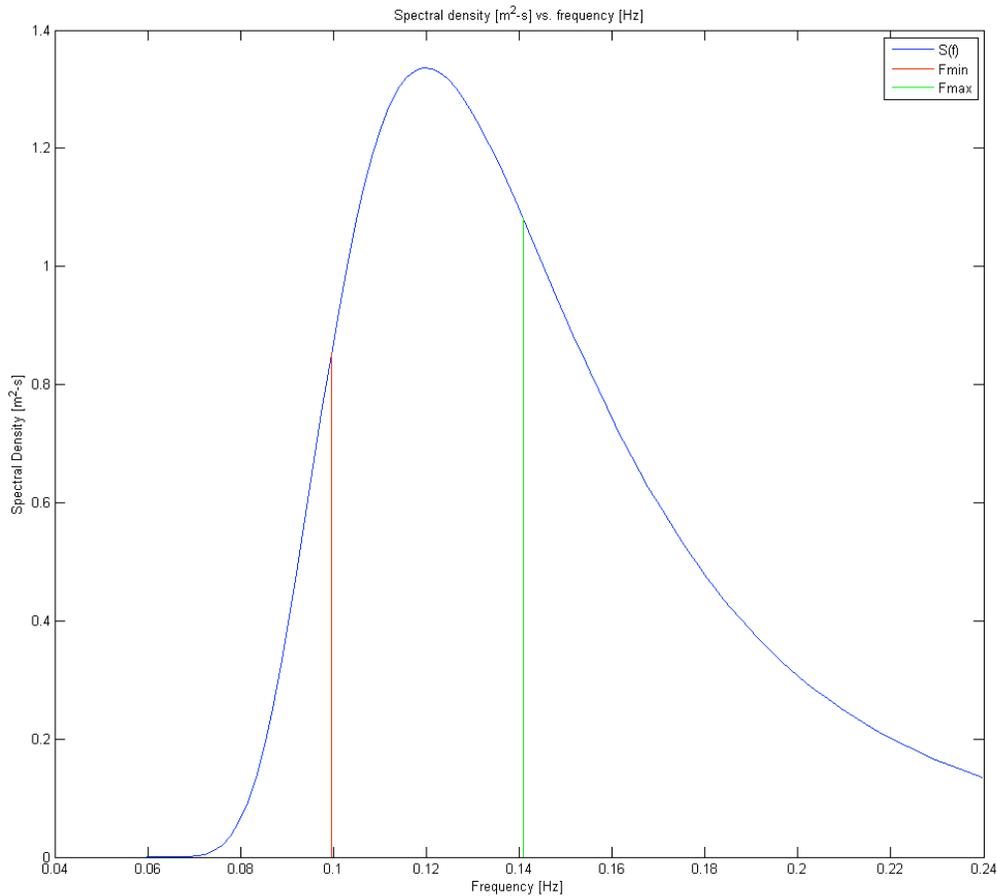
Figure 47: Spectral density vs. frequency for Delaware Bay study region

Virginia Beach, VA

This 3-meter discus buoy is owned and maintained by the National Data Buoy Center and is located at 36°36'40" N 74°50'11" W.   It resides at a water depth of 47.5 meters.

Significant wave height [m]: 1.706688702

Mean frequency [Hz]: 0.120387583

Rotor pitch: 78.0314 [m]

Rotor radius: 0.4267 [m]

with a minimum frequency of 0.1000 [Hz] and maximum frequency of 0.1414 [Hz]
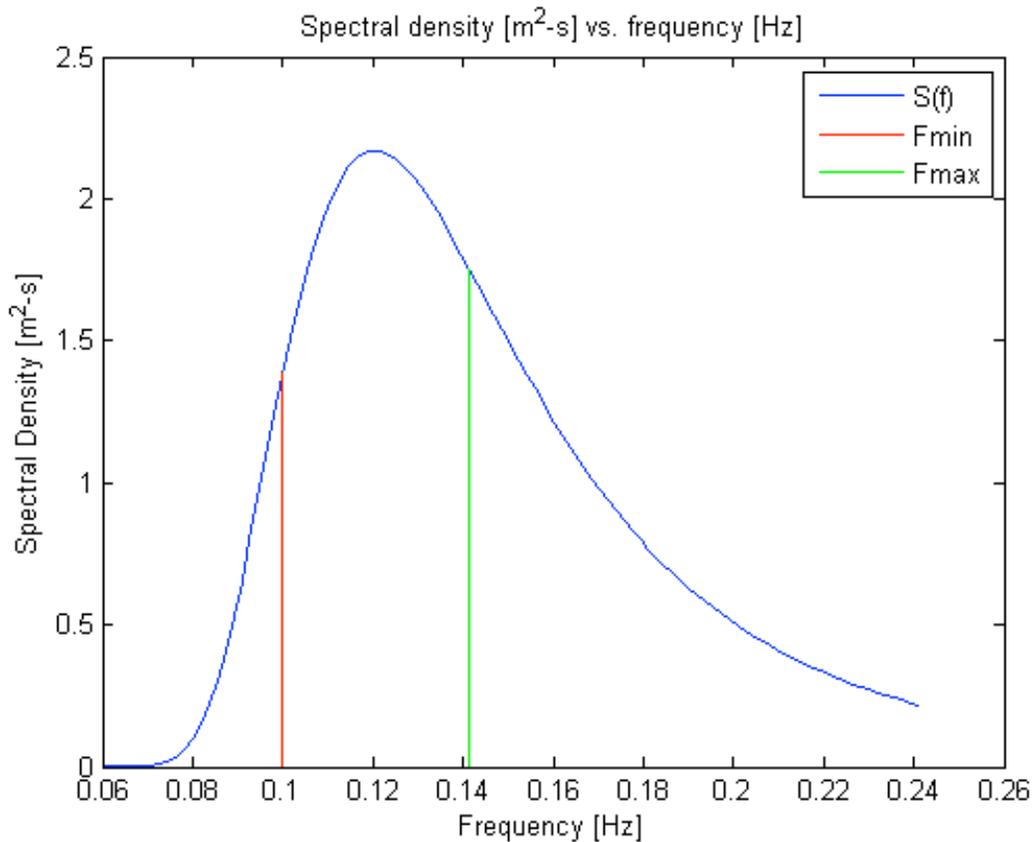
Figure 48: Spectral density vs. frequency for Virginia Beach study region

Cape Henry, VA

This Waveride Buoy's information was submitted by Scripps Institution of Oceanography and is located at 36°54'14" N 75°45'23" W.   It resides at a water depth of 18.9 meters.

Significant wave height [m]: 1.014619912

Mean frequency [Hz]: 0.112819017

Rotor pitch: 88.8522 [m]

Rotor radius: 0.2537 [m]

with a minimum frequency of 0.0937 [Hz] and maximum frequency of 0.1325 [Hz]
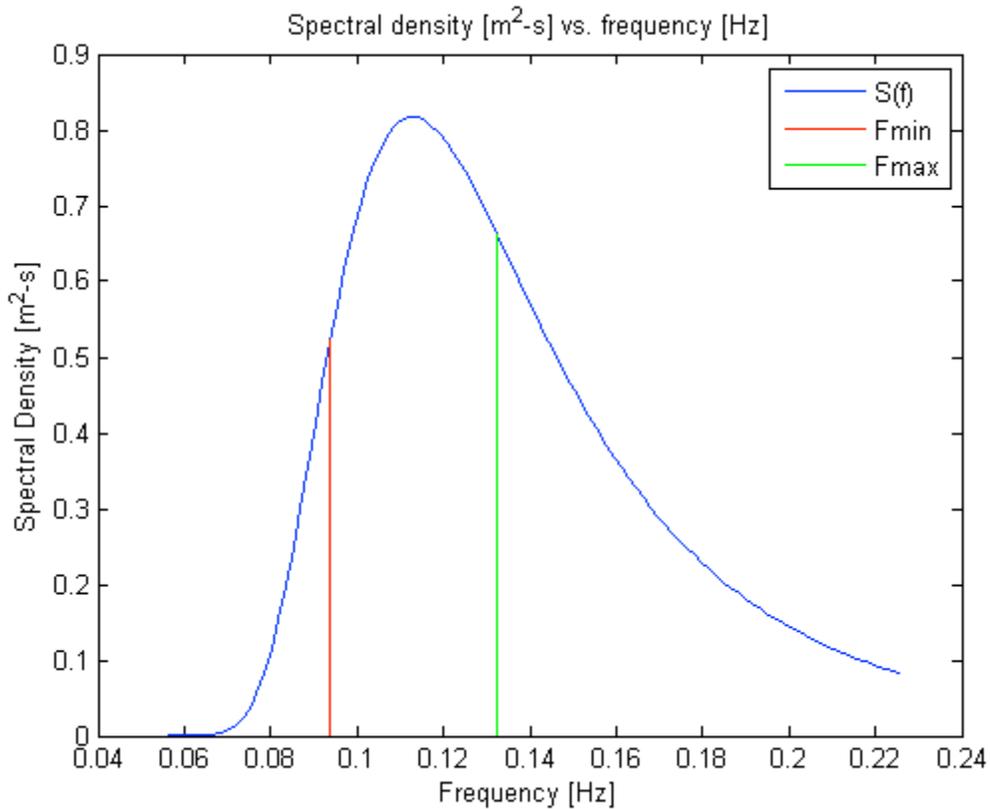
Figure 49: Spectral density vs. frequency for Cape Henry study region

The pitch was calculated as the wavelength divided by 1.38, following the team's optimal

ratio in the lab. Using the rotor pitch, the rotor length was calculated as 1.5 times the pitch,

following the proportions of the R-WEC.

	Dominant Wave Period (sec)	Significant Wave Height (m)	Average Wave Frequency (Hz)	Wavelength (m)	Radius (m)	Pitch (m)	Length (m)
Delaware Bay	8.341	1.338	0.1199	108.6	0.3344	78.69	118.0
Virginia Beach	8.307	1.707	0.1204	107.7	0.4267	78.03	117.1
Cape Henry	8.864	1.015	0.1128	122.7	0.2537	88.85	133.3

Next, the team chose a suitable material for the scaled up device. After researching the

material choices of several wave energy collectors and ocean buoys, the team decided upon mild

steel, also known as carbon steel. 1018 Cold Rolled Mild Steel has a density of 7860 kg/m^3

and a yield strength of 370 Mega-Pascals (MatWeb, 2011). This material is versatile for

machining, forming, welding, and heat treatment. The pricing of the device was computed

from online quotes of a national metal supplier. 1018 Cold Finish Mild Steel was selected from

OnlineMetals.com. A 0.003175 m (0.125 in) thickness was selected and the pricing was based

on sheets that were 0.1016 m (4 in) wide and 2.4384 m (96 in) long, at $21.87 per sheet. The

price per volume was calculated to be $27,804 per cubic meter of steel.

Next, using the calculated radius (outer helix radius) and length of the device, the volume

of the helix and rod were calculated for each region. This calculation also considered the inner

helix radius, rod outer radius, rod inner radius, thickness of the metal, and the moment of inertia

of the helix-rod rotor system. These calculations were similar to those in section 3.2 and

detailed in Equation 2Equation 4. However, the density of the water changed to 1027 kg/m^3,

to accommodate saltwater. The moment of inertia calculation also changed and is outlined in

Appendix O:.

The rod inner radius value remained constant at 0.002 m for all three regions, which

provided reasonable safety factors in the range of 2.098 to 7.838.   Due to the light material of

the device and its hollow nature, the device will require additional weight – ballast or anchors –

to offset the buoyancy force when implemented.   For complete calculations and load, shear,

moment, stress, and safety factor diagrams, see Appendix P:.

Figure 50 below depicts the various dimensions of the rod-rotor system:
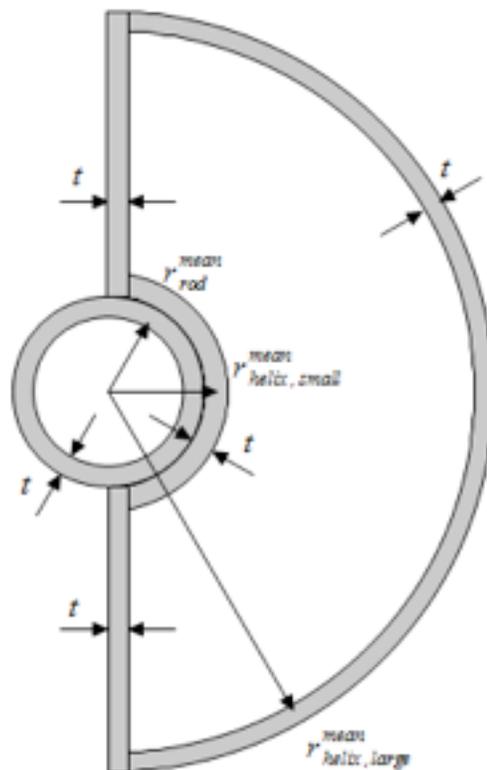
Figure 50: Rod-Rotor System Dimensions

The following chart displays the dimension for each rotor.

Table 6: Scaled up rotor dimensions

	Larger Helix Outer Radius (m)	Larger Helix Inner Radius (m)	Smaller Helix Outer Radius (m)	Smaller Helix Inner Radius (m)	Rod Outer Radius (m)	Rod Inner Radius (m)
Delaware Bay	0.334	0.331	0.008	0.005	0.005	0.002
Virginia Beach	8.864	1.015	0.008	0.005	0.005	0.002
Cape Henry	0.254	0.251	0.008	0.005	0.005	0.002

The following chart displays the moment of inertia, volume, and safety factor.

Table 7: Scaled up moment of inertia, volume, and safety factor

	Moment of Inertia (m^4)	Helix Volume (m^3)	Rod Volume (m^3)	Total Volume (m^3)	Safety Factor
Delaware Bay	0.0000474	0.5107	0.0084	0.5191	4.699
Virginia Beach	0.0000989	0.6468	0.0084	0.6552	7.838
Cape Henry	0.0000205	0.4368	0.0095	0.4463	2.098

Using the dominant wave period, significant wave height, gravity, and density of saltwater, the power flux equation, outlined in Section 4.1 and Equation 10, was used to calculate the available power per meter. Next, the available power per meter was multiplied by the 4.5% efficiency calculated from the team's laboratory data for multi-frequency waves in tethered mooring, which best fit the implementation conditions of the scaled-up rotor.

The available power was then multiplied by the pitch. This effectively models the rotor's behavior in a parallel wave farm configuration – multiple rotors in parallel with the distance of one pitch between each rotor. The pitch value was chosen to normalize the power instead of the diameter because the rotor can also draw energy from waves reflected by

neighboring rotors or from energy drawn in by turbulent flow.

Then, the total cost for the helix-rod rotor system was calculated to be $27,804/m^3 times the rotor volume, then multiplied by five (5). This factor of five provided a conservative estimate of the total costs of the rotor, as it accounted for the cost of shipping, welding, the generator, additional parts, and the labor needed to build each rotor system. The factor of five is a typical number used in the industry, as recommended by Mr. John Zseleczky of the U.S. Naval Academy. Lastly, the cost per kilowatt was calculated.

The following chart displays the price, power, and cost/KW.

	Available power (watts)	Available power (KW/m)	Available power after efficiency (KW/m)	Available power after efficiency, multiplied by pitch (KW)	Estimated steel cost	Estimated total cost	Cost per KW
Delaware Bay	7310	7.310	0.3290	25.90	$14,455	$72,275	$2,791.03
Virginia Beach	11850	11.85	0.5332	41.62	$18,218	$91,090	$2,188.42
Cape Henry	4469	4.468	0.2011	17.87	$12,410	$62,050	$3,471.41

This value was compared against the operating cost per KW for a coal power plant ($1290/KW) and photovoltaic cells ($4751/KW). As the estimated total costs increased, the cost per KW decreased. With the average U.S. household consuming about 1 KW of power, each device contains the potential to power approximately 25-60 homes. Optimally, the devices would be installed in farms, which would help to reduce the estimated total cost. The device may be able to power networks like marinas or small coastal communities.

5.5 *Limitations and Future Directions*

Limitations, such as the size of the wave tank available, and the allowable budget,

dictated the parameters of the experiments conducted.   The tank dimensions determined the rotor size, and the budget determined both the construction method and materials.

One of the most notable results we found was the ideal wavelength that resulted in optimal power extraction from the R-WEC.   As mentioned before the ideal wavelength of incoming waves should be 1.38 times the pitch of the R-WEC.   While this result confirms the original data collected by DeMenthon, this result was not expected.   If the device were to perform exactly as it is intended to, the spiral curve of the R-WEC would follow along the profile of the incoming waves.   This occurs when the pitch of the spiral, and the incoming wavelength are equal.   However, it seems that the device behaves more smoothly with an incoming wavelength slightly larger than the pitch of the rotor.   This factor of 1.38 may be influenced by the length of the rotor, and more specifically, by the length to pitch ratio of the device.   In this study, the R-WEC prototype had a 1.5 length to pitch ratio, and the ideal wavelength was in between the pitch and the length of the R-WEC (1.38 times the pitch). Further experiments would have to be conducted to determine which physical parameters have a greater effect on the optimal wavelength.   In particular it would be useful to understand how the optimal wavelength changes as a function of length to pitch ratio.

There are several limitations of the economic analysis, which serves as a basic look into the economic feasibility of the R-WEC in real-world conditions.   These limitations lead into further areas of study.   First, maintenance and repair costs were not taken into account.   Future studies could be focused on the life-cycle cost of the device.   Second, mild steel may not be the most suitable material for the device and future studies could examine the loading and structural integrity of the device in dynamic conditions.   Third, the pricing of the steel was based on online quotes from a metals supplier that does not sells metals in low quantities, not for industrial

use.   The actual cost per device may decrease if the steel is a larger quantity from a larger supplier.   Last, the team's data, which the 4.5% efficiency was derived from, was based on the 6-foot long rotor.   Since the rotor was not tested in larger dimensions or actual seas, the team assumed a linear scaling up factor.   Future studies could create several rotors in increasing size, each with a certain efficiency.   Using a curve of best fit, the scaled-up efficiencies could be determined.

The conclusions of the team's research led them to determine several factors that could be examined under future research or different testing conditions.   Wave farm configurations, a major factor in wave energy conversion, is one area the team would propose for future research. The efficiencies and conclusions of the team's study pose various questions regarding how the rotor would perform if multiple devices were placed into a wave farm configuration.

During testing and analysis, the team assumed that the activity happening on the right side of the rotor is the same as what is happening on the left side.   If multiple rotors were placed in a parallel or stacked configuration, the individual interaction of one rotor with the waves could have an impact on the remaining rotors, falsifying this assumption.   Future testing would require a larger wave tank where multiple rotors could be set up for each test.   The test scenarios would examine many parameters including: the optimal number of rotors within the configuration, whether a parallel or staggered configuration is more efficient, and what the optimal spacing between rotors.   These tests would offer additional insight into the efficiency and capabilities of the rotor when installed under realistic, real-world conditions.

Appendix A: Glossary

Amplitude: the vertical distance from the horizontal axis to either the crest or trough; half the wave height

Attenuator: long, multi-segmented wave energy converters which pivot at the segment joints as a wave passes by the device; a hydraulic pump at the hinged joints is used to convert the energy into usable power

Beam Theory: a simplification of the theory of elasticity which allows the load carrying and deflection characteristics of beams to be somewhat easily calculated

Benthic community: organisms that live in and on the bottom of the ocean floor including worms, clams, crabs, lobsters, sponges, and other tiny organisms that live in the bottom sediments

Catenary Mooring: an arrangement of mooring lines in which the lowest portion of the line rests on the ocean floor; results in the anchors only needing to withstand horizontal forces; has a large footprint and is not suitable for deep water mooring

Characteristic Zero Crossing Period: generalizes the period of a sea state to be that of a pure sinusoid; noted by Tz

Closed-cell foam: foams with a make-up that resist the entrance of air and other corrosive fluids

Crest: the peak of a wave; the highest point on the wave

Energy Flux: the amount of power contained in a unit width of wave crest

Frequency: the number of waves passing a given point per unit of time

Hydrography: the science that deals with the measurement and description of the physical features of bodies of water and the land areas that are affected by those bodies of water

Hydrostatic Equilibrium: a state when the compression due to gravity is equally balanced by the pressure gradients in the opposite direction (under the water level); used to analyze the buoyancy of the design

Hydrostatics: the study of the pressures exerted and other characteristics of fluids at rest

Ichthyofauna: the indigenous fish of a region

Leading Edge: the edge of the helical rotor which follows the crest of the propagating wave

Linear Wave Theory: a theory that gives a linearized description of the propagation of waves on the surface of the ocean; assumes the fluid has a uniform mean depth and that the flow is inviscid, incompressible, and irrotational

Multi Leg Mooring: a mooring system in which two or more mooring lines are used to restrain a floating structure; minimizes the motion of the floating object and increases the stability of the system from that of a single point system

Multi-Component Waves Pattern: a wave form defined by the superposition of two or more waves of differing parameters (i.e. amplitude, frequency, phase, direction).

Open-cell foam: foams with a make-up that does not resist the entrance of air and fluids; also has a smaller specific strength and rigidity compared to closed-cell foam

Oscillating Water Column: a partially submerged, hollow device which encompasses a "column" of part air, part water; the vertical rise and fall of the water column causes compression and decompression of the air within the device; the air flow causes a turbine to rotate producing electricity

Oscillating Wave Surge Converter: wave energy converter device which uses the motion of the

water particles within the waves to extract the horizontal energy; consists of a paddle arm which pivots on a horizontal axis and a hydraulic pump which absorbs the energy associated with the oscillation of the paddle arm

Overtopping Device: wave energy converter device composed of a collector, which collects the water of passing waves, a ramp, which channels the water towards a reservoir, and a reservoir, which stores the water until it is released; as the water in the reservoir is released, it turns hydro-turbines, which converts the stored energy into usable power

Pitch: the horizontal distance along the rotor that is required for the helical shape to make one complete spiral rotation

Point Absorber: a wave energy converter in which the components of the device move relative to each other, causing the relative motion to drive and electromechanical or hydraulic energy converter; can be classified as a floating point absorber or a submerged pressure differential device

Rotary Wave Energy Converter: a wave energy conversion device that floats at mean water level and rotates due to the pressure differential between the leading edge and the trailing edge

Sea State: a wave situation that is constant over a given time interval

Semi Taut Mooring: a variation of the taut mooring line arrangement in which the lines are not under constant tension but still remain partially taut at all times

Significant Wave Height: the average of the upper-third of the size-ordered sample of all wave heights for the specific time interval; noted by Hs

Single Frequency Waves: a wave form defined by a single set of parameters (i.e. amplitude, frequency, phase, direction).

Single Point Mooring: a simple mooring system consisting of one float (usually a buoy of

111

some sort), one line, and one anchor

Taut Mooring: an arrangement of mooring lines in which the lines are under constant tension, thus reducing the footprint from that of catenary mooring lines; requires the anchors to withstand vertical forces as well as horizontal forces

Trailing Edge: the edge of the helical rotor that is opposite of the leading edge

Trough: the lowest point on a wave

Wave climate: the temporal distribution of wave height, period, and direction

Wave Energy Converter: a device used to convert the energy which is stored in ocean waves into usable power

Wave Energy Farm: a strategic placement of wave energy converters in order to optimize the energy extraction capabilities of the devices; can be parallel, where the devices are aligned next to each other in a parallel formation, or staggered, where the devices are offset by a certain distance

Wave Height: the vertical distance from the crest of the wave to the trough of the wave

Wave Length: the horizontal distance between peaks (crests) of a wave; also the horizontal distance between troughs on a wave

Wave regime: the average wave properties along a coast

Appendix B: Stress Analysis Data Tables

Table 8: Parameters for stress analysis

Parameter	Units	Value
Foam Density	slug/in^3	0.00579
Aluminum Density	slug/in^3	0.09754
Water Density	slug/in^3	0.03613
Aluminum Yield Strength	lbf/in^2	32000
Helix Radius	in	2.000
Rod Outer Radius	in	0.500
Rod Inner Radius	in	0.250
Helix Length	in	72.00
Rod Length	in	72.00
Helix Volume	in^3	282.7433
Rod Volume	in^3	42.4115
Total Volume	in^3	14.1372
Displaced Fluid Volume	in^3	162.5774
Moment of Inertia	in^4	0.04602
Helix Weight	lbf	1.6362
Rod Weight	lbf	4.1370
Gravity Force	lbf	5.7732
Buoyancy Force	lbf	5.8735
Resultant Force	lbf	0.1003

Table 9: Load, shear, and moment data for stress analysis

Position	Load	Shear	Moment	Stress	Safety Factor
in	lbf/in	lbf	lbf-in	lbf/in^2	-
0.00	-0.05746	2.8866	0.000	0.00	
2.25	-0.06065	2.7537	6.347	68.96	464.06
4.50	-0.06385	2.6137	12.386	134.58	237.78
6.75	-0.06705	2.4664	18.103	196.69	162.69
9.00	-0.07024	2.3120	23.480	255.11	125.44
11.25	-0.07344	2.1503	28.501	309.67	103.34
13.50	-0.07663	1.9815	33.151	360.18	88.84
15.75	-0.07983	1.8055	37.413	406.49	78.72
18.00	-0.08302	1.6223	41.270	448.40	71.36
20.25	-0.08622	1.4319	44.707	485.75	65.88
22.50	-0.08942	1.2343	47.708	518.35	61.73
24.75	-0.09155	1.0299	50.256	546.03	58.60
27.00	-0.09155	0.8239	52.342	568.69	56.27
29.25	-0.09155	0.6179	53.964	586.32	54.58
31.50	-0.09155	0.4120	55.123	598.91	53.43
33.75	-0.09155	0.2060	55.818	606.46	52.77
36.00	-0.09155	0.0000	56.050	608.98	52.55
38.25	-0.09155	-0.2060	55.818	606.46	52.77
40.50	-0.09155	-0.4120	55.123	598.91	53.43
42.75	-0.09155	-0.6179	53.964	586.32	54.58
45.00	-0.09155	-0.8239	52.342	568.69	56.27
47.25	-0.09155	-1.0299	50.256	546.03	58.60
49.50	-0.08942	-1.2343	47.708	518.35	61.73
51.75	-0.08622	-1.4319	44.707	485.75	65.88
54.00	-0.08302	-1.6223	41.270	448.40	71.36
56.25	-0.07983	-1.8055	37.413	406.49	78.72
58.50	-0.07663	-1.9815	33.151	360.18	88.84
60.75	-0.07344	-2.1503	28.501	309.67	103.34
63.00	-0.07024	-2.3120	23.480	255.11	125.44
65.25	-0.06705	-2.4664	18.103	196.69	162.69
67.50	-0.06385	-2.6137	12.386	134.58	237.78
69.75	-0.06065	-2.7537	6.347	68.96	464.06
72.00	-0.05746	-2.8866	0.000	0.00	

Appendix C: Stress Analysis Diagrams
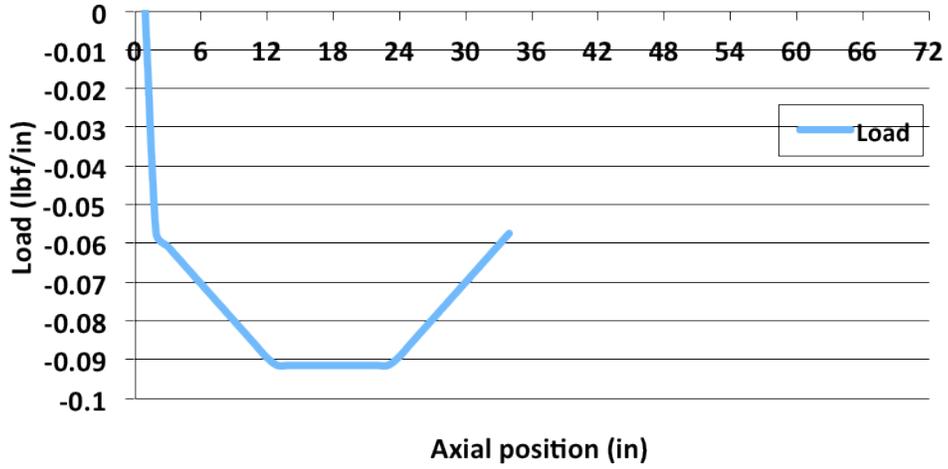
Figure 51: Calculated load applied to device
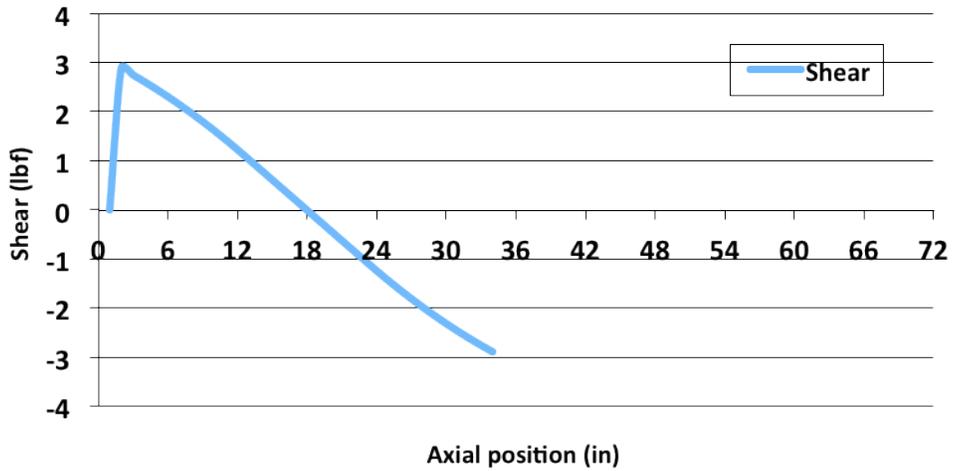
Figure 52: Calculated shear applied to device
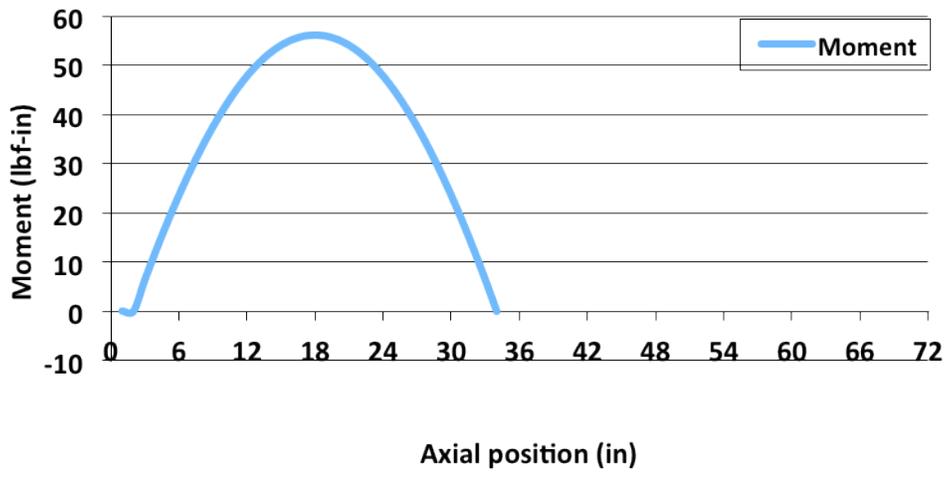
Figure 53: Calculated moment applied to device

Appendix D: Common Laboratory Setup Instructions

1) Before going to the side of the wave maker with the computer equipment, go to the circuit breaker (currently, outside of the curtain isolating the wave maker from construction). The circuit breaker is labeled "Next to New Tank".

2) On circuit breaker, check switch 4 labeled '2D+T Wave Maker'. If the switch is not set to 'on' (to the left), do so.

3) Unless otherwise advised, the carriage should be moved towards the beach to avoid interference with the mooring structure. Doing so requires two people, one on each side of the tank.

4) Near the computer equipment, set the large gray circuit switch to the on position. Turn large white power strip, located on large black box, to the on position.

5) If the computer is not turned on, do so. Acquire access to the computer via a laboratory personnel present if the proper credentials are not known.

6) Double-click the icon labeled 'BWG.EXE' on the desktop. Wait for application to open.

7) On the menu bar, select 'Access Privilege – Extended'.

8) On the menu bar, select 'File – Restore Settings', a file dialog appears. In the file dialog, choose the file 'C:\Program Files\wedge wavemaker\Gemstone project\091110.set'. Click 'OK'.

9) In the menu bar, select 'Operations – Board Programs', a window appears. In the window, select 'Board #1', a file dialog appears. In the file dialog, chose a file from the C:\Program Files\wedge wavemaker\Gemstone project\final testing project' folder with the desired

frequency.   Click 'OK'.

10) In the menu bar, select 'Display – Oscilloscope', the 'Board Program' window appears.   In the window, click 'A' and select 'Board #1 Program'.   In the window, click 'B' and select 'Board #1 Displacement'.

11) On the main window, click 'Reset'.   On the 'Board Program' window, click 'Reset'.

12) If all or some of the lights on the main window or the 'Board Program' window are not green (i.e. red), ensure that the emergency brake (red button next to computer equipment) is released.   To release, twist up button.

13) Check behind the wave maker to ensure that no objects and/or personnel are obstructing the wave maker's path.

14) With one person on each side of the tank, lower the beach into the water.

15) On the 'Board Program' window, set 'Power' to 'On'.   Select 'Home' for 'Setpoint'.

16) If and only if all lights in both the main window and 'Board Program' window are green, press 'Start'.

17) In the case that the wave maker is producing a noise not heard normally during operation, press the 'Emergency Brake' button.

18) Once the program has completed, press 'Stop'.

19) On the 'Board Program' window, set 'Power' to 'Off'.

20) Repeat Steps 11 through 20 the desired number of times.

21) Quit program and turn all the power off (i.e. computer, power strip, both circuits).

22) With one person on each side of the tank, raise the beach out of the water.

23) Run the multi-component profile script.

Appendix E: Simplified Script for Wave Maker Input

```
%This code was adapted from the code for making dispersively focused wave
%packets.  It is designed to make a sinusoidal wave motion with a given
%frequency, wave-maker amplitude, and number of waves.  All theo ther input
%parameters are commented out by J. Diorio (11/20/09).  Some of the
%parameters in this file may be superfluous.



clear all
%
XBB = 6.0;           %   /* breaking distance in frequency      */
XB = 10.0;          %/* breaking position              */
Z0 = 30.0;           % /* start position                     */
Z1 = 27.0;           %/* ending position                   */
TM = 12.0;           % /* running time                     */
 FREQ = 1.15;            % /* frequency of wavemaker         */
 NW   = 10.0;               %/* number of waves (crests)        */
 TA1 =  1.0;            %/* start time frame function         */
% // The followings are changed for new tank, by Liu08/25/03
TANKDEP = 1016.0;       % Depth of water in tank*/
%  /*This WATERL is only for NRL RADAR project by Liu 08/18/00 */
% /* #define WATERL          277.0; */
WATERL = 178.0;            % /* water level from the ruler in mm*/
SUBM = 0.35792;           %/* Submergence                */
AMPLIFAC= 0.0405;        % /* Amplification Factor           */
% #define RATIO          0.6            /* Time ratio for tp
*/
% #define DELTAO         -0.1           /* (omega2-omega1)/omegaave
*/
 BETA = 5.0;
 FHI= 90.0 ;             %/* phase                         */
% /*This initial SN is 200.0. It is changed by Liu for RPI 1/22/2001*/
SN =  100.0; %          /* sample # in one second (400 changed 04/13/04)
*/
PI =  3.14159265;
DFOAF =     0.6666;          %/* delta freq. over ave. freq.        */
GRAV = 9.81;     % /* gravity in m/s/s                */

% #define TDLY             0.5              /* time delay after wavemaker
*/
% // XX3 is modified after new tank is built. Old value is 300.0
XX3 = 170.0;          %  /* motion distance in inches         */
XXDOT = 31.5;          %   /* velocity in inches per second     */
XXDDOT = 30.0;  %          /* accelerat. in inches per second^2*/
TDLY = 0.5;

disp('/');
disp('/');
disp('The wavemaker input!!!!')
disp('/');
disp('/');
```

```matlab
  freq = input('Wave frequency (0.7 - 4.0 [Hz], default = 1.15)  freq =');
     if (freq == 0.0)   freq = FREQ; end;
     if ((freq < 0.7) | (freq > 4.0)),
        freq = input('Wrong frequency. Please input again. freq = ');
   end;

  scalfac= GRAV/2.0/PI/freq/freq; %/*scalfac is the wavelength in m*/

  %waterl = input('Water level (in the ruler in mm, [-700.0-300.0], default =
178.0), waterl = ');
  waterl = 0.0;
     if (waterl == 0.0)  waterl = WATERL; end;
     if ((waterl < -700.0) | (waterl > 300.0))
        waterl = input('Wrong water level. Please input again. waterl =');
   end;

  %subm = input('Scaled submergence,  (0.0-0.5, default = 0.35792), subm =
');
  subm = 0.0;
     if (subm == 0.0)   subm = SUBM; end;
     if ((subm < 0.0) | (subm > 0.5)),
        subm = input('Wrong scaled submergence. Please input again. subm =
');
   end;
  tsubm=subm*scalfac;
%     if (tsubm > 0.5)  {
%          printf("Submergence, %8.4f meters, out of range. \n", tsubm);
%          printf("Wrong data. Please input again. \n"); goto lpsubm; }
     subm=tsubm*1000.0;  %/*subm is now the submergence in mm*/

  amplifac = input('Scaled amplitude (0.0-0.06, default = 0.0405), amplifac =
');
     if ((amplifac < 0.0) | (amplifac > 0.06)),
        amplifac = input('Wrong scaled amplitude. Please input it again.
amplifac =');
   end;
     if (amplifac == 0.0)   amplifac = AMPLIFAC; end;
     ampt=amplifac*scalfac;
%     if ((ampt < 0.0) || (ampt > 0.15)) {
%          printf("Amp, %8.4f meters, out of range. \n", ampt);
%          printf("Wrong data. Please input again. \n"); goto lpc; }

% Commented on March 18, 2005

% % %   dfoaf = input('Delta freq. / ave. freq.  (0.0-1.6, default = 0.6666):
dfoaf = ');
% % %       if ((dfoaf < 0.0) | (dfoaf > 1.6)),
% % %         dfoaf = input('Wrong data. Please input it again. dfoaf =');
% % %      end;
% % %       if (dfoaf == 0.0)   dfoaf = DFOAF; end;
% % %
% % %    nw = input('Number of components  (0 - 100, default = 32):  nw =');
% % %       if ((nw < 0) | (nw > 100))
% % %         nw = input('Wrong data. Please input it again. nw=');
% % %      end;
% % %       if (nw == 0)    nw = NW; end;
% % %
```

```matlab
% % %    xbb = input('Break. dist. in wavelength (0.0 - 20.0, default = 6.0):
xbb = ');
% % %          if ((xbb < 0.0) | (xbb > 30.0)),
% % %            xbb = input('{Wrong data. Please input it again. xbb=');
% % %        end;
% % %          if (xbb == 0.0)   xbb = XBB; end;

   nw = input('Number of waves  (0 - 40, default = 10):  nw =');
      if ((nw < 0) | (nw > 40))
         nw = input('Wrong data. Please input it again. nw=');
      end;
        if (nw == 0)   nw = NW; end;

 %beta = input('Beta, slope for front window (0.0-10.0, default = 5.0):  beta
= ');
 beta = 0.5;
      if ((beta < 0.0) | (beta > 10.0)),
         beta = input('Wrong data. Please input it again. beta=');
      end;
        if (beta == 0.0),   beta = BETA; end;

 %beta2 = input('Beta, slope for back window (0.0-10.0, default = 5.0):
beta2 = ');
 beta2 = 1.0;
      if ((beta2 < 0.0) | (beta2 > 10.0)),
         beta2 = input('Wrong data. Please input it again. beta2=');
      end;
        if (beta2 == 0.0),   beta2 = BETA; end;


  %ta1 = input('start time for frame function, (0.0-6.0, default = 1.2): ta1
= ');
  ta1 = 0.0;
      if ((ta1 < 0.0) | (ta1 > 6.0)),
         tal = input('Wrong data. Please input it again.  ta1=');
      end;
        if (ta1 == 0.0),    ta1 = TA1; end;

  %fhi = input('phase in degree  ([-180.0 180.0], default = 90.0): fhi = ');
  fhi = 0.0;
      if ((fhi < -180.0) | (fhi > 180.0)),
         fhi = input('Wrong data. Please input it again. fhi=');
      end;
        if (fhi == 0.0)    fhi = FHI; end;

        fhi = fhi * PI / 180.0; %/* conversion degree into rad */

   fi = 0.0;  sn = SN;

%   /* Convert from dimensionless input to dimensional parameters */
%   /* This is changed by Liu, 08/24/99 for keeping constant water level in
tank. */
% /*  waterl = TANKDEP-(TANKDEP-waterl)*scalfac; */
% // For NRL RADAR, the following line was marked to change water level, by
Liu, 08/18/00
% //  waterl = TANKDEP-(TANKDEP-waterl)*1.1806; marked by Liu for new tank
%  // z0 = (subm + waterl + 137.0) / 25.4+5.0;  marked by Liu for new tank
```

122

```
%
%  z0 = subm/25.4 + 19.087 + (waterl -178.0)/25.4; %This is changed in the
%  MTS program
  z0= 0.0;
% % %   xb = xbb * scalfac;

% % %   delf = dfoaf * freq;
% % %   aveom = freq * 2.0 * PI;
% % %   delom = delf * 2.0 * PI;
% % %   om1 = aveom - delom / 2.0;
% % %   dom = delom / (nw - 1);
% % %   for i=1: nw,
% % %       om(i) = om1 + (i-1)* dom;
% % %       kk(i) = om(i) * om(i) / GRAV;
% % %       cgg(i) = om(i) / (2.0 * kk(i));
% % % %  //     ai[i] = 2.0*PI/kk[i]/scalfac/nw; marked by Liu 09/23/03
% % % %  //     ai[i] = 5.0*PI/kk[i]/sqrt(om[i])/scalfac/nw;  marked by
Duncan 09/26/03
% % %       ai(i) = 1.8605*PI/kk(i)/sqrt(om(i)/aveom)/scalfac/nw;
% % %   end

   omg = 2*pi*freq;
   cgg = GRAV/omg/2.0;
   kk = omg*omg/GRAV;
   %SPH 02/22/2010
   %this is why the amplitude changes
   ai = 2.0*PI/kk;%<--

% % %   cgave=0.0;
% % %   for i=1:nw,
% % %       cgave=cgave+cgg(i);
% % %   end;
% % %   cgave=cgave/nw;
% % %
% % %   for i=1:nw,
% % %       phase(i)=xb*(om(i)/cgave-kk(i))+fhi;
% % %   end;



%   t1 =  ta1*xb*(1.0/cgave-1.0/cgg(nw));
%   t2 =  ta1*xb*(1.0/cgave-1.0/cgg(1));
% %   tm =   2.0*(t2-t1);
%   tm = t2-t1;
  nfr= beta*freq;
  nfr2 = beta2*freq;
  t1 = 3.0/nfr;
  t2 = 2*t1+ nw/freq+4.0/nfr2;
  tm = t2-t1;


% Carriage input
% disp('/');
% disp('/');
% disp('The carriage input!!!!')
% disp('/');
% disp('/');
```

```matlab
sn = SN;

  %tdly = input('Time delay after wavemaker (0.0- , default = 0.5  sec):
tdly=');
  tdly = 0.0;
      if (tdly < 0.0),
         tdly = input('Wrong data. Please input it again. tdly=');
    end;
      if (tdly == 0.0), tdly = TDLY; end;

  %xx3 = input('Distance of towing motion= (0-180, default = 170.0 in): xx3 =
');
  xx3 = 0.0;
      if ((xx3 < 0.0) | (xx3 > 180.0)),
         xx3 = input('Wrong data. Please input it again. xx3 =');
    end;
      if (xx3 == 0.0)        xx3 = XX3; end;
  %xxdot = input('Speed of towing motion= (0.0-49.0, default = 31.5 in/sec):
xxdot =');
  xxdot = 0.0;
      if ((xxdot < 0.0) | (xxdot > 49.0)),
         xxdot = input('Wrong data. Please input it again. xxdot =');
    end;
      if (xxdot == 0.0)        xxdot = XXDOT; end;

  %xxddot = input('Acceleration of towing motion= (0-40, default = 30.0
in/sec/sec): xxddot =');
  xxddot = 0.0;
      if ((xxddot < 0.0) | (xxddot > 40.0)),
         xxddot = input('Wrong data. Please input it again. xxddot =');
    end;
      if (xxddot == 0.0)        xxddot = XXDDOT; end;

 tdy = tdly*sn;
 dtt = xx3/xxdot;
 pdt =xxdot/xxddot;
 it9 = round(pdt*sn);
 it1 = tdy + it9;
 it2 = it1 + round(dtt*sn);
 it3 = it2 + it9;
 xddd = xxddot*xxddot/2./xxdot;
 total_point = max(it3, round(sn*(t2+1)));

 clear zz;
 % Wave maker motion
%   total_point = round(sn/freq*(tm+10));
  for i = 1:total_point,
      ti(i) =(i-1)/sn;
      ztemp = ai*cos(fhi-omg*ti(i));
% % %           ztemp = 0.0;
% % %           for j = 1:nw,
% % %              ztemp = ztemp + ai(j)*cos(phase(j) - om(j)*ti(i));
% % %         end
        w = 0.25*(tanh(nfr * (ti(i) - t1)) + 1.0) *(1.0 - tanh(nfr2 * (ti(i)
- t2)));
        zz(i) = z0 - amplifac * 39.37 * w * ztemp;
    end
```

```matlab
  %carriage motion array

%   clear speed_carr;
%   clear x_carr;
 for i=1:tdy,
     speed_carr (i) = 0;
 end
 for i=tdy:it1,
     rmvolt = xxdot/2.+xxddot*(i-it1)/sn;
     dvolt = xddd*(i-it1)/sn*(i-it1)/sn;
     speed_carr(i) = rmvolt + dvolt;
 end
 for i=it1:it1+it9,
     rmvolt = xxdot/2.+xxddot*(i-it1)/sn;
     dvolt = xddd*(i-it1)/sn*(i-it1)/sn;
     speed_carr(i) = rmvolt - dvolt;
 end

 for i=it1+it9:it2-it9,
     speed_carr(i) = xxdot;
 end
 for i=it2-it9: it2,
     rmvolt = xxdot/2.- xxddot*(i-it2)/sn;
     dvolt = xddd*(i-it2)/sn*(i-it2)/sn;
     speed_carr(i) = rmvolt-dvolt;
 end
  for i=it2:it3,
     rmvolt = xxdot/2.- xxddot*(i-it2)/sn;
     dvolt = xddd*(i-it2)/sn*(i-it2)/sn;
     speed_carr(i) = rmvolt+dvolt;
 end
 for i=it3:total_point,
     speed_carr(i) = 0;
 end

x_carr(1) = 0;
for i=2:total_point,
    x_carr(i) = x_carr(i-1) - speed_carr(i)/sn;
end

figure(1)
plot(zz)

figure(2)
plot(speed_carr)
hold on
plot(x_carr, 'r');
hold off

for i=1:total_point,
    carr_wedge(i, 1) = zz(i);
    carr_wedge(i, 2) = x_carr(i);
end

% save('test_dat.txt','carr_wedge','-ASCII');
```

```matlab
%save('test_dat.txt','carr_wedge','-float');
fidd = fopen('output_fall_2009.txt','w');
% fprintf(fidd, '%12.8f', 1/sn);
fprintf(fidd, '%12.8f \t %12.8f\n', [zz; x_carr]);
fclose(fidd);
```

Appendix F: Multi-component Profile Script

```
%%  Multi-component wave profile generator
%
% Purpose:   Takes as input the significant wave height, frequency
%            range, and number of frequency components in the wave
%            packet.  Gives as output a signal comprised of a series
%            of sinusoidal waves.  The components shall have
%            frequencies uniformly distributed on a given range.  The
%            components shall have wave heights distributed across a
%            power spectrum.
%
% Author:    Sean Henely
%
% Language:  MATLAB 7.10
%
% *===============================================*
% |   University of Maryland College Park         |
% |                                               |
% |     Honors College                            |
% |     Gemstone Program                          |
% |     Cohort of 2011                            |
% |                                               |
% |     Glenn L. Martin Institute of Technology   |
% |     A. James Clark School of Engineering      |
% |     Department of Mechanical Engineering      |
% |     The Burgers Program for Fluid Dynamics    |
% |     Hydrodynamics Laboratory                  |
% *===============================================*
%
% *===============================================*
% |  Water and Versatile Energy Systems (WAVES)   |
% |                                               |
% |    Sean Henely                                |
% |    Laura Hereford                             |
% |    Mary Jung                                  |
% |    Tatsuya Saito                              |
% |    Edward Toumayan                            |
% |    Sarah Watt                                 |
% |    Melanie Wong                               |
% |                                               |
% |  Mentor:    Dr. James Duncan                  |
% |  Librarian: Ms. Nevenka Zdravkovsk            |
% *===============================================*


%%  Revision History
%
% Date          Author      Change Summary
% ----          ------      --------------
% 01/08/2011    shenely     Translation from Python 2.6 to MATLAB 7.10
% 01/10/2011    shenely     Removed gravity constant, changed
%                           everything to English units
```

```
% 01/17/2011    shenely    Runs for constant time, amplitudes based
%                          on average wave height
% 01/19/2011    shenely    Corrected window function, separate runs
%                          now repeatable, added wave hieght and
%                          frequency inputs, reworked wedge
%                          displacement
% 01/21/2011    shenely    Saves figures after displaying
% 02/20/2011    shenely    Renamed to be more appropriate


%% Constant Section
REV_TO_RAD  = 2 * pi;%Revolutions to radians

WAVE_HEIGHT   = 4.0;%Average wave height (RMS) [in]
MAX_AMPLITUDE = 6.0;%Maximum displacement of wedge [in]

FREQUENCY_MIN_LIMIT = 0.7;%Wedge lower frequency limit [Hz]
FREQUENCY_MIN = 0.8;%Minimum frequency [Hz]
FREQUENCY_MAX = 1.2;%Maximum frequency [Hz]
FREQUENCY_MAX_LIMIT = 4.0;%Wedge upper frequency limit [Hz]

SAMPLE  = 1e2;%Sampling rate [Hz]

HARMONICS   = 2;%Number of wave frequencies (harmonics)
HARMONICS_MAX= 5;%Maximum number of harmonics

RUN_TIME = 40.0;%Total run time (s)

ITERATIONS = 10;%Number of iterations

WINDOW_SLOPE  = 5;%Window slope  factor (both sides)
WINDOW_OFFSET = 3;%Window offset factor (both sides)

%Wave power spectrum - Bretschneider
BRETSCHNEIDER = @(f,Hsig,fM,a,b)...
             a * (Hsig ^ 2 / fM) * (f / fM) .^ - 5 .* ...
             exp(- b * (f / fM) .^ - 4);

%Output filename format
OUTPUT_FORMAT = 'output_sig%3.2f_min%3.2f_max%3.2f_num%d';


%% Determine significant wave height
%
% BEGIN
%   WHILE loop not broken
%     Propmt for wave height
%       Range:  0.0-12.0
%       Default:  4.0
%
%     IF a number is given
%       IF number is range
%         BREAK out of loop
%       ELSE
%         Invalid wave height given
%     ELSE IF no number is given
%       Set wave height to default
```

128

```matlab
%      BREAK out of loop
%    ELSE
%      Non-numeric value given
%    END IF
%   END WHILE
% END

while (1)
  str = input('Significant wave height (0-6.0, default = 4.0):  ','s')

  [Hsig,isdigit] = str2num(str);
  if (isdigit == 1)
    if ((Hsig > 0) & (Hsig <= 2 * MAX_AMPLITUDE))
      break
    else
      printf('Wave height not in range.')
    end
  elseif strcmp(str,'')
    Hsig = WAVE_HEIGHT;
    break
  else
    printf('Not a numeric value.')
  end
end


%%  Determine range of frequencies
%
% BEGIN
%   WHILE loop not broken
%     Prompt for minimum frequency
%       Range:  0.7-4.0
%       Default:  0.8
%
%     Prompt for maximum frequency
%       Range:  0.7-4.0
%       Default:  1.2
%
%     IF a numbers is given
%       IF numbers are in range
%         BREAK out of loop
%       ELSE
%         Invalid frequency given
%     ELSE IF no numbers is given
%       Set minimum frequency to default
%       Set maximum frequency to default
%       BREAK out of loop
%     ELSE
%       Non-numeric values given
%     END IF
%   END WHILE
% END

while (1)
  str1 = input('Minimum frequency (0.7 - 4.0 [Hz], default = 0.8):  ','s');
  str2 = input('Maximum frequency (0.7 - 4.0 [Hz], default = 1.2):  ','s');
```

129

```matlab
    [Fmin,isdigit1] = str2num(str1);
    [Fmax,isdigit2] = str2num(str2);
    if ((isdigit1 == 1) && (isdigit2 == 1))
      if (((Fmin >= FREQUENCY_MIN_LIMIT) && (Fmin <= FREQUENCY_MAX_LIMIT)) & ...
          ((Fmin >= FREQUENCY_MIN_LIMIT) && (Fmin <= FREQUENCY_MAX_LIMIT)))
        break
      else
        printf('Frequecies not in range.')
      end
    elseif (strcmp(str1,'') && (strcmp(str2,'')))
      Fmin = FREQUENCY_MIN;
      Fmax = FREQUENCY_MAX;
      break
    else
      printf('Not numeric values.')
    end
end


%% Determine number of harmonics
%
% BEGIN
%   WHILE loop not broken
%     Propmt for number of harmonics
%       Range: 1-50
%       Default: 10
%
%     IF a number is given
%       IF number is is range
%         BREAK out of loop
%       ELSE
%         Invalid number of harmonics given
%       ELSE IF no number is given
%       Set number of harmonics to default
%       BREAK out of loop
%     ELSE
%       Non-numeric value given
%     END IF
%   END WHILE
% END

while (1)
  str = input('Number of harmonics (1-5, default = 2): ','s');

  [n,isdigit] = str2num(str);
  if (isdigit == 1)
    if ((n > 0) && (n <= HARMONICS_MAX))
      break
    else
      printf('Number of harmonics not in range.')
    end
  elseif strcmp(str,'')
    n = HARMONICS;
    break
  else
    printf('Not a numeric value.')
  end
```

```matlab
    end

%%  Time domain
t = 0:(1 / SAMPLE):RUN_TIME;

%Frequency mean and difference
Fmean = (Fmax + Fmin) / 2;
Fdiff = (Fmax - Fmin) / 2;

%% Iteration to caputer divergence of frequency
for ii = 0:ITERATIONS

  %%  Frequency domain
  f = linspace(Fmean - ii * Fdiff / ITERATIONS,...
            Fmean + ii * Fdiff / ITERATIONS,n + 1);

  %%  Compute power spectrum
  S = BRETSCHNEIDER(f,Hsig,Fmean,0.3125,1.25);

  %%  Wave properties
  a     = sqrt(4 .* S .* Fdiff ./ n);%Amplitude [in]
  omega = f * REV_TO_RAD;            %Frequency [rad/s]
  %phi   = REV_TO_RAD * rand(1,n + 1);      %Phase [rad]
  phi   = zeros(1,n + 1);            %Phase [rad]

  %%  Window function properties
  beta = WINDOW_SLOPE ./ f;%Front and back slope
  t1   = WINDOW_OFFSET ./ beta;%Front slope offset
  t2   = t(end) - t1;        %Back  slope offset


  %%  Wedge displacement
  %
  % BEGIN
  %   Set wedge displacement to zero (0)
  %   FOR each harmonic
  %     Calculate wave profile
  %     Calculate window function
  %
  %     Subtract product of wave profile and window function from
  %      wedge displacement
  %   END FOR
  % END

  z = zeros(size(t));
  for (jj = 1:(n + 1))
    eta = a(jj) * sin(omega(jj) * t - phi(jj));
    win = (1 + tanh(beta(jj) * (t - t1(jj)))) .*...
          (1 - tanh(beta(jj) * (t - t2(jj)))) / 4;

    z = z - eta .* win;
  end

  %%  Create plot of wedge displacement vs. time
  figure(ii+1);
  plot(t,z);
  title('Wedge displacement [in] vs. time[s]')
```

131

```matlab
    xlabel('Time [s]');
    ylabel('Displacement [in]');

saveas(figure(ii+1),strcat(sprintf(OUTPUT_FORMAT,Hsig,f(1),f(end),n),'.bmp'))
;

    %%  Print wedge displacement to file
    fout = fopen(strcat(sprintf(OUTPUT_FORMAT,Hsig,f(1),f(end),n),'.txt'),'w');
    fprintf(fout,'%12.8f\t0.0\n',z);
    fclose(fout);
end
```

Appendix G: Multi-component Wave Profiles Used During Experimentation
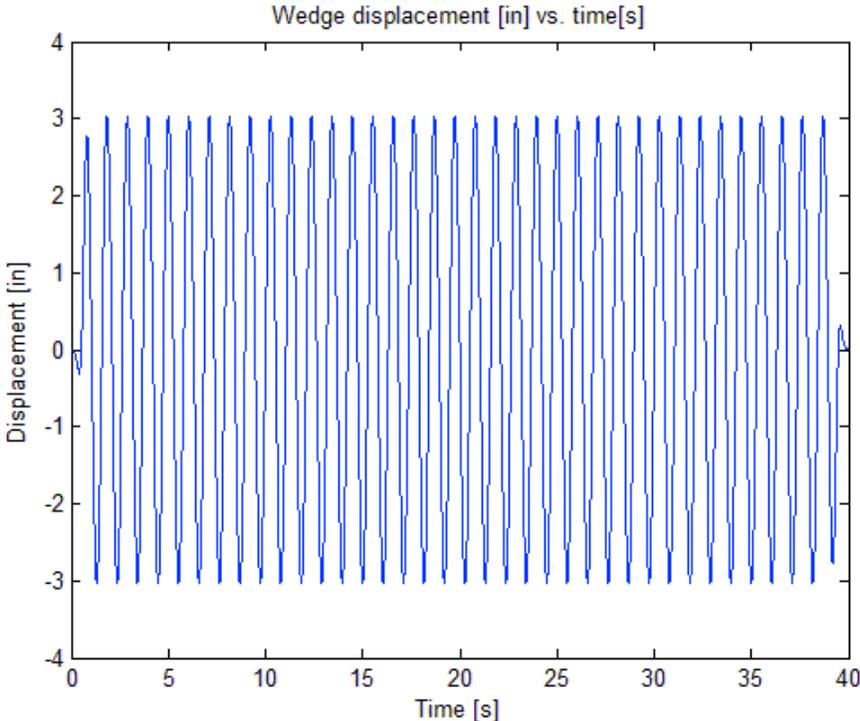
Figure 54: Multi-component wave form: Hsig=6in, Fmin=0.950Hz, Fmax=0.950Hz
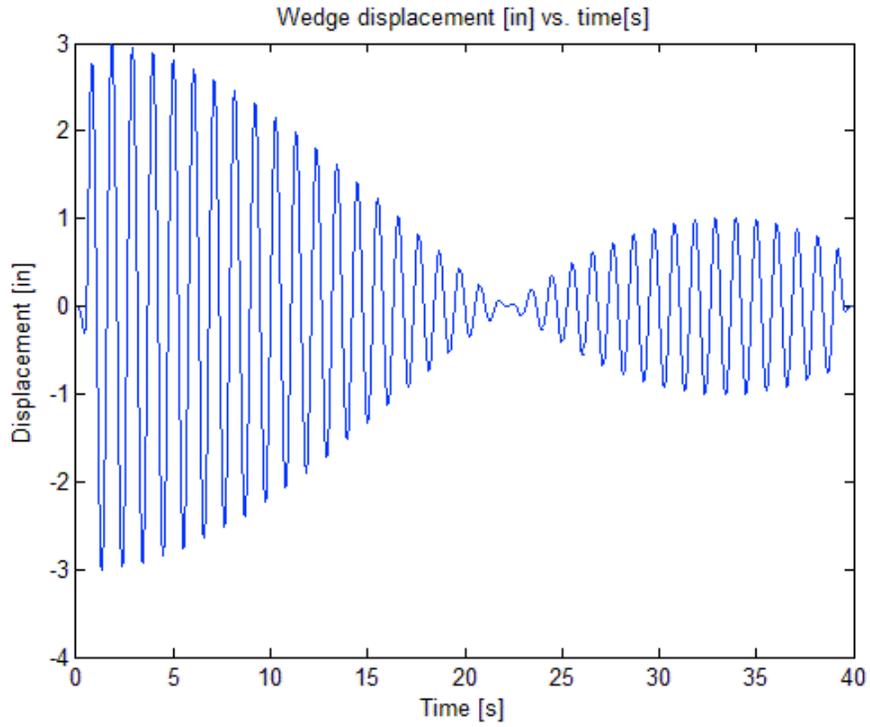
Figure 55: Multi-component wave form: Hsig=6in, Fmin=0.935Hz, Fmax=0.965Hz
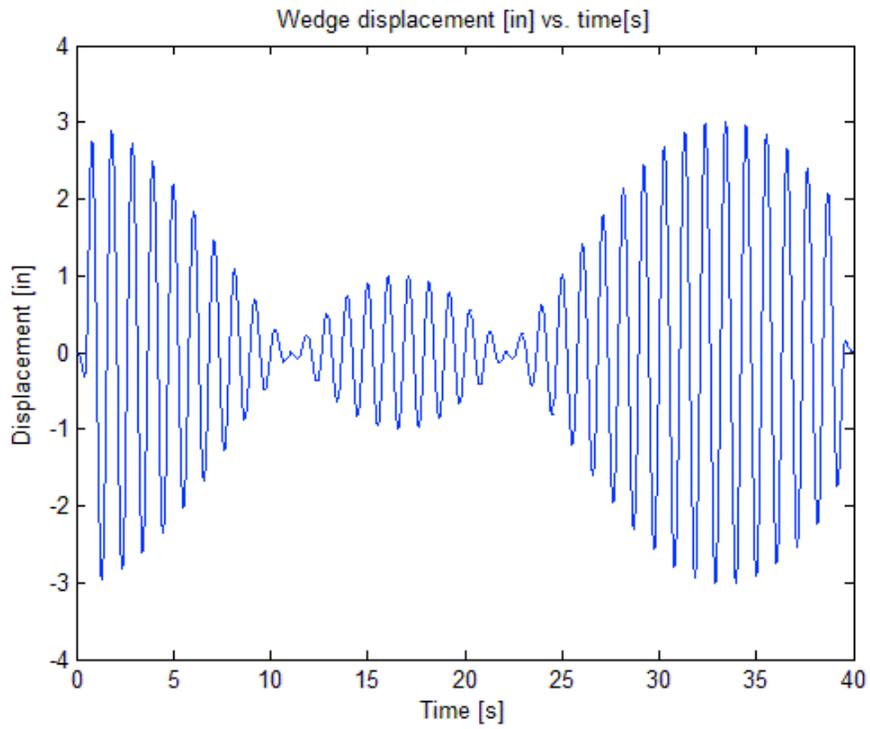
Figure 56: Multi-component wave form: Hsig=6in, Fmin=0.920Hz, Fmax=0.980Hz

134
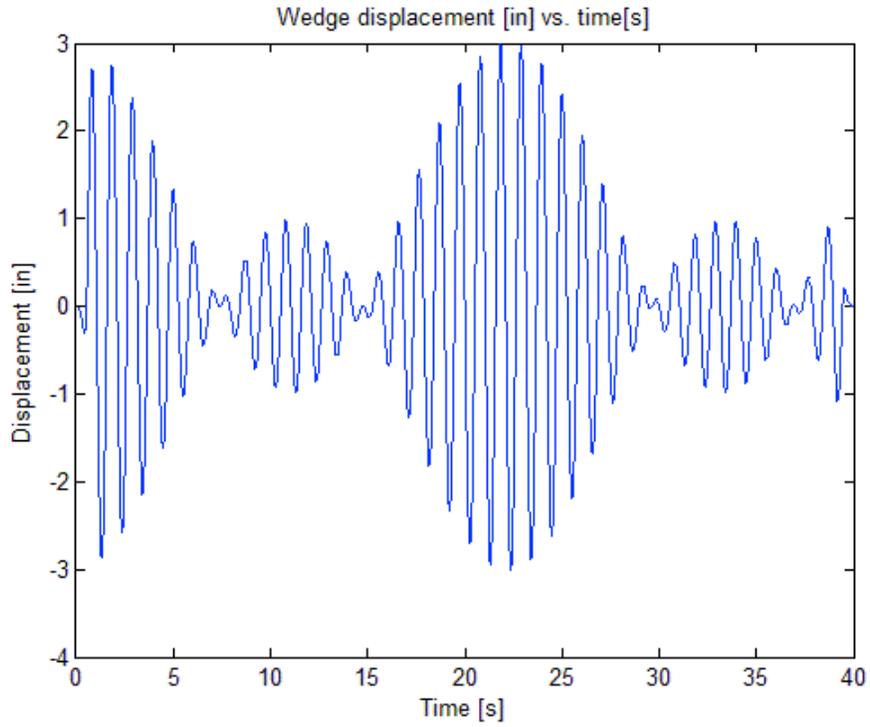
Figure 57: Multi-component wave form: Hsig=6in, Fmin=0.905Hz, Fmax=0.995Hz
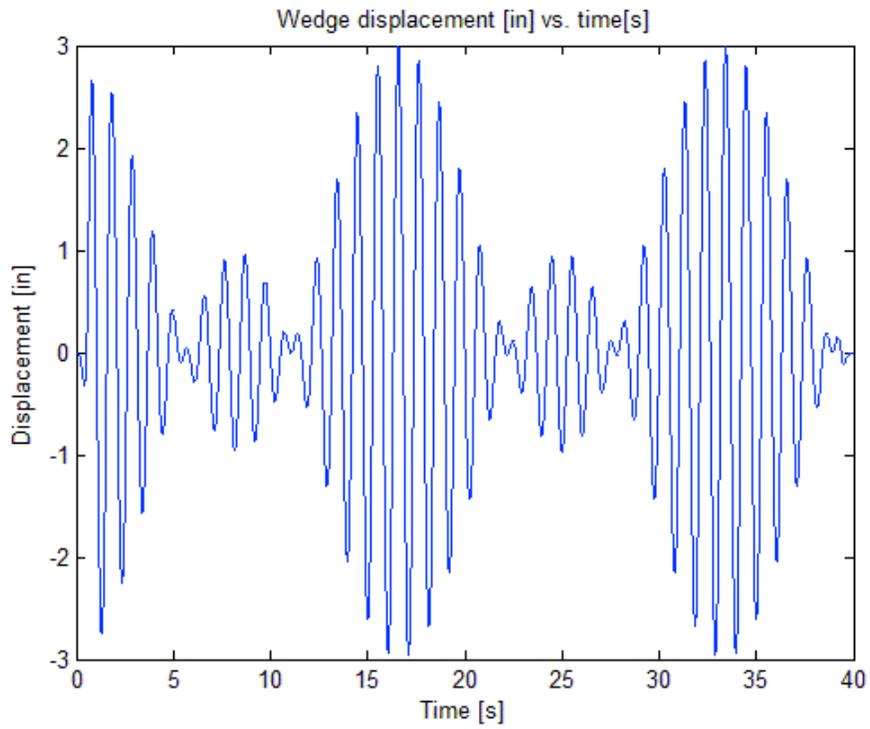
Figure 58: Multi-component wave form: Hsig=6in, Fmin=0.890Hz, Fmax=1.010Hz
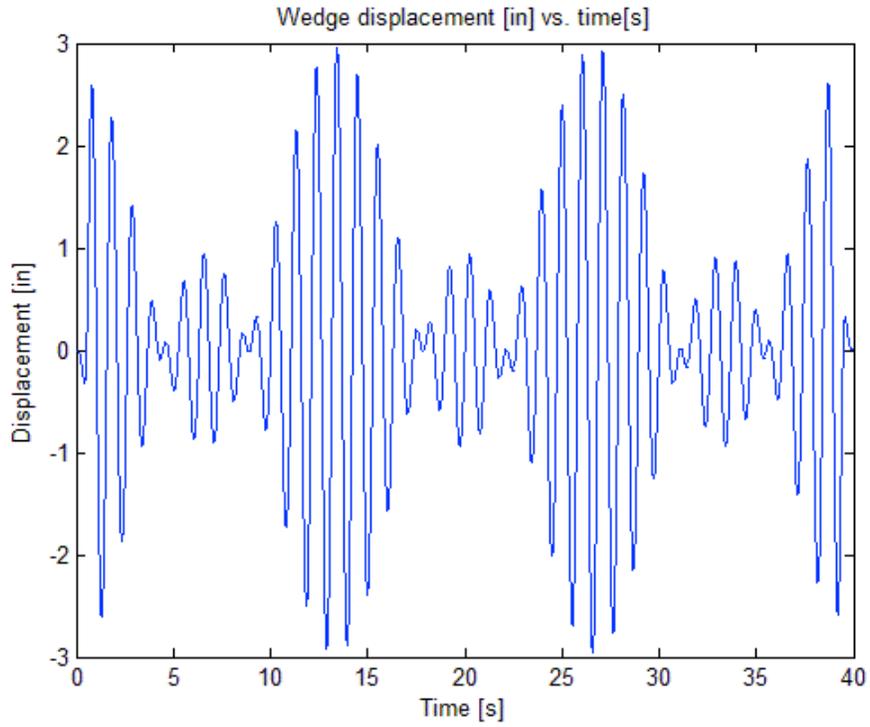
Figure 59: Multi-component wave form: Hsig=6in, Fmin=0.875Hz, Fmax=1.025Hz
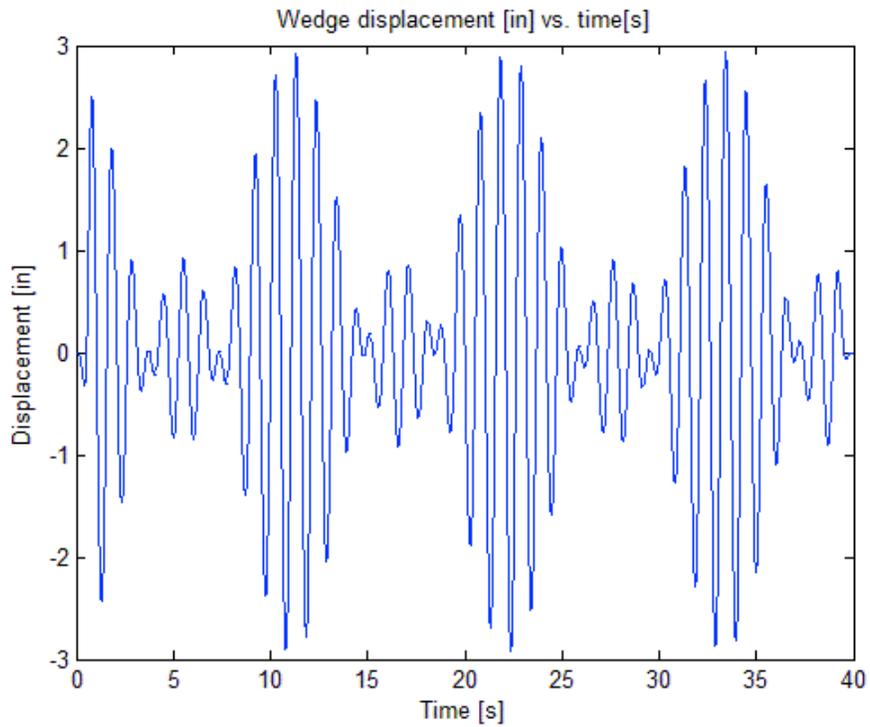
Figure 60: Multi-component wave form: Hsig=6in, Fmin=0.860Hz, Fmax=1.040Hz

136
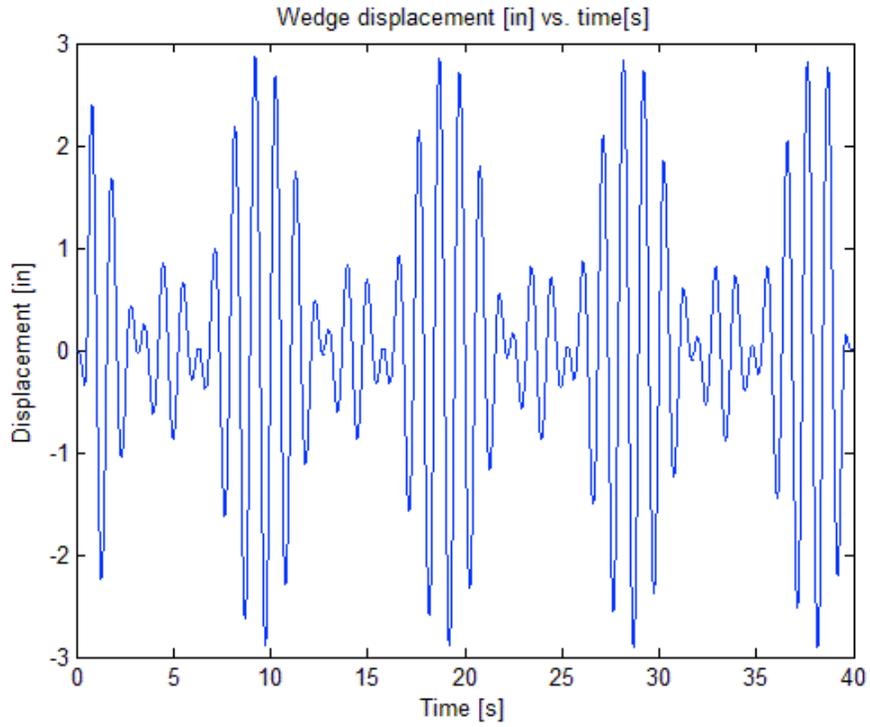
Figure 61: Multi-component wave form: Hsig=6in, Fmin=0.845Hz, Fmax=1.055Hz
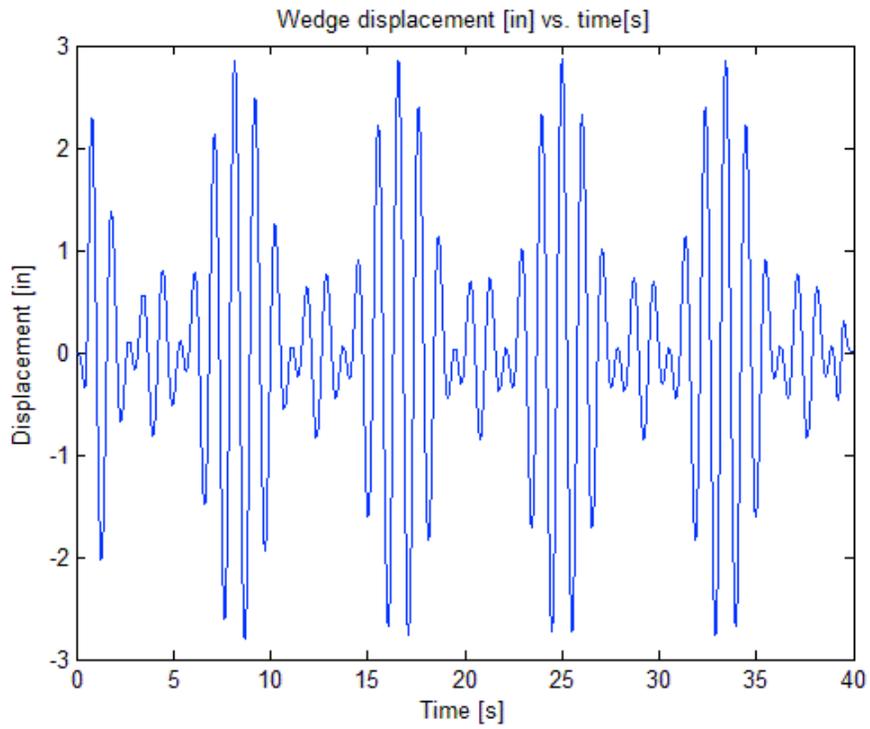
Figure 62: Multi-component wave form: Hsig=6in, Fmin=0.830Hz, Fmax=1.070Hz

137
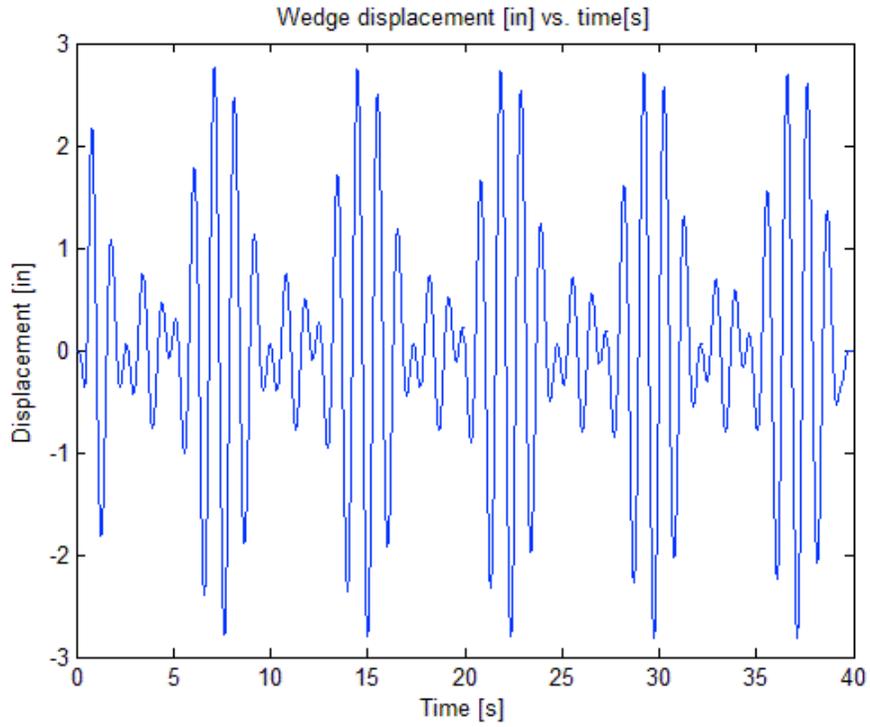
Figure 63: Multi-component wave form: Hsig=6in, Fmin=0.815Hz, Fmax=1.085Hz
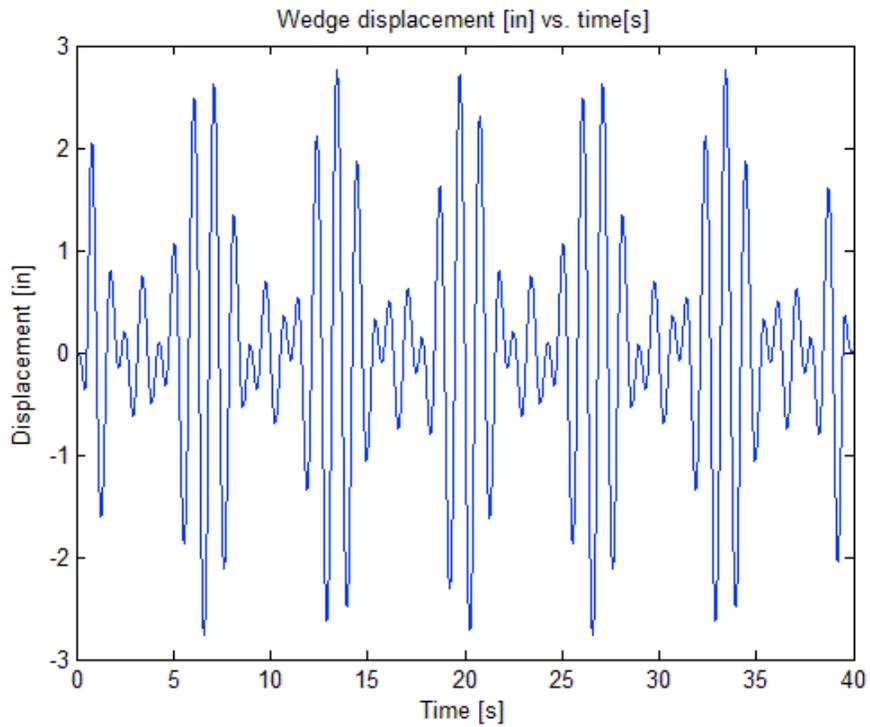
Figure 64: Multi-component wave form: Hsig=6in, Fmin=0.800Hz, Fmax=1.100Hz

Appendix H: Wave Amplitude Data

Table 10: Wave amplitude data, single frequency wave profiles

1/25/2010							
Water Level: 7 1/4"							
Amplitude Factor: 0.0405							
Frequency: 0.855 Hz							
Wavelength: 7 '							
Trial	1	2	3	Average			
Amplitude (Inches)	1.50	1.4375	1.5	1.48			
1/26/2010							
Water Level: 7 3/16"							
Amplitude Factor: 0.0405							
Frequency: 1.13 Hz							
Wavelength: 4 '							
Trial	1	2	3	Average			
Amplitude (Inches)	1.375	1.375	1.3125	1.35			
2/4/2010							
Water Level: 7 1/4"							
Amplitude Factor: 0.0405							
Frequency: 1.066 Hz							
Wavelength: 4.5 '							
Trial	1	2	3	4	5	6	Average
Amplitude (Inches)	2.125	2.125	2.125	2.1875	2.188	2.25	2.167
2/25/2010							
Water Level: 7 3/16"							
Frequency: 1.13 Hz							
Wavelength: 4 '							
Trial	1	2	3	Average			
Amplitude (Inches)	1.563	1.500	1.563	1.54			
Frequency: 1.066 Hz							
Wavelength: 4.5 '							
Trial	1	2	3	Average			
Amplitude (Inches)	1.625	1.625	1.563	1.60			
Frequency: 1.012 Hz							
Wavelength: 5 '							
Trial	1	2	3	Average			
Amplitude (Inches)	1.500	1.438	1.438	1.46			

Frequency: 0.965 Hz							
Wavelength: 5.5 '							
Trial	1	2	3	4	Average		Average Without Trial 3
Amplitude (Inches)	1.438	1.438	0.438	1.10	1.438		1.325
Frequency: 0.924 Hz							
Wavelength: 6 '							
Trial	1	2	3	Average			
Amplitude (Inches)	1.438	1.438	1.500	1.46			
Frequency: 0.887 Hz							
Wavelength: 6.5 '							
Trial	1	2	3	4	Average		
Amplitude (Inches)	1.625	1.625	1.625	1.500	1.63		
Frequency: 0.855 Hz							
Wavelength: 7 '							
Trial	1	2	Average				
Amplitude (Inches)	1.938	1.938	1.94				
3/26/2010							
Water Level: 7 1/4"							
Frequency: 0.826 Hz							
Wavelength: 7.5 '							
Trial	1	2	3	Average			
Amplitude (Inches)	2.125	2.250	2.000	2.13			
Frequency: 0.800 Hz							
Wavelength: 8 '							
Trial	1	2	3	Average			
Amplitude (Inches)	1.875	2.000	2.000	1.96			

Appendix I: Energy Flux Calculation

The equation for the energy flux in a wave is given by the following equation:

$$Q = \frac{\rho g^2 A^2 T}{8\pi}$$

Where Q is the energy flux in kilowatts per meter of wave crest, ρ is the density of the medium, g is the acceleration of gravity, A is the wave amplitude (one half of the wave height) in meters, and T is the period of the wave in seconds.

This equation is then multiplied by the width of the tank (1.2192 m) to find the amount of power contained in each wave profile.   This is reflected in the equation below, which produces power in watts, where w is the width of wave crest.

$$P = Q * w = \frac{\rho g^2 A^2 T}{8\pi} * w$$

For example:

$$P = \frac{1000 * 9.8^2 * (0.392)^2 * 0.88}{8 * \pi} * 1.219 = .00628 \; kilowatts$$

To convert to watts, we can multiply this number by 1000.

Appendix J: Raw Data, Fixed Mooring, Single Frequency Wave Profiles

Table 11: Data for fixed mooring, single frequency wave profiles

12/3/2009						
Water Level: 7 3/16" (Gemstone Ruler)						
Amplitude Factor: 0.0405						
Frequency: 0.95 Hz						
Wavelength: 5.67 '						
Weight (G)	Rise Height (Inches)					
200g #1	6					
Trial	1	2	3	4	5	
Time (Sec)	1.81	1.81	1.82	1.78	1.75	
Average Time (Sec)	1.79					
Standard Deviation	0.028809721	Uncertainty	0.05			
Weight (G)	Rise Height (In)					
500g	6					
Trial	1	2	3			
Time (Sec)	1.93	2.25	1.78			
Average Time (Sec)	1.99					
Standard Deviation	0.240069434	Uncertainty	0.05			
Weight (G)	Rise Height (In)					
500g	12					
Trial	1	2	3	4	5	
Time (Sec)	3.16	3.41	3.50	3.38	3.50	
Average Time (Sec)	3.39					
Standard Deviation	0.139283883	Uncertainty	0.05			
12/4/2009						
Water Level: 7 3/16" (Gemstone Ruler)						
Amplitude Factor: 0.0405						
Frequency:0.95 Hz						
Wavelength: 5.67 '						
Weight (G)	Rise Height (In)					
200g #1	12					
Trial	1	2	3	4	5	
Time (Sec)	3.36	3.39	3.31	3.39	3.38	
Average Time (Sec)	3.37					
Standard Deviation	0.033615473	Uncertainty	0.05			
Weight (G)	Rise Height (In)					

200g #1+100g	12					
Trial	1	2	3	4	5	
Time (Sec)	3.43	3.45	3.38	3.39	3.43	
Average Time (Sec)	3.42					
Standard Deviation	0.036055513	Uncertainty	0.05			
1/21/2010						
Water Level: 7 3/16"						
Amplitude Factor: 0.0405						
Frequency: 1.13 Hz						
Wavelength: 4 '						
Weight (G)	Rise Height (In)					
200g #2	12					
Trial	1	2	3			
Time (Sec)	4.49	5.59	4.91			
Average Time (Sec)	5.00					
Standard Deviation	0.555097589	Uncertainty	0.05			
Frequency: 0.9235 Hz						
Wavelength: 6 '						
Weight (G)	Rise Height (In)					
200g #2	12					
Trial	1	2	3	4	5	
Time (Sec)	3.51	3.51	3.5	3.46	3.5	
Average Time (Sec)	3.50					
Standard Deviation	0.005773503	Uncertainty	0.05			
Frequency: 1.306 Hz						
Wavelength: 3 '						
Weight (G)	Rise Height (In)					
200g #2	12					
Note: The Weight Could Not Be Lifted With This Wavelength						
Frequency: 0.754 Hz						
Wavelength: 9 '						
Weight (G)	Rise Height (In)					
200g #2	12					
Time: 7.02 Sec						
Note: The Rotor Did Not Have Uniform Motion At This Wavelength						

Frequency: 0.855 Hz						
Wavelength: 7 '						
Weight (G)	Rise Height (In)					
200g #2	12					
Trial	1	2	3	4	5	
Time (Sec)	3.8	3.73	3.73	3.69	3.72	
Average Time (Sec)	3.73					
Standard Deviation	0.040414519	Uncertainty	0.05			
1/25/2010						
Water Level: 7 1/4"						
Amplitude Factor: 0.0405						
Frequency: 0.9235 Hz						
Wavelength: 6 '						
Weight (G)	Rise Height (In)					
200g #2+100g	12					
Trial	1	2	3	4	5	
Time (Sec)	3.34	3.28	3.41	3.28	3.35	
Average Time (Sec)	3.33					
Standard Deviation	0.065064071	Uncertainty	0.05			
Frequency: 1.13 Hz						
Wavelength: 4 '						
Weight (G)	Rise Height (In)					
200g #2+100g	12					
Trial	1	2	3	4		
Time (Sec)	6.36	8.14	8.79	8.52		
Average Time (Sec)	7.95					
Standard Deviation	1.258027557	Uncertainty	0.05			
Frequency: 0.855 Hz						
Wavelength: 7 '						
Weight (G)	Rise Height (In)					
200g #2+100g	12					
Trial	1	2	3	4	5	
Time (Sec)	3.48	3.44	3.51	3.48	3.5	
Average Time (Sec)	3.48					
Standard Deviation	0.035118846	Uncertainty	0.05			
Amplitude (Inches)	1.50	1.4375	1.5	Average:	1.48	
1/26/2010						
Water Level: 7 3/16"						

Amplitude Factor: 0.0405						
Frequency: 1.13 Hz						
Wavelength: 4 '						
Weight (G)	Rise Height (In)					
100g	12					
Trial	1	2	3	4	5	
Time (Sec)	2.76	2.74	2.69	2.66	2.76	
Average Time (Sec)	2.72					
Standard Deviation	0.036055513	Uncertainty	0.05			
Amplitude (Inches)	1.375	1.375	1.3125	Average:	1.35	
Frequency: 1.13 Hz						
Wavelength: 4 '						
Weight (G)	Rise Height (In)					
200g #2	12					
Trial	1	2	3	4	5	
Time (Sec)	4.61	4.73	5.52	7.49	5.38	
Average Time (Sec)	5.55					
Standard Deviation	0.494401996	Uncertainty	0.05			
Frequency: 1.13 Hz						
Wavelength: 4 '						
Weight (G)	Rise Height (In)					
200g #2+100g	6					
Trial	1	2	3	4	5	
Time (Sec)	6.86	5.16	6.6	6.72	7.3	
Average Time (Sec)	6.53					
Standard Deviation	0.915714657	Uncertainty	0.05			
2/4/2010						
Water Level: 7 1/4"						
Amplitude Factor: 0.0405						
Frequency: 1.13 Hz						
Wavelength: 4 '						
Weight (G)						
200g #2+200g #1	Rise Height (In)					
Note: This Wave Length Could Not Lift 400g	6					
Frequency: 1.066 Hz						
Wavelength: 4.5 '						
Weight (G)						

100g	Rise Height (In)					
Trial	12					
Time (Sec)	1	2	3	4	5	
Average Time (Sec)	2.96	3.02	3.01	2.94	3	
Standard Deviation	2.99					
Amplitude (Inches)	0.032145503	Uncertainty	0.05			
	2.125	2.125	2.125	2.1875	Average:	2.125
Frequency: 1.066 Hz						
Wavelength: 4.5 '						
Weight (G)						
200g #2	Rise Height (In)					
Trial	12					
Time (Sec)	1	2	3	4	5	
Average Time (Sec)	2.88	2.94	2.86	2.91	2.96	
Standard Deviation	2.91					
Amplitude (Inches)	0.04163332	Uncertainty	0.05			
	2.188	2.25	Average:	2.219		
4/2/2010						
Water Level: 7 3/16"						
Amplitude Factor: 0.0405						
Frequency: 1.066 Hz						
Wavelength: 4.5 '						
Weight (G)						
100g + 200g #2	Rise Height (In)					
Trial	12					
Time (Sec)	1	2	3	4		
Average Time (Sec)	5.72	8.24	8.09	9.14		
Standard Deviation	7.80					
Note: The Rotations Started Off Smooth But Became Hesitant After A While. Oscillations Became Random	1.413612394	Uncertainty	0.05			
Frequency: 1.012 Hz						
Wavelength: 5 '						
Weight (G)						
100g	Rise Height (In)					

Trial	12					
Time (Sec)	1	2	3			
Average Time (Sec)	3.13	3.12	3.15			
Standard Deviation	3.13					
	0.015275252	Uncertainty	0.05			
Frequency: 1.012 Hz						
Wavelength: 5 '						
Weight (G)						
200g #2	Rise Height (In)					
Trial	12					
Time (Sec)	1	2	3			
Average Time (Sec)	3.17	3.13	3.11			
Standard Deviation	3.14					
	0.030550505	Uncertainty	0.05			
4/9/2010						
Water Level: 7 3/16"						
Amplitude Factor: 0.0405						
Frequency: 1.012 Hz						
Wavelength: 5 '						
Weight (G)						
100g + 200g #2	Rise Height (In)					
Trial	12					
Time (Sec)	1	2	3			
Average Time (Sec)	3.34	3.30	3.27			
Standard Deviation	3.30					
	0.035118846	Uncertainty	0.05			
Frequency: 1.012 Hz						
Wavelength: 5 '						
Weight (G)						
200g #1 + 200g #2	Rise Height (In)					
Trial	12					
Time (Sec)	1	2	3	4	5	
Average Time (Sec)	3.41	3.32	3.21	3.16	3.24	
Standard Deviation	3.27					
	0.100166528	Uncertainty	0.05			
Frequency: 1.012 Hz						

Wavelength: 5 '						
Weight (G)						
500g	Rise Height (In)					
Trial	12					
Time (Sec)	1	2	3			
Average Time (Sec)	3.88	3.72	3.69			
Standard Deviation	3.76					
	0.10214369	Uncertainty	0.05			
Frequency: 0.965 Hz						
Wavelength: 5.5 '						
Weight (G)						
100g	Rise Height (In)					
Trial	12					
Time (Sec)	1	2	3			
Average Time (Sec)	3.30	3.35	3.27			
Standard Deviation	3.31					
	0.040414519	Uncertainty	0.05			
Frequency: 0.965 Hz						
Wavelength: 5.5 '						
Weight (G)						
200g #2	Rise Height (In)					
Trial	12					
Time (Sec)	1	2	3			
Average Time (Sec)	3.28	3.31	3.23			
Standard Deviation	3.27					
	0.040414519	Uncertainty	0.05			
Frequency: 0.965 Hz						
Wavelength: 5.5 '						
Weight (G)						
100g + 200g #2	Rise Height (In)					
Trial	12					
Time (Sec)	1	2	3	4		
Average Time (Sec)	3.66	3.35	3.40	3.33		
Standard Deviation	3.44					
	0.16643317	Uncertainty	0.05			
Frequency: 0.965 Hz						
Wavelength: 5.5 '						

Weight (G)						
200g #1 + 200g #2	Rise Height (In)					
Trial	12					
Time (Sec)	1	2	3	4		
Average Time (Sec)	3.44	3.53	3.37	3.37		
Standard Deviation	3.43					
	0.080208063	Uncertainty	0.05			
Frequency: 0.965 Hz						
Wavelength: 5.5 '						
Weight (G)						
500g	Rise Height (In)					
Trial	12					
Time (Sec)	1	2	3			
Average Time (Sec)	3.23	3.33	3.57			
Standard Deviation	3.38					
	0.174737899	Uncertainty	0.05			
Frequency: 0.924 Hz						
Wavelength: 6 '						
Weight (G)						
100g	Rise Height (In)					
Trial	12					
Time (Sec)	1	2	3	4		
Average Time (Sec)	3.58	3.61	3.70	3.61		
Standard Deviation	3.63					
	0.06244998	Uncertainty	0.05			
Frequency: 0.924 Hz						
Wavelength: 6 '						
Weight (G)						
200g #2	Rise Height (In)					
Trial	12					
Time (Sec)	1	2	3			
Average Time (Sec)	3.40	3.54	3.58			
Standard Deviation	3.51					
	0.094516313	Uncertainty	0.05			
Frequency: 0.924 Hz						
Wavelength: 6 '						
Weight (G)						

100g + 200g #2	Rise Height (In)					
Trial	12					
Time (Sec)	1	2	3			
Average Time (Sec)	3.58	3.52	3.49			
Standard Deviation	3.53					
	0.045825757	Uncertainty	0.05			
Frequency: 0.924 Hz						
Wavelength: 6 '						
Weight (G)						
200g #1 + 200g #2	Rise Height (In)					
Trial	12					
Time (Sec)	1	2	3			
Average Time (Sec)	3.37	3.34	3.42			
Standard Deviation	3.38					
	0.040414519	Uncertainty	0.05			
Frequency: 0.887 Hz						
Wavelength: 6.5 '						
Weight (G)						
100g	Rise Height (In)					
Trial	12					
Time (Sec)	1	2	3			
Average Time (Sec)	3.78	3.82	3.69			
Standard Deviation	3.76					
	0.066583281	Uncertainty	0.05			
Frequency: 0.887 Hz						
Wavelength: 6.5 '						
Weight (G)						
200g #2	Rise Height (In)					
Trial	12					
Time (Sec)	1	2	3			
Average Time (Sec)	3.78	3.78	3.81			
Standard Deviation	3.79					
	0.017320508	Uncertainty	0.05			
Frequency: 0.887 Hz						
Wavelength: 6.5 '						
Weight (G)						
100g + 200g #2	Rise Height (In)					

Trial	12						
Time (Sec)	1	2	3	4			
Average Time (Sec)	4.02	3.79	3.72	3.75			
Standard Deviation	3.82						
	0.156950098	Uncertainty	0.05				
Frequency: 0.887 Hz							
Wavelength: 6.5 '							
Weight (G)							
200g #1 + 200g #2	Rise Height (In)						
Trial	12						
Time (Sec)	1	2	3	4			
Average Time (Sec)	4.05	3.66	3.70	3.85			
Standard Deviation	3.82						
	0.214553801	Uncertainty	0.05				
Frequency: 0.887 Hz							
Wavelength: 6.5 '							
Weight (G)							
500g	Rise Height (In)						
Trial	12						
Time (Sec)	1	2	3				
Average Time (Sec)	3.69	3.64	3.84				
Standard Deviation	3.72						
	0.1040833	Uncertainty	0.05				
Frequency: 0.855 Hz							
Wavelength: 7 '							
Weight (G)							
100g	Rise Height (In)						
Trial	12						
Time (Sec)	1	2	3	4			
Average Time (Sec)	3.70	3.56	3.57	3.57			
Standard Deviation	3.60						
	0.078102497	Uncertainty	0.05				
Frequency: 0.855 Hz							
Wavelength: 7 '							
Weight (G)							
200g #2	Rise Height (In)						
Trial	12						

Time (Sec)	1	2	3			
Average Time (Sec)	3.60	3.58	3.57			
Standard Deviation	3.58					
	0.015275252	Uncertainty	0.05			
Frequency: 0.855 Hz						
Wavelength: 7 '						
Weight (G)						
100g + 200g #2	Rise Height (In)					
Trial	12					
Time (Sec)	1	2	3	4		
Average Time (Sec)	3.27	3.72	3.69	3.57		
Standard Deviation	3.56					
	0.251594913	Uncertainty	0.05			
Frequency: 0.855 Hz						
Wavelength: 7 '						
Weight (G)						
200g #1 + 200g #2	Rise Height (In)					
Trial	12					
Time (Sec)	1	2	3	4		
Average Time (Sec)	3.75	3.36	3.25	3.48		
Standard Deviation	3.46					
	0.262741952	Uncertainty	0.05			
Frequency: 0.826 Hz						
Wavelength: 7.5 '						
Weight (G)						
100g	Rise Height (In)					
Trial	12					
Time (Sec)	1	2	3	4		
Average Time (Sec)	4.00	3.78	3.43	4.03		
Standard Deviation	3.81					
	0.27676705	Uncertainty	0.05			
Frequency: 0.826 Hz						
Wavelength: 7.5 '						
Weight (G)						
200g #2	Rise Height (In)					
Trial	12					
Time (Sec)	1	2	3	4	5	

Average Time (Sec)	3.64	3.34	3.27	3.63	4.32	
Standard Deviation	3.64					
	0.415150575	Uncertainty	0.05			
Frequency: 0.826 Hz						
Wavelength: 7.5 '						
Weight (G)						
100g + 200g #2	Rise Height (In)					
Trial	12					
Time (Sec)	1	2	3	4		
Average Time (Sec)	3.81	3.61	3.91	3.91		
Standard Deviation	3.81					
	0.141421356	Uncertainty	0.05	Total Uncert:		
Frequency: 0.826 Hz						
Wavelength: 7.5 '						
Weight (G)						
200g #1 + 200g #2	Rise Height (In)					
Trial	12					
Time (Sec)	1	2	3	4		
Average Time (Sec)	3.76	3.73	4.04	3.76		
Standard Deviation	3.82					
	0.145688023	Uncertainty	0.05			
Frequency: 0.800 Hz						
Wavelength: 8 '						
Weight (G)						
100g	Rise Height (In)					
Trial	12					
Time (Sec)	1	2	3			
Average Time (Sec)	4.06	3.95	4.05			
Standard Deviation	4.02					
	0.060827625	Uncertainty	0.05			
Frequency: 0.800 Hz						
Wavelength: 8 '						
Weight (G)						
200g #2	Rise Height (In)					
Trial	12					
Time (Sec)	1	2	3			

Average Time (Sec)	4.11	4.00	4.03			
Standard Deviation	4.05					
	0.056862407	Uncertainty	0.05			
Frequency: 0.800 Hz						
Wavelength: 8 '						
Weight (G)						
100g + 200g #2	Rise Height (In)					
Trial	12					
Time (Sec)	1	2	3			
Average Time (Sec)	3.90	4.03	3.96			
Standard Deviation	3.96					

Appendix K: Power Extraction Calculation

To compute the power extracted by the rotor was computed using the following equation:

$$P = \frac{mgh}{t}$$

Where P is power in watts, m is the mass in grams, g is the acceleration of gravity in m/s^2, h is the height in meters, and t is the time in seconds.

An example calculation is shown below:

$$P = (0.09986 * 9.8 * 0.3040)/2.72 = 0.1097 \ W$$

Appendix L: Power Extraction Data, Fixed Mooring, Single Frequency Waves

Table 12: Power extraction data for fixed mooring, single frequency wave profiles

Wavelength (feet)	Mass (g)	Distance (m)	Work (J)	Time(sec)	Power (W)	Uncertainty
4	99.86	0.3048	0.2983	2.72	0.1097	0.0056
4	199.73	0.3048	0.5966	5	0.1193	0.0060
4	199.73	0.3048	0.5966	5.55	0.1075	0.0054
4	299.59	0.1524	0.4474	6.53	0.0685	0.0069
4	299.59	0.3048	0.8949	7.95	0.1126	0.0056
4.5	99.86	0.3048	0.2983	2.99	0.0998	0.0051
4.5	199.73	0.3048	0.5966	2.91	0.2050	0.0105
4.5	299.73	0.3048	0.8953	7.8	0.1148	0.0058
5	99.86	0.3048	0.2983	3.13	0.0952	0.0048
5	199.73	0.3048	0.5966	3.14	0.1902	0.0097
5	299.59	0.3048	0.8949	3.3	0.2709	0.0138
5	399.47	0.3048	1.1932	3.27	0.3651	0.0186
5	499.43	0.3048	1.4918	3.76	0.3964	0.0201
5.5	99.86	0.3048	0.2983	3.31	0.0902	0.0046
5.5	199.73	0.3048	0.5966	3.27	0.1823	0.0093
5.5	299.59	0.3048	0.8949	3.44	0.2605	0.0132
5.5	399.47	0.3048	1.1932	3.43	0.3481	0.0177
5.5	499.43	0.3048	1.4918	3.38	0.4418	0.0224
5.67	199.74	0.1524	0.2983	1.79	0.1667	0.0169
5.67	199.74	0.3048	0.5966	3.37	0.1770	0.0090
5.67	299.6	0.3048	0.8949	3.42	0.2617	0.0133
5.67	499.43	0.1524	0.7459	1.99	0.3748	0.0379
5.67	499.43	0.3048	1.4918	3.39	0.4401	0.0224
6	99.86	0.3048	0.2983	3.63	0.0823	0.0042
6	199.73	0.3048	0.5966	3.5	0.1705	0.0087
6	199.73	0.3048	0.5966	3.51	0.1701	0.0086
6	299.59	0.3048	0.8949	3.33	0.2687	0.0137
6	299.59	0.3048	0.8949	3.53	0.2535	0.0129
6	399.47	0.3048	1.1932	3.38	0.3534	0.0180
6.5	99.86	0.3048	0.2983	3.76	0.0793	0.0040
6.5	199.73	0.3048	0.5966	3.79	0.1574	0.0080
6.5	299.59	0.3048	0.8949	3.82	0.2343	0.0119

6.5	399.47	0.3048	1.1932	3.82	0.3128	0.0158
6.5	499.43	0.3048	1.4918	3.72	0.4007	0.0203
7	99.86	0.3048	0.2983	3.6	0.0829	0.0042
7	199.73	0.3048	0.5966	3.58	0.1665	0.0084
7	199.73	0.3048	0.5966	3.73	0.1599	0.0081
7	299.59	0.3048	0.8949	3.48	0.2572	0.0131
7	299.59	0.3048	0.8949	3.56	0.2512	0.0127
7	399.47	0.3048	1.1932	3.46	0.3449	0.0175
7.5	99.86	0.3048	0.2983	3.81	0.0783	0.0040
7.5	199.73	0.3048	0.5966	3.64	0.1639	0.0083
7.5	299.59	0.3048	0.8949	3.81	0.2349	0.0119
7.5	399.47	0.3048	1.1932	3.82	0.3122	0.0158
8	99.86	0.3048	0.2983	4.02	0.0742	0.0038
8	199.73	0.3048	0.5966	4.05	0.1474	0.0075
8	299.59	0.3048	0.8949	3.96	0.2258	0.0114

Appendix M: Power Extraction Data, Tethered Mooring, Single Frequency Waves

Table 13: Power extraction data for tethered mooring single frequency wave profiles

Wavelength (ft)	Average time (s)	Distance (m)	Weight (g)	Work (J)	Power (W)
4	7.69	0.381	172	0.6422	0.0835
4.5	4.88	0.381	222	0.8289	0.1699
5	3.38	0.381	234	0.8737	0.2585
5.5	2.89	0.381	236	0.8812	0.3049
6	3.48	0.381	258	0.9633	0.2768
6.5	3.39	0.381	258	0.9633	0.2842
7	3.38	0.381	234	0.8737	0.2585
7.5	3.48	0.381	258	0.9633	0.2768
8	3.65	0.381	270	1.0081	0.2762

Appendix N: Scaling Up MATLAB Script

```matlab
%%  Scaling Up Analysis
%
% Purpose:
%
% Author:     Sean Henely
%
% Language:  MATLAB 7.10
%
% *================================================*
% |   University of Maryland College Park        |
% |                                              |
% |     Honors College                          |
% |     Gemstone Program                        |
% |     Cohort of 2011                          |
% |                                              |
% |     Glenn L. Martin Institute of Technology  |
% |     A. James Clark School of Engineering     |
% |     Department of Mechanical Engineering     |
% |     The Burgers Program for Fluid Dynamics   |
% |     Hydrodynamics Laboratory                 |
% *================================================*
%
% *================================================*
% |  Water and Versatile Energy Systems (WAVES)   |
% |                                              |
% |     Sean Henely                             |
% |     Laura Hereford                          |
% |     Mary Jung                               |
% |     Tatsuya Saito                           |
% |     Edward Toumayan                         |
% |     Sarah Watt                              |
% |     Melanie Wong                            |
% |                                              |
% | Mentor:     Dr. James Duncan                 |
% | Librarian:  Ms. Nevenka Zdravkovsk          |
% *================================================*


%%  Revision History
%
% Date          Author      Change Summary
% ----          ------      --------------
% 02/22/2011    shenely     Start of implementation


%%  Constant Section
REV_TO_RAD  = 2 * pi;%Revolutions to radians

GRAVITY = 9.806;%Acceleration of gravity
```

```matlab
%Wave power spectrum - Bretschneider
BRETSCHNEIDER = @(f,Hsig,Fmean,a,b)...
            a * (Hsig ^ 2 / Fmean) * (f / Fmean) .^ - 5 .* ...
            exp(- b * (f / Fmean) .^ - 4);

Hsig  = input('Significant wave height [m]: ');
Fmean = input('Mean frequency [Hz]: ');

% [Hsig ,isdigit] = str2num(Hsig);
% [Fmean,isdigit] = str2num(Fmean);

S = @(f) BRETSCHNEIDER(f,Hsig,Fmean,0.3125,1.25);

pitch  = GRAVITY / Fmean ^ 2 / REV_TO_RAD / 1.38;
radius = Hsig / 4;

Fmin  = sqrt(GRAVITY / pitch / REV_TO_RAD / 2);
Fmax  = sqrt(GRAVITY / pitch / REV_TO_RAD);

Pmax = (Hsig / 4) ^ 2;
P    = quad(S,Fmin,Fmax);

f = linspace(Fmean / 2,2 * Fmean,101);

plot(f,S(f),'Color','b');
title('Spectral density [m^2-s] vs. frequency [Hz]');
xlabel('Frequency [Hz]');
ylabel('Spectral Density [m^2-s]');
line([Fmin Fmin],[0 S(Fmin)],'Color','r');
line([Fmax Fmax],[0 S(Fmax)],'Color','g');
legend('S(f)','Fmin','Fmax');

fprintf('Rotor pitch:\t%6.4f [m]\n',pitch);
fprintf('Rotor radius:\t%6.4f [m]\n',radius);
fprintf('% Power available:\t%6.4f\n',P / Pmax);
fprintf('\twith minimum frequency of %6.4f [Hz]\n',Fmin);
fprintf('\t and maximum frequency of %6.4f [Hz]\n',Fmax);
```

Appendix O: Moment of Inertia Calculation

The following proof is the moment of inertia calculation.   It simulates the "worst" or most stressful configuration as when the cross sectional area is, on average, closest to the center of rotation.

$$I = \int x^2 \, dA$$

$$I = 2t \int_{r_{helix,small}^{mean}}^{r_{helix,large}^{mean}} r^2 \, dr \; \square \; \square \left(r_{helix,small}^{mean}\right)^3 \square \left(r_{helix,large}^{mean}\right)^3 \square t \int_{-\square/2}^{\square/2} \sin^2 \square \square \square d \square \; \square \square \; r_{rod}^{mean\,3} \, t \int_{0}^{2\square} \sin^2 \square \square \square d \square$$

$$I = \frac{2}{3} t \; \square \left(r_{helix,large}^{mean}\right)^3 - \left(r_{helix,small}^{mean}\right)^3 \square \square \frac{\square}{2} t \; \square \left(r_{helix,small}^{mean}\right)^3 \square \left(r_{helix,large}^{mean}\right)^3 \square \square \; \square t \, r_{rod}^{mean\,3}$$

Appendix P: Scaling Up Calculations

Delaware Bay Region

Parameter	Units	Value
Gravity	L/T^2	9.81
Helix Density	M/L^3	7.860E+03
Rod Density	M/L^3	7.860E+03
Water Density	M/L^3	1.027E+03
Aluminum Yield Strength	M/L/T^2	386000000
Larger Helix Outer Radius, Ro	L	0.334
Larger Helix Inner Radius, Ri	L	0.331
Rod Outer Radius = ri	L	0.005
Rod Inner Radius	L	0.002
Helix Length	L	118.03
Rod Length	L	118.03
Helix Volume	L^3	0.5107
Rod Volume	L^3	0.0084
Inner Volume	L^3	0.0015
Displaced Fluid Volume	L^3	14.0780
Moment of Inertia	L^4	4.74E-005
Helix Weight	ML/T^2	39359.8951
Rod Weight	ML/T^2	651.0830
Gravity Force	ML/T^2	40010.9781
Buoyancy Force	ML/T^2	141775.8031
Resultant Force	ML/T^2	101764.8250
Total Volume	L^3	0.5191
Rmean	L	0.333
rMEAN	L	0.007
Thickness	L	0.003
Smaller Helix Outer Radius, rO	L	0.008
Smaller Helix Inner Radius, ri	L	0.005
Price/m^3		27803.9434
Price of Device		$14,433.482

Position	Load	Shear	Moment	Stress	Safety Factor
L	M/T^2	ML/T^2	ML^2/T^2	M/L/T^2	-
0.00	-5.51607	20005.4890	0.000	0.00	
1.64	-26.35750	19979.3629	32779.418	3582416.30	107.75
3.28	-47.19894	19919.0702	65488.000	7157091.06	53.93
4.92	-68.04037	19824.6110	98069.735	10717902.90	36.01
6.56	-88.88180	19695.9851	130468.612	14258730.43	27.07
8.20	-109.72323	19533.1927	162628.619	17773452.25	21.72
9.84	-130.56467	19336.2338	194493.746	21255946.97	18.16
11.48	-151.40610	19105.1082	226007.981	24700093.21	15.63
13.11	-172.24753	18839.8161	257115.312	28099769.56	13.74
14.75	-193.08896	18540.3573	287759.729	31448854.64	12.27
16.39	-213.93039	18206.7321	317885.220	34741227.05	11.11
18.03	-234.77183	17838.9402	347435.775	37970765.41	10.17
19.67	-255.61326	17436.9818	376355.380	41131348.32	9.38
21.31	-276.45469	17000.8567	404588.027	44216854.39	8.73
22.95	-297.29612	16530.5652	432077.702	47221162.24	8.17
24.59	-318.13756	16026.1070	458768.396	50138150.45	7.70
26.23	-338.97899	15487.4822	484604.096	52961697.66	7.29
27.87	-359.82042	14914.6909	509528.792	55685682.46	6.93
29.51	-380.66185	14307.7330	533486.471	58303983.46	6.62
31.15	-401.50328	13666.6086	556421.124	60810479.28	6.35
32.79	-422.34472	12991.3175	578276.738	63199048.51	6.11
34.43	-443.18615	12281.8599	598997.303	65463569.77	5.90
36.07	-464.02758	11538.2357	618526.807	67597921.67	5.71
37.71	-484.86901	10760.4449	636809.238	69595982.81	5.55
39.34	-505.71045	9948.4876	653788.586	71451631.81	5.40
40.98	-505.71045	9119.4470	669418.175	73159767.50	5.28
42.62	-505.71045	8290.4063	683688.669	74719369.65	5.17
44.26	-505.71045	7461.3657	696600.069	76130438.26	5.07
45.90	-505.71045	6632.3251	708152.373	77392973.34	4.99
47.54	-505.71045	5803.2844	718345.583	78506974.88	4.92
49.18	-505.71045	4974.2438	727179.699	79472442.88	4.86
50.82	-505.71045	4145.2032	734654.719	80289377.34	4.81
52.46	-505.71045	3316.1625	740770.645	80957778.26	4.77
54.10	-505.71045	2487.1219	745527.477	81477645.64	4.74
55.74	-505.71045	1658.0813	748925.213	81848979.49	4.72
57.38	-505.71045	829.0406	750963.855	82071779.80	4.70
59.02	-505.71045	0.0000	751643.403	82146046.56	4.70
60.66	-505.71045	-829.0406	750963.855	82071779.80	4.70
62.30	-505.71045	-1658.0813	748925.213	81848979.49	4.72
63.93	-505.71045	-2487.1219	745527.477	81477645.64	4.74
65.57	-505.71045	-3316.1625	740770.645	80957778.26	4.77
67.21	-505.71045	-4145.2032	734654.719	80289377.34	4.81
68.85	-505.71045	-4974.2438	727179.699	79472442.88	4.86
70.49	-505.71045	-5803.2844	718345.583	78506974.88	4.92
72.13	-505.71045	-6632.3251	708152.373	77392973.34	4.99
73.77	-505.71045	-7461.3657	696600.069	76130438.26	5.07
75.41	-505.71045	-8290.4063	683688.669	74719369.65	5.17
77.05	-505.71045	-9119.4470	669418.175	73159767.50	5.28

163

78.69	-505.71045	-9948.4876	653788.586	71451631.81	5.40
80.33	-484.86901	-10760.4449	636809.238	69595982.81	5.55
81.97	-464.02758	-11538.2357	618526.807	67597921.67	5.71
83.61	-443.18615	-12281.8599	598997.303	65463569.77	5.90
85.25	-422.34472	-12991.3175	578276.738	63199048.51	6.11
86.89	-401.50328	-13666.6086	556421.124	60810479.28	6.35
88.53	-380.66185	-14307.7330	533486.471	58303983.46	6.62
90.16	-359.82042	-14914.6909	509528.792	55685682.46	6.93
91.80	-338.97899	-15487.4822	484604.096	52961697.66	7.29
93.44	-318.13756	-16026.1070	458768.396	50138150.45	7.70
95.08	-297.29612	-16530.5652	432077.702	47221162.24	8.17
96.72	-276.45469	-17000.8567	404588.027	44216854.39	8.73
98.36	-255.61326	-17436.9818	376355.380	41131348.32	9.38
100.00	-234.77183	-17838.9402	347435.775	37970765.41	10.17
101.64	-213.93039	-18206.7321	317885.220	34741227.05	11.11
103.28	-193.08896	-18540.3573	287759.729	31448854.64	12.27
104.92	-172.24753	-18839.8161	257115.312	28099769.56	13.74
106.56	-151.40610	-19105.1082	226007.981	24700093.21	15.63
108.20	-130.56467	-19336.2338	194493.746	21255946.97	18.16
109.84	-109.72323	-19533.1927	162628.619	17773452.25	21.72
111.48	-88.88180	-19695.9851	130468.612	14258730.43	27.07
113.12	-68.04037	-19824.6110	98069.735	10717902.90	36.01
114.76	-47.19894	-19919.0702	65488.000	7157091.06	53.93
116.39	-26.35750	-19979.3629	32779.418	3582416.30	107.75
118.03	-5.51607	-20005.4890	0.000	0.00	

	SF	4.699

Load M/T^2

164
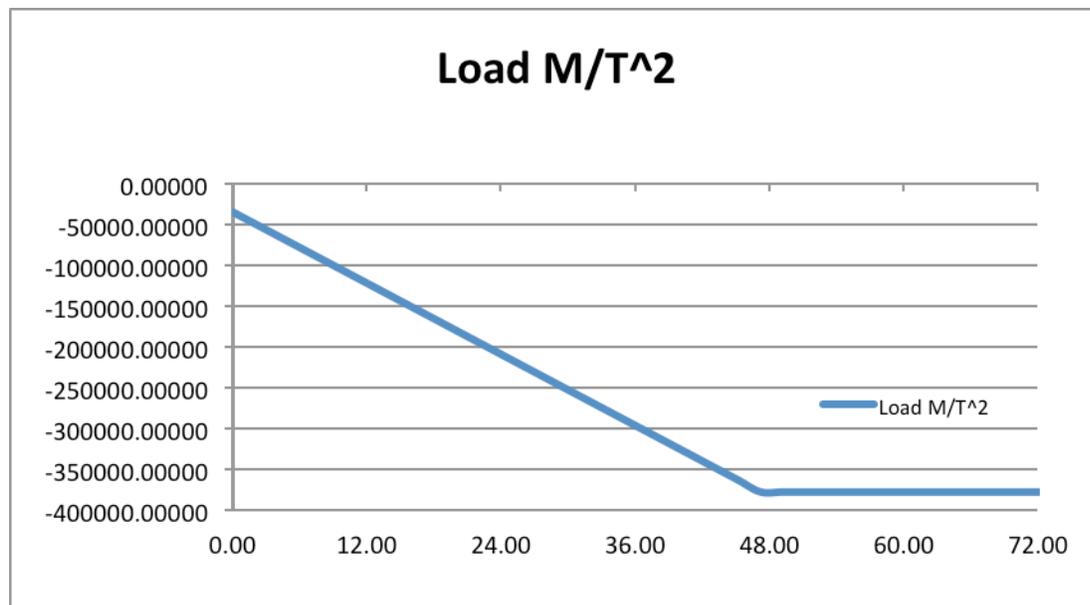
Shear ML/T^2
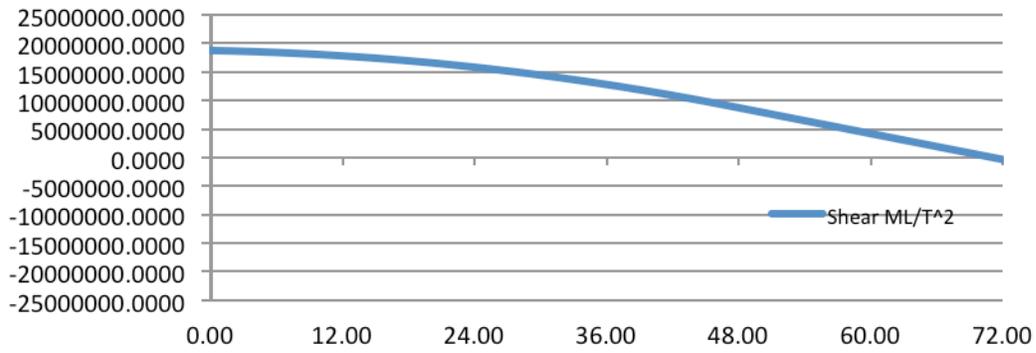
Moment ML^2/T^2
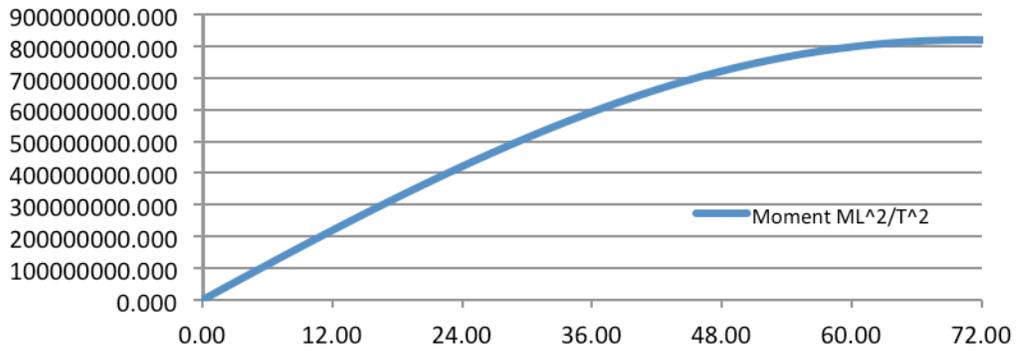
Stress M/L/T^2
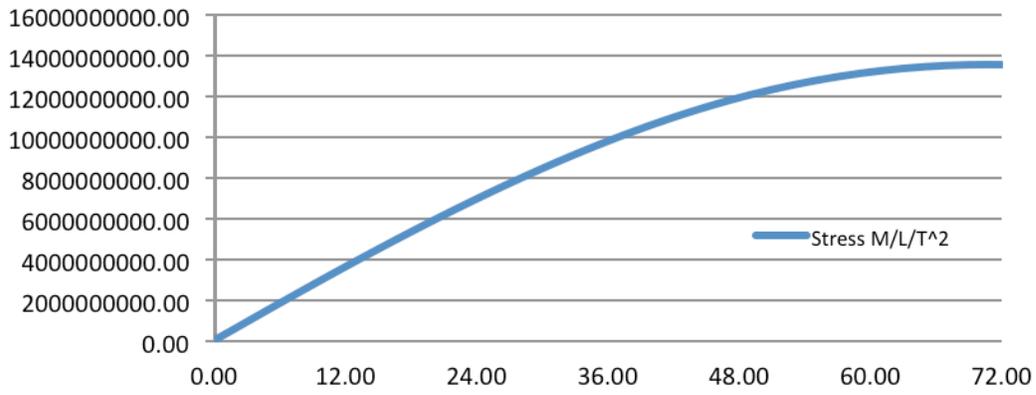
Safety Factor -
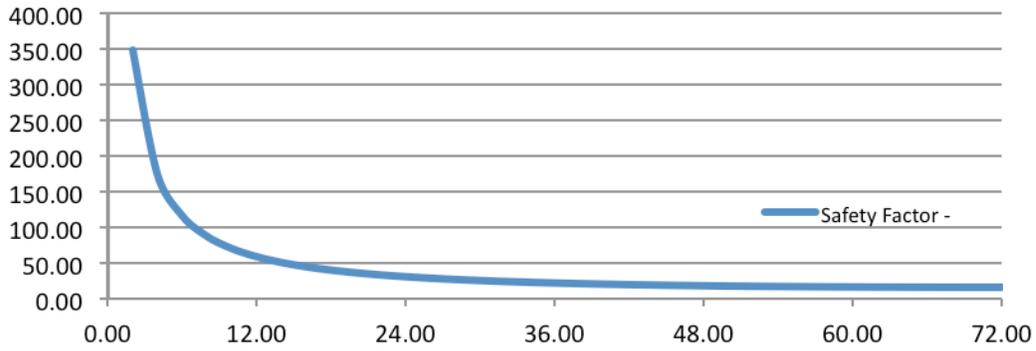
Virginia Beach Region

Parameter	Units	Value
Gravity	L/T^2	9.81
Helix Density	M/L^3	7.860E+03
Rod Density	M/L^3	7.860E+03
Water Density	M/L^3	1.027E+03
Aluminum Yield Strength	M/L/T^2	386000000
Larger Helix Outer Radius, Ro	L	0.427
Larger Helix Inner Radius, Ri	L	0.424
Rod Outer Radius = ri	L	0.005
Rod Inner Radius	L	0.002
Helix Length	L	117.05
Rod Length	L	117.05
Helix Volume	L^3	0.6468
Rod Volume	L^3	0.0084
Inner Volume	L^3	0.0015
Displaced Fluid Volume	L^3	22.6395
Moment of Inertia	L^4	9.89E-005
Helix Weight	ML/T^2	49855.4277
Rod Weight	ML/T^2	645.6403
Gravity Force	ML/T^2	50501.0680
Buoyancy Force	ML/T^2	227996.6661
Resultant Force	ML/T^2	177495.5981
Total Volume	L^3	0.6552
Rmean	L	0.425
rMEAN	L	0.007
Thickness	L	0.003
Smaller Helix Outer Radius, rO	L	0.008
Smaller Helix Inner Radius, ri	L	0.005
Price/m^3		27803.9434
Price of Device		$18,217.657

L	M/T^2	ML/T^2	ML^2/T^2	M/L/T^2	-
0.00	-5.51607	25250.5340	0.000	0.00	
1.63	-32.13753	25219.9281	41029.621	2146139.67	179.86
3.25	-58.75898	25146.0450	81974.311	4287836.82	90.02
4.88	-85.38044	25028.8846	122763.716	6421411.44	60.11

6.50	-112.00190	24868.4468	163327.481	8543183.53	45.18
8.13	-138.62335	24664.7319	203595.253	10649473.08	36.25
9.75	-165.24481	24417.7396	243496.678	12736600.09	30.31
11.38	-191.86626	24127.4700	282961.402	14800884.55	26.08
13.01	-218.48772	23793.9232	321919.071	16838646.44	22.92
14.63	-245.10918	23417.0991	360299.331	18846205.77	20.48
16.26	-271.73063	22996.9977	398031.829	20819882.53	18.54
17.88	-298.35209	22533.6190	435046.210	22755996.71	16.96
19.51	-324.97355	22026.9631	471272.121	24650868.31	15.66
21.13	-351.59500	21477.0298	506639.207	26500817.32	14.57
22.76	-378.21646	20883.8193	541077.116	28302163.72	13.64
24.38	-404.83791	20247.3315	574515.492	30051227.52	12.84
26.01	-431.45937	19567.5664	606883.982	31744328.71	12.16
27.64	-458.08083	18844.5241	638112.232	33377787.28	11.56
29.26	-484.70228	18078.2044	668129.889	34947923.23	11.05
30.89	-511.32374	17268.6075	696866.598	36451056.54	10.59
32.51	-537.94519	16415.7333	724252.005	37883507.22	10.19
34.14	-564.56665	15519.5818	750215.757	39241595.25	9.84
35.76	-591.18811	14580.1530	774687.499	40521640.63	9.53
37.39	-617.80956	13597.4470	797596.878	41719963.36	9.25
39.02	-644.43102	12571.4636	818873.541	42832883.41	9.01
40.64	-644.43102	11523.8417	838458.857	43857334.13	8.80
42.27	-644.43102	10476.2197	856341.103	44792702.18	8.62
43.89	-644.43102	9428.5977	872520.278	45638987.56	8.46
45.52	-644.43102	8380.9758	886996.381	46396190.27	8.32
47.14	-644.43102	7333.3538	899769.414	47064310.30	8.20
48.77	-644.43102	6285.7318	910839.376	47643347.67	8.10
50.40	-644.43102	5238.1099	920206.266	48133302.36	8.02
52.02	-644.43102	4190.4879	927870.086	48534174.38	7.95
53.65	-644.43102	3142.8659	933830.835	48845963.73	7.90
55.27	-644.43102	2095.2439	938088.512	49068670.41	7.87
56.90	-644.43102	1047.6220	940643.119	49202294.41	7.85
58.52	-644.43102	0.0000	941494.654	49246835.75	7.84
60.15	-644.43102	-1047.6220	940643.119	49202294.41	7.85
61.77	-644.43102	-2095.2439	938088.512	49068670.41	7.87
63.40	-644.43102	-3142.8659	933830.835	48845963.73	7.90
65.03	-644.43102	-4190.4879	927870.086	48534174.38	7.95
66.65	-644.43102	-5238.1099	920206.266	48133302.36	8.02
68.28	-644.43102	-6285.7318	910839.376	47643347.67	8.10
69.90	-644.43102	-7333.3538	899769.414	47064310.30	8.20
71.53	-644.43102	-8380.9758	886996.381	46396190.27	8.32
73.15	-644.43102	-9428.5977	872520.278	45638987.56	8.46
74.78	-644.43102	-10476.2197	856341.103	44792702.18	8.62
76.41	-644.43102	-11523.8417	838458.857	43857334.13	8.80
78.03	-644.43102	-12571.4636	818873.541	42832883.41	9.01
79.66	-617.80956	-13597.4470	797596.878	41719963.36	9.25
81.28	-591.18811	-14580.1530	774687.499	40521640.63	9.53
82.91	-564.56665	-15519.5818	750215.757	39241595.25	9.84
84.53	-537.94519	-16415.7333	724252.005	37883507.22	10.19
86.16	-511.32374	-17268.6075	696866.598	36451056.54	10.59
87.79	-484.70228	-18078.2044	668129.889	34947923.23	11.05
89.41	-458.08083	-18844.5241	638112.232	33377787.28	11.56
91.04	-431.45937	-19567.5664	606883.982	31744328.71	12.16
92.66	-404.83791	-20247.3315	574515.492	30051227.52	12.84

168

94.29	-378.21646	-20883.8193	541077.116	28302163.72	13.64
95.91	-351.59500	-21477.0298	506639.207	26500817.32	14.57
97.54	-324.97355	-22026.9631	471272.121	24650868.31	15.66
99.16	-298.35209	-22533.6190	435046.210	22755996.71	16.96
100.79	-271.73063	-22996.9977	398031.829	20819882.53	18.54
102.42	-245.10918	-23417.0991	360299.331	18846205.77	20.48
104.04	-218.48772	-23793.9232	321919.071	16838646.44	22.92
105.67	-191.86626	-24127.4700	282961.402	14800884.55	26.08
107.29	-165.24481	-24417.7396	243496.678	12736600.09	30.31
108.92	-138.62335	-24664.7319	203595.253	10649473.08	36.25
110.54	-112.00190	-24868.4468	163327.481	8543183.53	45.18
112.17	-85.38044	-25028.8846	122763.716	6421411.44	60.11
113.80	-58.75898	-25146.0450	81974.311	4287836.82	90.02
115.42	-32.13753	-25219.9281	41029.621	2146139.67	179.86
117.05	-5.51607	-25250.5340	0.000	0.00	

SF   7.838

Load M/T^2
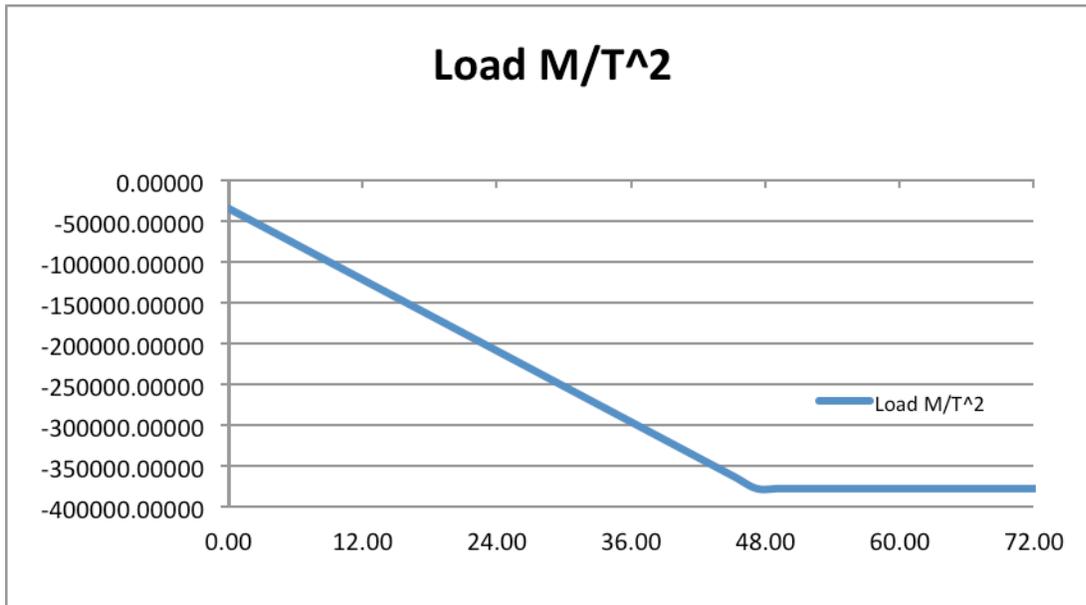
Shear ML/T^2
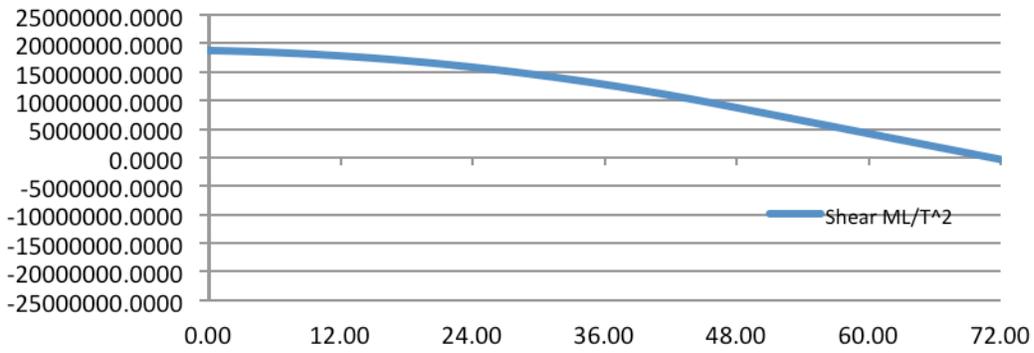
Moment ML^2/T^2
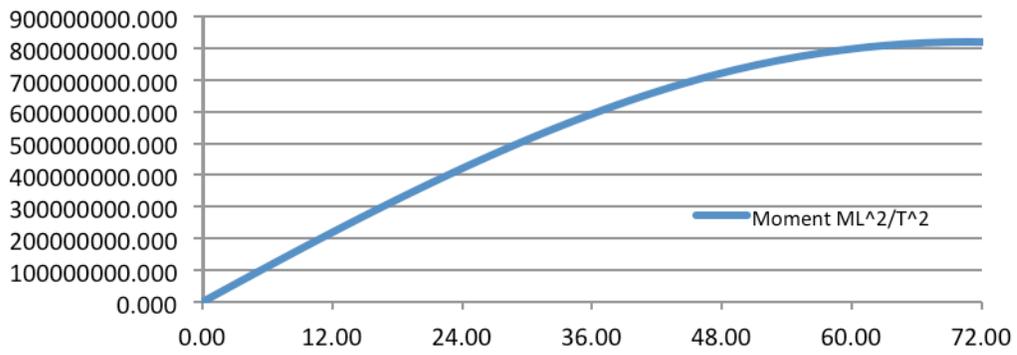
Stress M/L/T^2
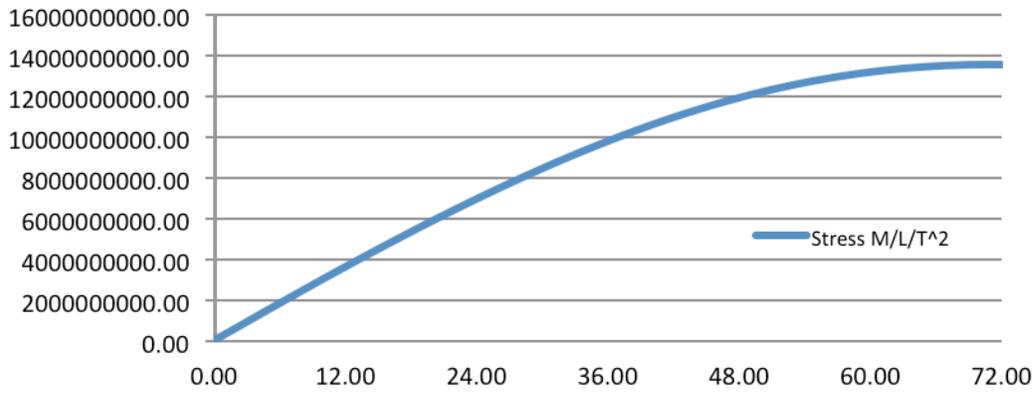
Safety Factor -
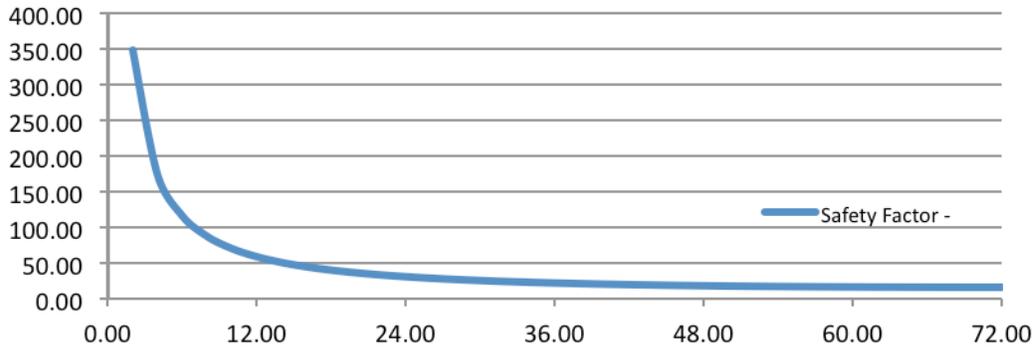
Cape Henry Region

Parameter	Units	Value
Gravity	L/T^2	9.81
Helix Density	M/L^3	7.860E+03
Rod Density	M/L^3	7.860E+03
Water Density	M/L^3	1.027E+03
Aluminum Yield Strength	M/L/T^2	386000000
Larger Helix Outer Radius, Ro	L	0.254
Larger Helix Inner Radius, Ri	L	0.251
Rod Outer Radius = ri	L	0.005
Rod Inner Radius	L	0.002
Helix Length	L	133.28
Rod Length	L	133.28
Helix Volume	L^3	0.4368
Rod Volume	L^3	0.0095
Inner Volume	L^3	0.0017
Displaced Fluid Volume	L^3	9.2040
Moment of Inertia	L^4	2.05E-005
Helix Weight	ML/T^2	33666.7921
Rod Weight	ML/T^2	735.1727
Gravity Force	ML/T^2	34401.9648
Buoyancy Force	ML/T^2	92691.2911
Resultant Force	ML/T^2	58289.3263
Total Volume	L^3	0.4463
Rmean	L	0.252
rMEAN	L	0.007
Thickness	L	0.003
Smaller Helix Outer Radius, rO	L	0.008
Smaller Helix Inner Radius, ri	L	0.005
Price/m^3		27803.9434
Price of Device		$12,410.098

Position	Load	Shear	Moment	Stress	Safety Factor
L	M/T^2	ML/T^2	ML^2/T^2	M/L/T^2	-
0.00	-5.51607	17200.9824	0.000	0.00	
1.85	-21.30390	17176.1594	31822.057	8030536.07	48.07
3.70	-37.09172	17122.1117	63571.115	16042650.47	24.06

5.55	-52.87955	17038.8393	95193.078	24022691.30	16.07
7.40	-68.66737	16926.3423	126633.848	31957006.69	12.08
9.26	-84.45520	16784.6207	157839.327	39831944.75	9.69
11.11	-100.24302	16613.6744	188755.418	47633853.61	8.10
12.96	-116.03085	16413.5035	219328.025	55349081.38	6.97
14.81	-131.81867	16184.1079	249503.048	62963976.19	6.13
16.66	-147.60650	15925.4877	279226.392	70464886.15	5.48
18.51	-163.39432	15637.6428	308443.958	77838159.38	4.96
20.36	-179.18215	15320.5733	337101.649	85070144.00	4.54
22.21	-194.96997	14974.2791	365145.369	92147188.12	4.19
24.06	-210.75780	14598.7603	392521.019	99055639.88	3.90
25.92	-226.54563	14194.0169	419174.502	105781847.38	3.65
27.77	-242.33345	13760.0488	445051.721	112312158.75	3.44
29.62	-258.12128	13296.8560	470098.578	118632922.10	3.25
31.47	-273.90910	12804.4386	494260.976	124730485.55	3.09
33.32	-289.69693	12282.7966	517484.818	130591197.23	2.96
35.17	-305.48475	11731.9299	539716.006	136201405.24	2.83
37.02	-321.27258	11151.8386	560900.443	141547457.72	2.73
38.87	-337.06040	10542.5226	580984.032	146615702.77	2.63
40.72	-352.84823	9903.9820	599912.674	151392488.53	2.55
42.58	-368.63605	9236.2167	617632.274	155864163.10	2.48
44.43	-384.42388	8539.2268	634088.733	160017074.60	2.41
46.28	-384.42388	7827.6246	649236.970	163839846.48	2.36
48.13	-384.42388	7116.0223	663067.969	167330203.40	2.31
49.98	-384.42388	6404.4201	675581.730	170488145.39	2.26
51.83	-384.42388	5692.8179	686778.253	173313672.42	2.23
53.68	-384.42388	4981.2156	696657.538	175806784.51	2.20
55.53	-384.42388	4269.6134	705219.585	177967481.66	2.17
57.38	-384.42388	3558.0112	712464.394	179795763.86	2.15
59.23	-384.42388	2846.4089	718391.965	181291631.12	2.13
61.09	-384.42388	2134.8067	723002.298	182455083.42	2.12
62.94	-384.42388	1423.2045	726295.393	183286120.79	2.11
64.79	-384.42388	711.6022	728271.250	183784743.21	2.10
66.64	-384.42388	0.0000	728929.869	183950950.68	2.10
68.49	-384.42388	-711.6022	728271.250	183784743.21	2.10
70.34	-384.42388	-1423.2045	726295.393	183286120.79	2.11
72.19	-384.42388	-2134.8067	723002.298	182455083.42	2.12
74.04	-384.42388	-2846.4089	718391.965	181291631.12	2.13
75.89	-384.42388	-3558.0112	712464.394	179795763.86	2.15
77.75	-384.42388	-4269.6134	705219.585	177967481.66	2.17
79.60	-384.42388	-4981.2156	696657.538	175806784.51	2.20
81.45	-384.42388	-5692.8179	686778.253	173313672.42	2.23
83.30	-384.42388	-6404.4201	675581.730	170488145.39	2.26
85.15	-384.42388	-7116.0223	663067.969	167330203.40	2.31
87.00	-384.42388	-7827.6246	649236.970	163839846.48	2.36
88.85	-384.42388	-8539.2268	634088.733	160017074.60	2.41
90.70	-368.63605	-9236.2167	617632.274	155864163.10	2.48
92.55	-352.84823	-9903.9820	599912.674	151392488.53	2.55
94.41	-337.06040	-10542.5226	580984.032	146615702.77	2.63
96.26	-321.27258	-11151.8386	560900.443	141547457.72	2.73
98.11	-305.48475	-11731.9299	539716.006	136201405.24	2.83
99.96	-289.69693	-12282.7966	517484.818	130591197.23	2.96
101.81	-273.90910	-12804.4386	494260.976	124730485.55	3.09
103.66	-258.12128	-13296.8560	470098.578	118632922.10	3.25

105.51	-242.33345	-13760.0488	445051.721	112312158.75	3.44
107.36	-226.54563	-14194.0169	419174.502	105781847.38	3.65
109.21	-210.75780	-14598.7603	392521.019	99055639.88	3.90
111.07	-194.96997	-14974.2791	365145.369	92147188.12	4.19
112.92	-179.18215	-15320.5733	337101.649	85070144.00	4.54
114.77	-163.39432	-15637.6428	308443.958	77838159.38	4.96
116.62	-147.60650	-15925.4877	279226.392	70464886.15	5.48
118.47	-131.81867	-16184.1079	249503.048	62963976.19	6.13
120.32	-116.03085	-16413.5035	219328.025	55349081.38	6.97
122.17	-100.24302	-16613.6744	188755.418	47633853.61	8.10
124.02	-84.45520	-16784.6207	157839.327	39831944.75	9.69
125.87	-68.66737	-16926.3423	126633.848	31957006.69	12.08
127.73	-52.87955	-17038.8393	95193.078	24022691.30	16.07
129.58	-37.09172	-17122.1117	63571.115	16042650.47	24.06
131.43	-21.30390	-17176.1594	31822.057	8030536.07	48.07
133.28	-5.51607	-17200.9824	0.000	0.00	

	SF	2.098

Load M/T^2
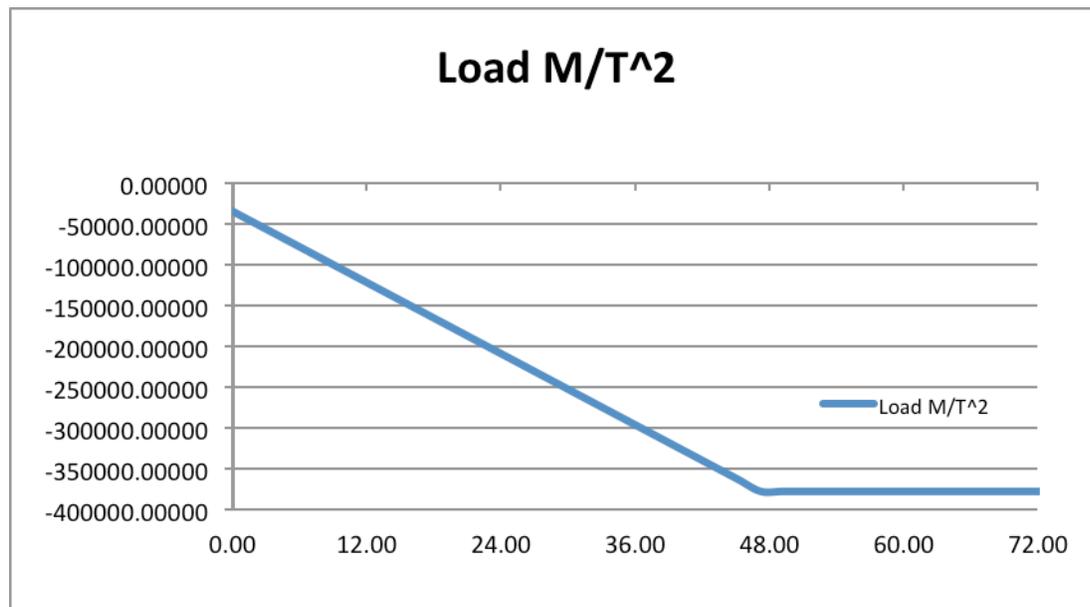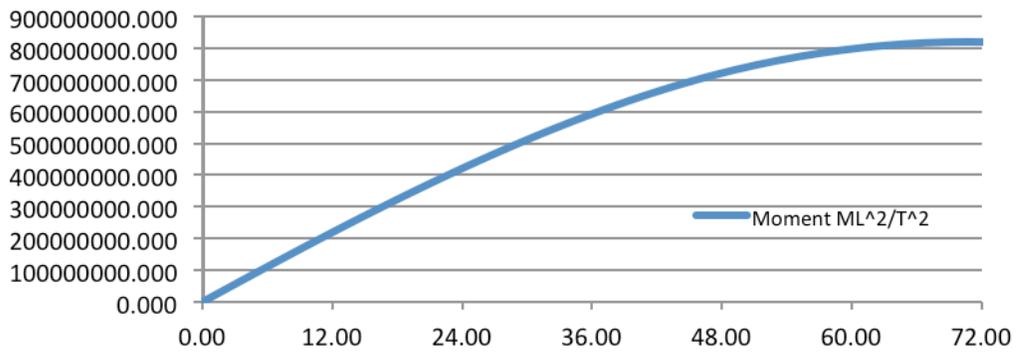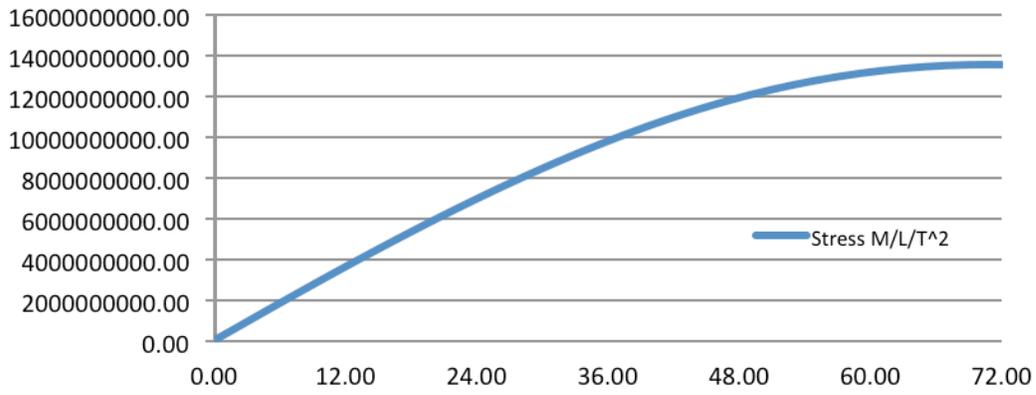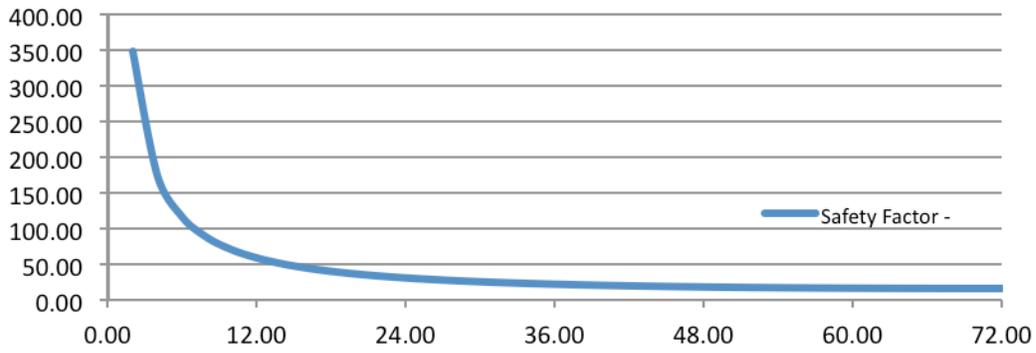
Shear ML/T^2
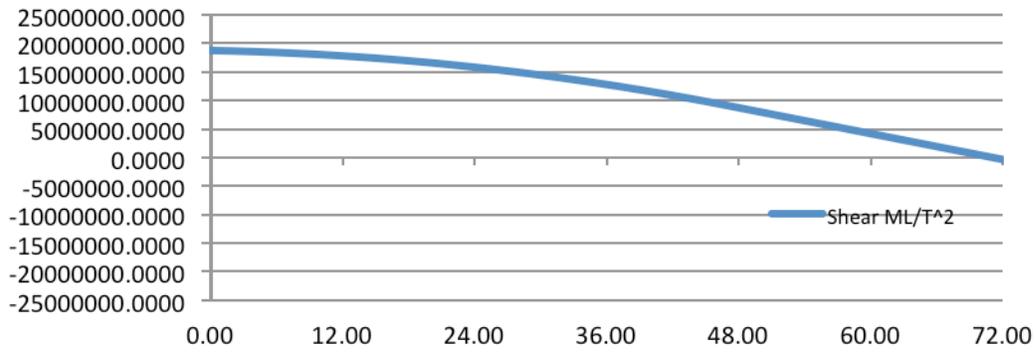
Moment ML^2/T^2

Stress M/L/T^2

Safety Factor -

Appendix Q: Bibliography

AquaBUOY wave energy technology advances (2006).   Retrieved from

       http://www.renewableenergyworld.com/rea/news/story?id=46165

Aquamarine – Oyster 2 unveiled. (2010). *Renewable Energy Focus*, 11(4), 13.

       doi:10.1016/S1755-0084(10)70084-3

Arena, F., & Filianoti, P. (2007, March). Small-scale field experiment on a submerged

       breakwater for absorbing wave energy. *Journal of Waterway, Port, Coastal & Ocean*

       Engineering, 133(2), 161-167. doi:10.1061/(ASCE)0733-950X(2007)133:2(161)

Bald, J., Del Campo, A., Franco. J., Galparsoro, I., Gonzalez, M., Liria, P., ... Mendez, G. (2010,

       October 6). Protocol to develop an environmental impact study of wave energy

       converters. 3rd International Conference on Ocean Energy. *Revista de investigacion*

       marina, 17(5).

Barras, Colin. (2010, May 11). Plenty of wave energy to be harvested close to shore. *New*

       Scientist, 2759.

Berteaux, H. O. (1976). *Buoy Engineering*. New York, NY: A Wiley-Interscience Publication.

Beyene, A., Wilson, J.H. (2008). *Challenges and issues of wave energy conversion*. Arlington,

       VA: Compass Publications.

Birol, F.   (2007 May). World energy prospects and challenges.   *Asia-Pacific Review, 14(1)*, 1-

       12.

Buggey, T. (2007, Summer). Storyboard for Ivan's morning routine. Diagram. *Journal of*

       Positive Behavior Interventions, *9*(3), 151. Retrieved December 14, 2007, from

       Academic Search Premier database.

Charlier, Roger H. & Finkl, Charles W. (2009). Current from Tidal Current. *Ocean Energy* (141-152). Berlin: Springer Berlin Heidelberg.

Cruz, J. (2008). Ocean wave energy: Current status and future perspectives. Germany: Spencer Verlag.

Daedalus Informatics (2008). Simple Oscillating Water Column Device Operating Principle and Flow Dynamics Stimulation. *Renewable Energy Technology – Wave Energy*.

Dementhon, Daniel. (1982). A Rotary Wave Energy Collector. *Offshore and Deepsea Systems Symposium*. Laurel: Hydronautics.

Dementhon, Daniel. (1983). U.S. Patent No 4,412,417. Washington, DC: U.S. Patent and Trademark Office.

de O. Flacao, A.F. Control of an Oscillating- Water-Column Wave Power Plant for Maximum Energy Production.

de O. Falcao, A., Gato, L., Justino, P., & Vicente, P. (2009). Renewable Energy: Leveraging Ocean and Waterways. *Applied Ocean Research, 31(267-281)*.

De Sousa Prado, M. G., Gardner, F. F., Damen, M. M., & Polinder, H. H. (2006). Modeling and test results of the Archimedes wave swing. *Proceedings of the Institution of Mechanical Engineers -Part A- Power & Energy*, 220(8), 855-868. doi:10.1243/09576509JPE284

El Marjani, A., Castro Ruiz, F., Rodriguez, M. A., & Parra Santos, M. T. (2008). Numerical modeling in wave energy conversion systems. *Energy, 33*(8), 1246-1253.

EMEC: European Marine Energy Centre. (2008). Retrieved from http://www.emec.org.uk/wave_energy_devices.asp

Eriksson, M., Waters, R., Svensson, O., Isberg, J., & Leijon, M. (2007). Wave power absorption: Experiments in open sea and simulation. *Journal of Applied Physics, 102*(8).

Evans, D.V. (1978). The Oscillating Water Column Wave-Energy Device. *Department of Mathematics, University of Bristol,22(423-233)*.

Folley, M., Whittaker, T. J. T., & Henry, A. (2007). The effect of water depth on the performance of a small surging wave energy converter. *Ocean Engineering,* 34(8-9), 1265-1274.

Folley, M., Whittaker, T., Osterried, M. (2005). The oscillating wave surge converter. *International Offshore and Polar Engineering Conference.* Belfast: The International Society of Offshore and Polar Engineers.

Holzman, D. C. (2007). Blue power: Turning tides into electricity. *Environmental Health Perspectives,* 115(12), A590-A593.

IEEE. (2007). Scotland to make a big splash in marine energy. *Engineering and Technology*, 2(3), 8-14. Retrieved from Academic Search Premiere.

Ionita, A., & Weitsman, Y. (2007). A model for fluid ingress in closed cell polymeric foams. *Mechanics of Materials, 39*, 434-444.

Johnson, B. & Onwuegbuzie, A. (2004). Mixed methods research: A research paradigm whose time has come. *Educational Researcher*. 33(7), 14-26.

Kofoed, J., Frigaard, P., Friis-Madsen, E., & Sorensen, H. (2004). Prototype testing of the wave energy converter wave dragon. *Renewable Energy*, 31(2), 181-189.

Koola, P., Ravindran, M., & Narayana, P. (1995, April). Model studies of oscillating water column wave-energy device. *Journal of Energy Engineering*, 121(1), 14. Retrieved from Academic Search Premier database.

Leedy, P., & Ormrod, J. (2005). *Practical research: Planning and design*. Upper Saddle River, NJ: Pearson.

Leung, C. (2005). CATCH A WAVE. *Canadian Business*, 78(18), 51. Retrieved from

  EBSCO*host*.

Low, Y.M. & Langley, R.S. (2006). Time and frequency domain coupled analysis of deepwater

  floating production systems. *Applied Ocean Research*, 28(6), 371-385.

Mao, Y., & Heron, M.L. (2008). The Influence of Fetch on the Response of Surface Currents to

  Wind Studied by HF Ocean Surface Radar. Journal of Physical Oceanography, 38(5),

  1107-1121.

MatWeb. (2011). AISI 1018 Steel. Retrieved from

  http://www.matweb.com/search/datasheettext.aspx?matid=6817

McCabe, A. P., & Aggidis, G. A. (2009). Optimum mean power output of a point-absorber wave

  energy converter in irregular waves. *Proceedings of the Institution of Mechanical*

  Engineers -- Part A -- Power & Energy, 223(7), 773-781. doi:10.1243/09576509JPE751

Moreno, Alejandro. (2008). Water Power. *United States Department of Energy*

NASA. (2008). Significant wave height. Retrieved from

  http://www.nasa.gov/mission_pages/ostm/multimedia/swh-20080730.html

NDBC. (2011). NDBC - Cape Henry. Retrieved from

  http://www.ndbc.noaa.gov/station_page.php?station=44099

NDBC. (2011). NDBC - Cape Henry Historical Data. Retrieved from

  http://www.ndbc.noaa.gov/station_history.php?station=44099

NDBC. (2011). NDBC - Delaware Bay. Retrieved from

  http://www.ndbc.noaa.gov/station_page.php?station=44009

NDBC. (2011). NDBC - Delaware Bay Historical Data. Retrieved from

  http://www.ndbc.noaa.gov/station_history.php?station=44009

NDBC. (2011). NBDC - Virginia Beach. Retrieved from

http://www.ndbc.noaa.gov/station_page.php?station=44014

NDBC. (2011). NDBC - Virginia Beach Historical Data. Retrieved from

http://www.ndbc.noaa.gov/station_history.php?station=44014

Nelson, Peter A. (2008, November). Developing wave energy in coastal California: potential

socio-economic and environmental effects. H. T. Harvey & Associates. California Energy

Commission Contract No. 500-07-036.

http://www.energy.ca.gov/2008publications/CEC-500-2008-083/CEC-500-2008-

083.PDF

Pascoal, R., Huang, S., Barltrop, N., & Soares, C.G. (2006). Assessment of the effect of mooring

systems on the horizontal motions with an equivalent force to model**.** *Ocean

Engineering,* 33(11), 1644-1668.

Qian, L., Mingham, C., Causon, D., Ingram, D., Folley, M., & Whittaker, T. (2005, December

20). Numerical simulation of wave power devices using a two-fluid free surface solver.

Modern Physics Letters B, 19(28-29), 1479-1482. Retrieved from Academic Search

Premier database.

Ocean Power Technologies (2008).   Retrieved from

http://www.oceanpowertechnologies.com/tech.htm

"OCS Alternative Energy and Alternate Use Programmatic EIS. (2010). Ocean Wave Energy.

Bureau of Ocean Energy, Management, Regulation, and Enforcement.

Ozcivici, E., & Singh, R (2005). Fabrication and characterization of ceramic foams based on

silicon carbide matrix and hollow alumino-silicate spheres. *Journal of the American

Ceramic Society, 88*(12), 3338-3345.

Patel, S. (2008). A new wave: Ocean power. *Power, 152*(5), 48.

Rusch, E. (2009). Catching a Wave. *Smithsonian*, 40(4), 66-71. Retrieved from EBSCO*host*.

Russell, P. (2010). New Jersey firm seeking power from Oregon's waves. *ENR: Engineering News-Record*, 264(13), 21. Retrieved from EBSCO*host*.

Setoguchi, T., & Takao, M. (2006, September). *Current Status of Self Rectifying Air Turbines for Wave Energy Conversion*. 47(15-16), 2382-2396.

Sorensen, H.C., Hansen, L.K., Hansen, R., and Hammarlund, K. (2002, October 29). *Social, Planning, and Environmental Impact.* European Thematic Network on Wave Energy. Brighton.

Staedter, T. (2002). Wave Power. *Technology Review*, 105(1), 86. Retrieved from EBSCO*host*.

Taylor, J., & Van Doren, P. (2008). In The concise encyclopedia of economics. Retrieved from http://www.econlib.org/library/Enc/Energy.html

Thakker, A., Jarvis, J., & Buggy, M. (2008, April 18). A novel approach to materials selection strategy case study: Wave energy extraction impulse turbine blade. *Materials and Design, 29,* 1973–1980.

Thiruvenkatasamy, K., Neelamani, S., & Sato, M. (2005, March). Nonbreaking wave forces on multiresonant oscillating water column wave power caisson breakwater. *Journal of Waterway, Port, Coastal & Ocean Engineering,* 131(2), 77-84. doi:10.1061/(ASCE)0733-950X(2005)131:2(77)

Vazquez-Hernandez, A. O. (2007). Reliability-based comparative study for mooring lines design criteria. *Applied Ocean Research, 28*(6), 398-406.

Von Jouanne, A. (2006, December). Harvesting the waves. Mechanical Engineering, 128(12), 24-27. Retrieved from Academic Search Premier database.

Wang L., Guo Z., & Yuan, F. (2010). Quasi-static three-dimensional analysis of suction anchor

    mooring system. *Ocean Engineering,* 37(13), 1128-1138.

Wu, F., Zhang, X., Ju, P., Sterling, M. (2008 August). Modeling and control of AWS-based

    wave energy conversion system integrated into power grid. *IEEE Transactions on Power*

    Systems, 23(3) 1196-1204.